Aus dem Centrum für Schlaganfallforschung Berlin,
Abteilung für Experimentelle Neurologie
der Medizinischen Fakultät Charité – Universitätsmedizin Berlin

DISSERTATION

Characterization of the PPPDE1 protein in neurons: intracellular localization, binding partners and functional implications

zur Erlangung des akademischen Grades
Doctor of Philosophy (PhD)

vorgelegt der Medizinischen Fakultät
Charité – Universitätsmedizin Berlin

von

Mariana de Souza Leão Cerdeira
aus Rio de Janeiro, Brasilien

Datum der Promotion: 01.03.2019

Table of Contents

List of Figures 3

List of Tables 4

List of Abbreviations 5

Abstract (English) 9

Abstract (German) 11

Introduction 13

The PPPDE1 protein 13

Ubiquitin and ubiquitin-like proteins 13

Potential functions and localization of PPPDE1 15

The endomembrane system 18

Potential implications in neurons 20

Project aims 21

Materials and Methods 23

Primary culture of mouse cortical neurons 23

Cloning of PPPDE1 overexpression and RNA interference vectors 23

Generation and titration of lentiviral particles 26

Live cell imaging 27

Immunoblot analysis 28

Immunocytochemistry 29

Colocalization analysis 30

Time lapse imaging after brefeldin A treatment 30

Immunocytochemistry for Structured Illumination Microscopy (SIM) imaging 30

SIM imaging, 3D rendering and nearest neighbor analysis 31

Fluorescence Recovery After Photobleaching (FRAP) 32

Propidium iodide incorporation.....32

Immunoprecipitation for proteomics analysis.....33

Preparation of samples for mass spectrometry (MS).....34

Liquid chromatography mass spectrometry (LC-MS) / MS analyses.....34

MS data analyses.....35

Results.....36

PPPDE1 localizes to tubular-shaped compartments in the perinuclear region of neurons.....36

PPPDE1 co-localizes with markers of the cis-Golgi and ER-Golgi intermediate compartment.....39

PPPDE1 is in close proximity with the cis-Golgi and ERGIC, but is closer to the cis-Golgi.....42

Brefeldin A causes rapid dispersion of PPPDE1-positive tubular structures.....45

PPPDE1 vesicles move bi-directionally through neuronal projections.....48

There is a faster- and a slower-moving pool of PPPDE1 molecules.....50

Exogenous PPPDE1 has a positive effect on survival of cultured cortical neurons.....52

PPPDE1 co-precipitates with ubiquitin, but not SUMO, and proteins involved in ER-Golgi vesicle trafficking.....55

PPPDE1 co-localizes with RAB1 and RAB2, but not with SAR1.....62

Annex.....64

Discussion.....66

References.....80

Affidavit.....96

Curriculum Vitae.....97

Acknowledgements.....100

List of Figures

Fig. 1. Schematic overview of the ubiquitin-like protein (UBL) conjugation and deconjugation cycle....15

Fig. 2. Sequence alignment and quaternary structure of mouse PPPDE2 compared to PPPDE1....17

Fig. 3. Schematic representation of the components of the endomembrane system in mammalian cells....18

Fig. 4. Schematic overview of the overexpression and knockdown vectors used and their respective non-targeting controls....26

Fig. 5. Comparison between two variants of PPPDE1-shRNAs and of control shRNAs 36

Fig. 6. Establishment of PPPDE1 knockdown and expression of EGFP-PPPDE1 after lentiviral-mediated transduction of mouse primary cortical neurons....38

Fig. 7. Immunocytochemical screening of markers of the endomembrane system for co-localization with PPPDE1....42

Fig. 8. Confirmation of EGFP fluorescence signal amplification and specificity for PPPDE1 after GFP immunostaining....43

Fig. 9. Spatial distribution of cis-Golgi and ERGIC in relation to PPPDE1....45

Fig. 10. Effect of brefeldin A (BFA) treatment on PPPDE1 in live cortical neurons....47

Fig. 11. Representative time lapse images of EGFP-PPPDE1 vesicles moving mono- or bi-directionally through neuronal projections over time....49

Fig. 12. Quantification of the fluorescence recovery after photobleaching (FRAP) in live cortical neurons expressing EGFP-PPPDE1....51

Fig. 13. Assessment of cell viability in cultured mouse cortical neurons after transduction with EGFP-PPPDE1....53

Fig. 14. Interactome analysis of binding partners of PPPDE1 by mass spectrometry ...59

Fig. 15. Gene ontology (GO) term classification of proteins in the PPPDE1 interactome 62

Fig. 16. Co-expression of EGFP-PPPDE1 and mRuby2-RAB1, -RAB2, -SAR1 or mRuby2 control in live cortical neurons....63

Fig. 17. Expression pattern of PPPDE1 immunostaining in mouse cortical neurons. 67

Fig. 18. Schematic representation of the intracellular localization of perinuclear PPPDE1, RAB1/RAB2 and SAR1 in neurons 76

List of Tables

Table 1. Primary antibodies used and their specifications 29

Table 2. Specifications of the proteins identified in the PPPDE1 interactome 65

List of Abbreviations

3D	three-dimensional
a.u.	arbitrary unit
ADP	adenosine diphosphate
AEBSF	4-(2-aminoethyl) benzenesulfonyl fluoride hydrochloride
ALS	amyotrophic lateral sclerosis
ANOVA	analysis of variance
ARF	ADP ribosylation factor
ATP	adenosine triphosphate
BFA	brefeldin A
bp	base pair
BSS	balanced salt solution
COP	coat/coatomer protein
D / Asp	aspartate
DAPI	4',6-diamidino-2-phenylindole
DeSI	de-SUMOylating isopeptidase
DIV	days in vitro
DMSO	dimethyl sulfoxide
DNA	deoxyribonucleic acid
dsRNA	double-stranded RNA
DTT	dithiothreitol
DUB	de-ubiquitinating enzyme
E / Glu	glutamic acid
EDTA	ethylenediaminetetraacetic acid
EEA1	early endosome antigen 1
EGFP	enhanced green fluorescent protein

ER	endoplasmic reticulum
ERES	endoplasmic reticulum exit site
ERGIC	endoplasmic reticulum-Golgi intermediate compartment
ERGIC-53	53 kDa ERGIC membrane protein
ESI	electrospray ionization
FDR	false discovery rate
FRAP	fluorescence recovery after photobleaching
GAP	GTPase activating protein
GAPDH	glyceraldehyde 3-phosphate dehydrogenase
GDP	guanosine diphosphate
GEF	guanine nucleotide exchange factor
GGA1	Golgi-associated, gamma adaptin ear containing, ARF binding protein 1
GM130	130 kDa Golgi matrix protein
GO	gene ontology
GOP	Golgi outpost
GTP	guanosine triphosphate
HA	human influenza hemagglutinin
HCD	higher-energy collisional dissociation
HEK	human embryonic kidney 293 cells
HEPES	4-(2-hydroxyethyl)-1-piperazineethanesulfonic acid
HPLC	high performance liquid chromatography
IB	immunoblot
K / Lys	lysine
kDa	kilodalton
KDEL	lysine - aspartate - glutamic acid - leucine
L / Leu	leucine

LC-MS	liquid chromatography mass spectrometry
LTR	long terminal repeat
MAP2	microtubule-associated protein 2
MOI	multiplicity of infection
mRNA	messenger RNA
MS	mass spectrometry
NEM	N-ethylmaleimide
NN	nearest neighbor
ORF	open reading frame
PBS	phosphate-buffered saline
PCR	polymerase chain reaction
PDB	protein data bank
PEG	polyethylene glycol
PI	propidium iodide
PLL	poly-L-lysine
PPPDE	permuted papain fold peptidases of dsRNA viruses and eukaryotes
PTM	post-translational modification
PVDF	polyvinylidene fluoride
RAB	Ras-related in brain protein
RIPA	radioimmunoprecipitation assay
RNA	ribonucleic acid
RNAi	RNA interference
ROI	region of interest
S / Ser	serine
SDS	sodium dodecyl sulfate
SENP	sentrin-specific protease

shRNA	short hairpin RNA
SIM	structured illumination microscopy
SUMO	small ubiquitin-like modifier
TBS-T	tris-buffered saline with Tween20
TGN	trans-Golgi network
Tris	tris(hydroxymethyl)aminomethane
TTC	tubular transport carrier
TU	tranducing units
UBL	ubiquitin-like protein
ULP	UBL-specific protease
VTC	vesicular tubular cluster
WPRE	woodchuck hepatitis virus post-transcriptional regulatory element

Abstract (English)

The PPPDE1 protein, a member of the Permuted Papain fold Peptidases of dsRNA viruses and Eukaryotes superfamily, is widely expressed in different tissues and conserved across several plant and animal species. Its exact cellular functions, however, still remain unclear. Scarce literature data suggests that this protein might be involved in post-translational deconjugation of ubiquitin or small ubiquitin-like modifier (SUMO) and in cell cycle modulation.

The goal of the present work was to characterize PPPDE1 in mouse neurons. We aimed to identify the intracellular localization, binding partners and cellular dynamics of this protein, investigate the effects of its expression and knockdown and describe its potential functional implications.

We constructed and delivered an EGFP-PPPDE1 fusion protein vector to mouse primary cortical neuronal cultures by lentiviral-mediated transduction. Using live cell imaging, immunocytochemistry and nearest neighbor analysis of structured illumination microscopy (SIM) images, we identified that PPPDE1 localizes to tubular structures in the perinuclear region. These were in close proximity with the *cis* end of the Golgi apparatus and the endoplasmic reticulum (ER)-Golgi intermediate compartment (ERGIC) and were functionally associated with the Golgi. Time lapse imaging revealed that PPPDE1 is also present in vesicular-shaped compartments moving rapidly and bi-directionally through neuronal projections. Fluorescent recovery after photobleaching (FRAP) confirmed the existence of a second, more mobile population of intracellular PPPDE1 molecules.

Interactome analysis showed that ubiquitin, but not SUMO, was significantly enriched by PPPDE1, indicating that PPPDE1 might have an effect on de-ubiquitination processes, but most likely not on de-SUMOylation, as previously assumed. Several proteins involved in intracellular trafficking were identified as potential binding partners of PPPDE1, such as the RAS-related RAB1 and RAB2 proteins, regulators of transport between the ER and Golgi, and SAR1, the initiating protein for COP-II coat assembly. Co-expression of PPPDE1 with these candidate proteins using distinct fluorescent markers showed that PPPDE1 co-localized with high correlation with RAB1 and RAB2, but in a lower degree and non-specifically with SAR1 in live neurons.

Regarding its functional impact, neuronal cultures overexpressing PPPDE1 exhibited significantly smaller rates of apoptotic and necrotic cells, suggesting that this protein might have a positive effect on neuronal survival.

Our findings provide, for the first time in neurons, evidence on the intracellular features and dynamics of the PPPDE1 protein, and indicate it as a potential contributing factor in the regulation of membrane trafficking between the ER and Golgi.

Abstract (German)

Das Protein PPPDE1, ein Mitglied der permutierten Papain-Faltung Peptidasen bei dsRNA Viren und Eukaryonten-Superfamilie, wird in einer Vielzahl von Geweben exprimiert und ist über mehrere Pflanzen- und Tierarten hinweg konserviert. Seine genauen zellulären Funktionen sind jedoch immer noch unklar. Es existieren nur wenige Veröffentlichungen über PPPDE1, die einen Zusammenhang mit der posttranslationalen Dekonjugation vom Ubiquitin oder vom SUMO (small ubiquitin-like modifier) oder einer Beteiligung an der Zellzyklusmodulation beschreiben.

Das Ziel der vorliegenden Arbeit war es, PPPDE1 in Mausneuronen zu charakterisieren. Dabei wurden die intrazelluläre Lokalisation, sowie die zelluläre Mobilität betrachtet und die Bindungspartner dieses Proteins identifiziert. Dazu wurden die Auswirkungen seiner Expression als fluoreszentes Fusionsprotein und während RNA-Interferenz untersucht, um Rückschlüsse auf seine potenzielle Funktion ziehen zu können.

Ein EGFP-PPPDE1-Fusionsproteinvektor wurde konstruiert und in primäre Kulturen von kortikalen Mausneuronen durch Lentivirus-vermittelte Transduktion exprimiert. Lebendzellbildgebung, Immunzytochemie und Nearest Neighbor Analyse von SIM-Superresolutions-Mikroskopie (structured illumination microscopy) Bildern zeigten, dass PPPDE1 an röhrenförmigen Strukturen in der perinukleären Region lokalisiert war. Diese lagen in unmittelbarer Nähe zum cis-Golgi-Apparat und dem ERGIC (endoplasmic reticulum (ER)-Golgi intermediate compartment) und waren funktionell mit dem Golgi assoziiert. Mittels zeitaufgelöster Videomikroskopie lokalisierte PPPDE1 auch an bidirektional durch neuronale Projektionen wandernden Vesikeln. FRAP (fluorescent recovery after photobleaching) bestätigte die Existenz einer zweiten Population von freier beweglicheren PPPDE1-Molekülen.

Interaktomanalysen zeigten, dass Ubiquitin, aber nicht SUMO, signifikant durch PPPDE1 angereichert wurde, was darauf hindeutet, dass PPPDE1 einen Einfluss auf Prozesse der Deubiquitinierung haben könnte, aber höchstwahrscheinlich nicht der DeSUMOylierung, wie bisher angenommen. Mehrere Proteine, die am intrazellulären Transport beteiligt sind, wurden als potentielle Bindungspartner von PPPDE1 identifiziert, wie die RAS-verwandten RAB1- und RAB2-Proteine, Regulatoren des

Transports zwischen ER und Golgi und SAR1, das initiierende Protein für die COP-II-Mantel-Bildung. Die Ko-Expression von PPPDE1 mit diesen Kandidaten unter Verwendung von verschiedenen Fluoreszenzmarkern zeigte, dass PPPDE1 mit hoher Korrelation mit RAB1 und RAB2 in lebenden Neuronen ko-lokalisiert war, jedoch weniger und unspezifisch mit SAR1.

In Bezug auf seine funktionellen Auswirkungen zeigten neuronale Kulturen, welche PPPDE1 exprimierten, signifikant geringere Raten von apoptotischen und nekrotischen Zellen, was darauf hindeutet, dass dieses Protein eine positive Auswirkung auf das neuronale Überleben haben könnte.

Diese Ergebnisse geben zum ersten Mal in Neuronen Hinweise auf die intrazellulären Eigenschaften und die Dynamik des PPPDE1-Proteins und legen nahe, dass es ein beeinflussender Faktor bei der Regulierung der Transportprozesse zwischen ER und Golgi sein könnte.

Introduction

The PPPDE1 protein

A member of the Permuted Papain fold Peptidases of dsRNA viruses and Eukaryotes superfamily, the PPPDE1 protein, sometimes also referred to as PNAS4, is widely expressed in different tissues and organs and highly conserved across several plant and animal species (He et al., 2013). Its broad expression and evolutionary conservation indicate that this protein must have an essential biological role. Nonetheless, its exact cellular functions still remain unclear.

The superfamily of PPPDE proteins was identified in 2004 (Iyer et al., 2004). As the name suggests, its members contain a circularly permuted papain-like fold and have been found in most eukaryotes, as well as in double-stranded RNA viruses, and one single-stranded DNA virus.

The few existing studies on PPPDE1 have pointed out a possible role of this protein in modulation of cell cycle and post-translational modifications (PTMs). PTMs refer to usually enzymatic alterations of proteins after their biosynthesis, by addition or cleavage of a chemical group or modifier. PTM processes are able to regulate protein conformation, localization, stability, interaction and activity in the cell (Knorre et al., 2009). They therefore represent a fast and reliable mechanism to modulate a wide variety of cellular pathways and functions in response to stimuli or disruption of the cell's homeostasis (Karve et al., 2011).

Ubiquitin and ubiquitin-like proteins

Ubiquitination, also known as ubiquitylation, is a frequent type of PTM consisting of the covalent attachment of an 8.5-kDa ubiquitin protein to lysine residues of a target protein (Khoury et al., 2011). Ubiquitin received this name for its ubiquitous presence in nature, i.e. it is found in all eukaryotic organisms and conserved throughout species (Goldstein et al., 1975), referring to the latin term *ubique*, or "everywhere".

Ubiquitination was first described as a mechanism to label intracellular proteins for subsequent degradation by the proteasome, popularly known as the "molecular kiss of

death", and this discovery was awarded the 2004 Nobel Prize in Chemistry (Hershko et al., 1980; Glickman & Ciechanover, 2002; Giles, 2004). But soon it became clear that ubiquitin conjugation has implications in several other cellular functions in addition to proteolysis signaling, including DNA repair, protein kinase activation and vesicle trafficking (Chen & Sun, 2009; Mukhopadhyay & Riezman, 2007).

One feature that contributes to this versatility is the fact that an ubiquitin molecule can be conjugated to another ubiquitin by linkage to one of its seven lysine residues or N-terminal methionine, forming varied types of ubiquitin chains (polyubiquitination). Alternatively, one single molecule can be added to a target protein (monoubiquitination) (Komander et al., 2009; Zhao & Ulrich, 2010). Ubiquitin chains are commonly represented by a letter, indicating the amino acid where linkage occurs (e.g. K or Lys for lysine), and a number, indicating he amino acid position. The most prevalent ubiquitin chains are K48-linked, well known to target proteins for proteasomal degradation, and K63-linked, involved in non-proteolytical cellular events (Swatek & Komander, 2016).

Several families of proteins that share structural similarities with ubiquitin, called ubiquitin-like proteins (UBL), have been identified in eukaryotes and plants. UBLs include the 12-kDa small ubiquitin-like modifier (SUMO), also known as sentrin (Johnson et al., 1997; Denuc & Marfany, 2010; Cappadocia & Lima, 2018). Conjugation of SUMO to target proteins (or SUMOylation) has been implicated in the regulation of different processes, such as transcription, cell cycle and transport between nucleus and cytoplasm (Müller et al., 2001).

Ubiquitin and UBLs are attached to target proteins usually through a three-step process requiring the sequential activity of activating (E1), conjugating (E2) and ligating (E3) enzymes (Fig. 1) (Schwartz & Hochstrasser, 2003). Both ubiquitination and SUMOylation are reversible reactions, as ubiquitin and SUMO can be removed from the substrate protein by the isopeptidase activity of de-ubiquitinating enzymes (DUBs) or SUMO proteases, respectively (Reyes-Turcu et al., 2009, Nayak & Müller, 2014).

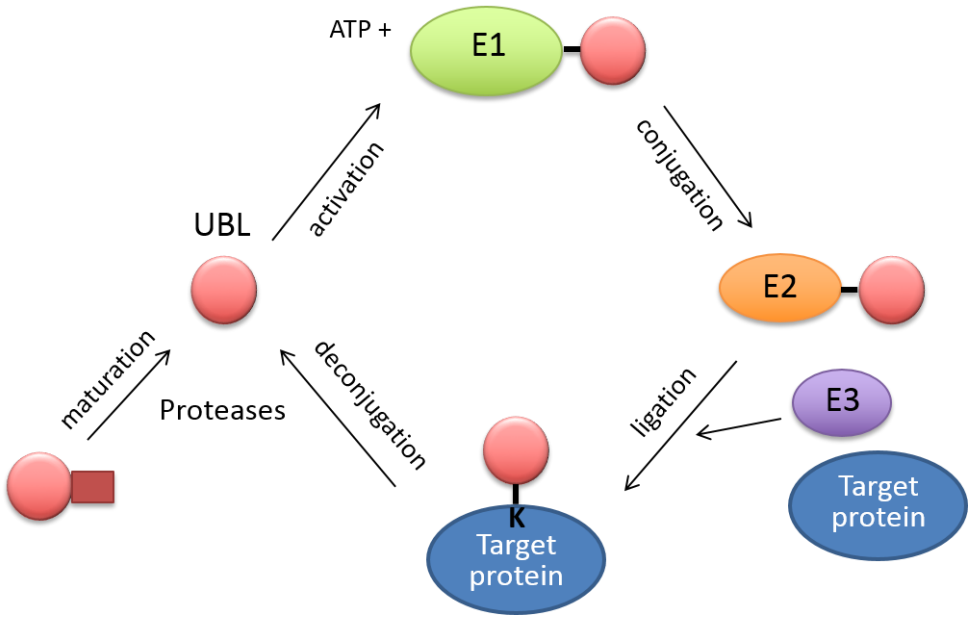

Fig. 1. Schematic overview of the ubiquitin-like protein (UBL) conjugation and deconjugation cycle. After maturation of UBL (red circle) by cleavage of its precursor by an UBL-specific protease (ULP), it is activated in an ATP-dependent manner, binding to the activating enzyme E1. It is then transferred to a conjugating enzyme E2. Conjugation of UBL to a lysine residue (K) of the target protein can occur either directly by E2, or in conjunction with an E3 enzyme. UBL can subsequently be deconjugated from the substrate protein via cleavage by ULPs, including de-ubiquitinating enzymes (DUBs) for ubiquitin, and SUMO isopeptidases for SUMO.

Potential functions and localization of PPPDE1

PPPDE1 has been reported to induce apoptosis and S-phase cell cycle arrest in different cancer cells (Yan et al., 2009; Deng et al., 2010; Li et al. 2013; Yuan et al., 2015), and to play a role in embryogenesis of the zebrafish, pig and frog (Yao et al., 2008; Mo et al., 2008; Yan et al., 2010). However, brain development in conditional knockout mice was not altered compared to wild-type mice (Cai et al., 2012), meaning that PPPDE1 likely has other functions in addition to apoptosis modulation.

A bioinformatics screening study using database searches and structural modeling predicted that proteins in the PPPDE superfamily might play a role in the ubiquitin signaling system as de-ubiquitinating enzymes (Iyer et al., 2004). More recently,

PPPDE1 was reported to have de-ubiquitinating activity *in vitro* in human carcinoma cell lines, acting on the ribosomal protein S7 (Xie et al., 2017).

The second member of the PPPDE family, both in humans and mice, is PPPDE2, whose amino acid sequence is 32% identical to that of its isoform, PPPDE1 – a homology usually considered to result in identical folds (Fig. 2). The similarity between the two isoforms – a value that includes non-identical amino acids that have similar chemical properties – is 53%.

PPPDE2 has been described to catalyze the deconjugation of SUMO, but not ubiquitin, from the BTB-ZF protein expressed in effector lymphocytes, named BZEL (Shin et al., 2012). For this reason, it received a new name of de-SUMOylating isopeptidase 1, or DeSI1. Because of the sequence similarity between the two isoforms, PPPDE1 was denominated DeSI2. However, no de-SUMOylating activity of DeSI2 or substrate proteins have been reported so far.

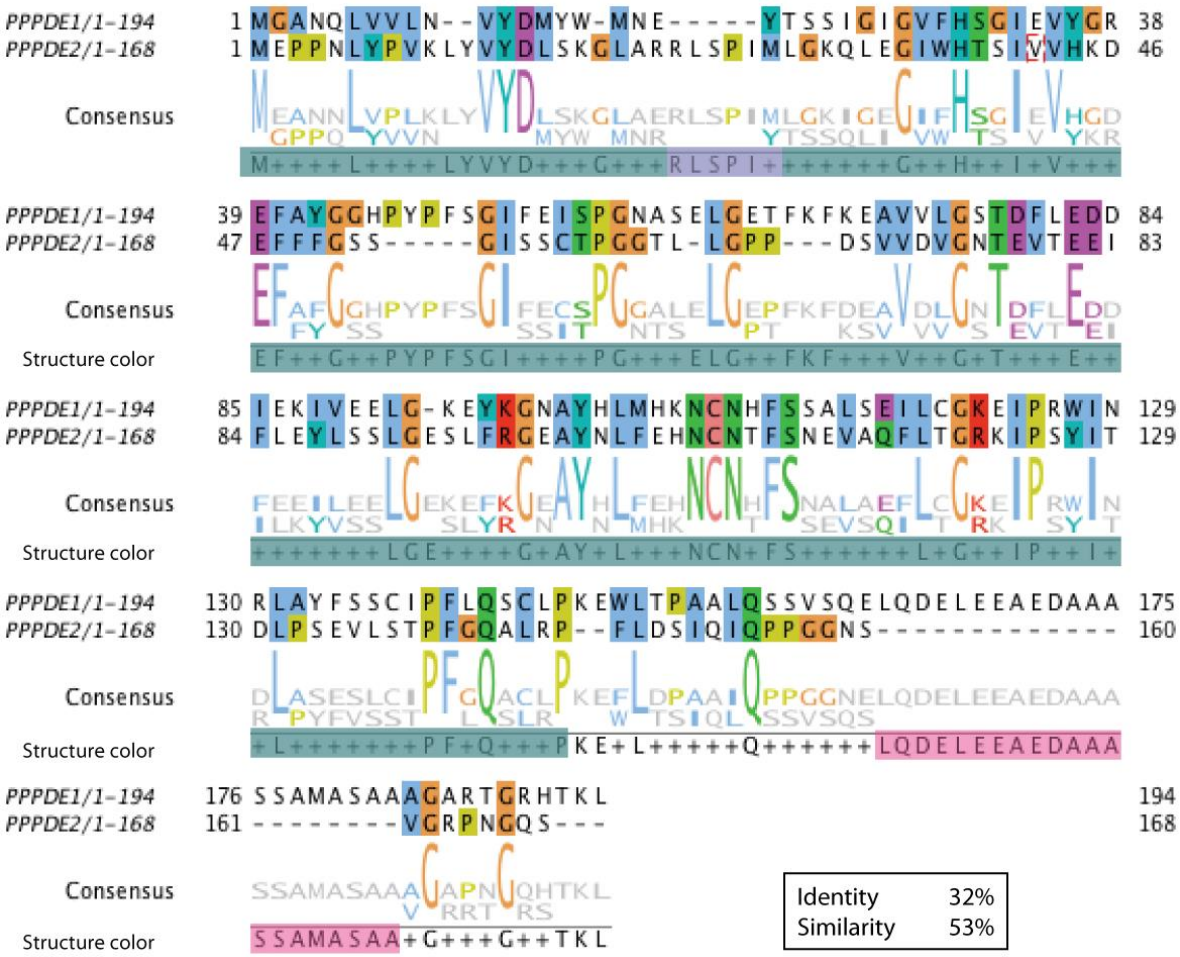

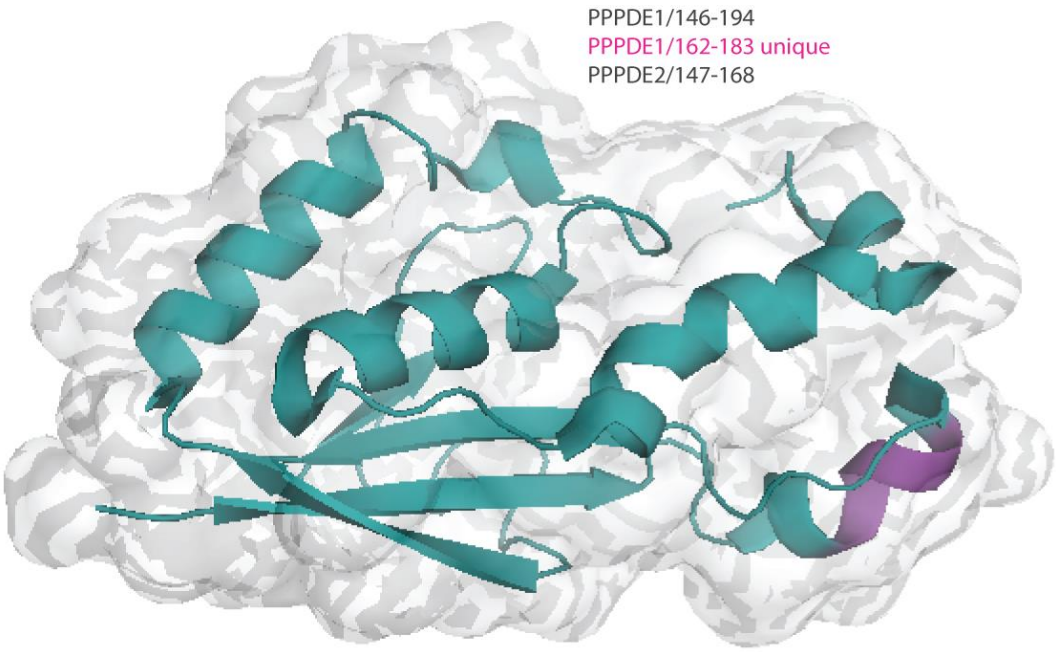

Fig. 2. Sequence alignment and quaternary structure of mouse PPPDE2 compared to PPPDE1. Amino acid sequences of murine PPPDE1 (NP_077244.1) and PPPDE2 (NP_598856.1) aligned using Jalview (version 2.10.1, Waterhouse et al., 2009) with default settings for Clustal Omega and Clustal X color code. The schematic representation of the quaternary structure of mouse PPPDE2 (Protein Data Bank, PDB 3ebq) exhibits the PPPDE2-specific insertion within the first N-terminal helix in purple and the remaining X-ray-determined structure in green. The consensus sequences corresponding to the structural features are represented in the same colors. C-termini of both proteins that are not displayed in the structure are annotated. A unique serine-rich stretch in PPPDE1 is highlighted in pink.

PPPDE1, or DeSI2, has been reported to localize in the cytoplasm, particularly concentrated in the perinuclear region, in human embryonic kidney 293 (HEK) cells (Yan et al., 2010; Deng et al., 2010; Shin et al., 2012). Two other studies in pig kidney epithelial cells (Mo et al., 2008) and in human HeLa cells (He et al., 2013) suggested that PPPDE1 is localized to the Golgi apparatus.

SUMOylation processes typically occur in the nuclear compartment. All isoforms of the previously known class of human SUMO proteases, the sentrin-specific proteases (SENP), as well as the SUMO E1, E2 and E3 conjugating enzymes, are located in the nucleus (Gong et al., 2000). Therefore, the fact that PPPDE1 could be a de-

SUMOylating isopeptidase with cytoplasmic activity raises a novel and intriguing possibility, as this type of post-translational modification is currently known to take place exclusively in the nucleus.

The claim that PPPDE1 localizes to the Golgi, however, has so far only been based on similarity of expression patterns between a PPPDE1 antibody signal and a Golgi tracker, and did not take into consideration other organelles from the endomembrane system that typically display a perinuclear organization.

The endomembrane system

Protein and lipid molecules are often not produced or modified at the site where they serve function. Therefore, specific trafficking of these molecules to their correct destination occurs via a system of internal membranous compartments, known as the endomembrane system (Morré & Mollenhauer, 1974; Harris, 1986). It consists of sequential intracellular membrane structures involved in the production, processing, packaging, transport, degradation, endocytosis and secretion of proteins and lipids (Fig. 3).

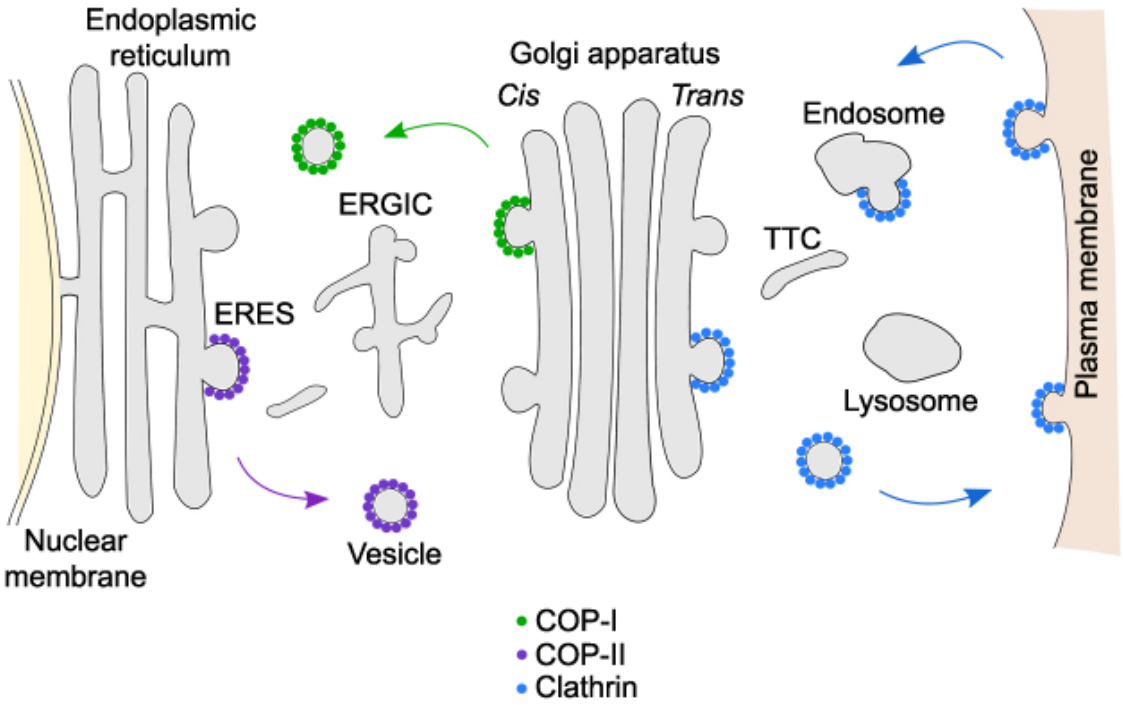

Fig. 3. Schematic representation of the components of the endomembrane system in mammalian cells. Intracellular trafficking of vesicular and tubular carriers

transporting protein and lipid cargo between organelle membranes. The contour lines represent phospholipid bilayers. ERES: endoplasmic reticulum exit site; ERGIC: endoplasmic reticulum-Golgi intermediate compartment; TTC: tubular transport carrier; COP: coat/coatomer protein. Based on Bonifacino & Glick, 2004.

In eukaryotes, the endomembrane system is comprised of the nuclear membrane, the endoplasmic reticulum (ER), the Golgi apparatus, lysosomes, endosomes, the plasma membrane and the vesicles that traffic between these organelles (Palade, 1975; Bonifacino & Glick, 2004). Mammalian cells contain, in addition, an ER-Golgi intermediate compartment (ERGIC), also referred to as vesicular tubular cluster (VTC), a relay station mediating trafficking and protein sorting between the ER and Golgi (Schweizer et al., 1988; Hauri & Schweizer, 1992; Appenzeller-Herzog & Hauri, 2006).

The outer nuclear membrane is continuous with the membranes of the endoplasmic reticulum (ER), the organelle responsible for the ribosomal synthesis and modification of lipids and proteins (English & Voeltz, 2013). Proteins are packaged into vesicles that bud off from ER exit sites (ERES) and are transported either directly to the Golgi apparatus or first to the ER-Golgi intermediate compartment (ERGIC), which facilitates the sorting of cargo and retrieves ER resident proteins back to this organelle (Martínez-Menárguez et al., 1999). The Golgi apparatus or complex is composed by cisternae or stacks, classified into two main networks: cis-Golgi, facing the ER, and trans-Golgi, facing the plasma membrane. In the Golgi, proteins and lipids undergo further sorting, modification, tagging and packaging into vesicles (Bentivoglio, 1999; Alberts et al., 2002).

Molecules destined for degradation are directed to lysosomes, where they are hydrolyzed by enzymatic activity (Mellman, 1989). Extracellular molecules are internalized via endocytosis by vesicles budding from the plasma membrane, which fuse to endosomes, usually classified as early or late, depending on the post-internalization stage. Contents are sorted in the endosome either for transport to lysosomes or for recycling back to the plasma membrane (Helenius et al., 1983; Mellman, 1996).

Transport vesicles containing cargo in the lumen bud from a donor membrane and later fuse to an acceptor membrane, delivering their cargo. These vesicles move through the cell with specific directionality by coupling to cytoskeletal proteins. Vesicles are carried along microtubules by the motor proteins kinesin and dynein, in anterograde or retrograde direction, respectively, fueled by ATP hydrolysis (Lodish et al., 2000).

Cytoplasmic coat proteins help select cargo molecules, shape the cargo-containing budding vesicles and encircle them during intracellular transport. Two sets of protein complexes, or coatomers, envelop vesicles transported between the ER and the cis-Golgi: COP-I in retrograde direction (Golgi-ER) and COP-II in anterograde direction (ER-Golgi). Clathrin and its adaptor proteins are responsible for coating vesicles between the trans-Golgi, lysosomes, endosomes and the plasma membrane (Aridor et al., 1995; Cooper, 2000; Lee et al., 2004).

In addition to the classical small, round and coated vesicles, a second structural type of membrane container mediates transport of proteins between organelles of the endomembrane system. These are larger, pleomorphic or tubular-shaped membranous structures facilitating both early-stage protein transport, between the ER, ERGIC and Golgi, and late-stage, post-Golgi transport (Bannykh et al., 1996; Hirschberg et al., 1998; Polishchuk et al., 2000; Blum et al., 2000).

These structures have received different names in the literature, such as large pleomorphic carriers or LPCs (Luini et al., 2005), tubular transport intermediates or TTIs (Simpson et al., 2006), and tubular transport carriers or TTCs (Polishchuck et al., 2009). Like vesicular carriers, transport of TTCs is assisted by the cytoskeleton (Toomre et al., 1999; Polishchuck et al., 2009). But unlike the classical coated structures, TTCs can fuse to the acceptor membrane without having detached from the donor membrane, thereby creating a tunnel between two compartments (Trucco et al., 2004; Marsh et al., 2004; Massol et al., 2005).

Potential implications in neurons

PTMs can have a major impact on cell cycle and response to stress. Changes in cellular levels of ubiquitin- or SUMO-conjugated proteins can be expected to strongly influence cell fate and survival (Kirkin & Dikic, 2007; Gilberto & Peter, 2017). Elimination of

damaged proteins through the ubiquitin signaling pathway is imperative for a proper response to different types of cellular stressors (Pickart, 1999; Flick & Kaiser, 2012). In addition, conjugation and expression of SUMO increase significantly following various harmful conditions, such as hypoxia, temperature change, and osmotic or nutrient stress (Lee et al., 2009; Guo & Henley, 2014). Therefore, ubiquitination and SUMOylation of particular proteins seem to act as regulatory mechanisms of endogenous protection and maintenance of cellular integrity after stress (Meller et al., 2008; Datwyler et al., 2011).

Despite its ubiquitous expression and conservation, very little is known about PPPDE1. There has been scarce evidence that this protein may have pro-apoptotic, de-SUMOylating or de-ubiquitinating activity, all of which is still unclear. Its properties and functions have not yet been correlated with its localization and remain to be validated particularly in neurons. Only one study so far has reported data of PPPDE1 in the nervous system (Cai et al., 2010).

Neurons are mostly post-mitotic cells, meaning that they generally do not divide and therefore must rely on fast and efficient endogenous responses to stress and adverse conditions (Herrup & Yang, 2007). Therefore, if PPPDE1 is in fact responsible for modulating common post-translational modifications or apoptosis in neurons, it could exert an impact on neuronal survival.

Project aims

The general goal of the present work was to perform a thorough characterization of PPPDE1 in mouse neurons, by investigating different aspects of this protein using varied methodologies. More specifically, this project aimed to:

- identify the intracellular localization of PPPDE1, taking into consideration different possibly related cellular compartments and organelles;
- investigate whether PPPDE1 might have an effect on either ubiquitin or SUMO processes;
- identify the binding partners and target proteins of PPPDE1 to better understand which molecules it interacts with and which cellular pathways it is involved in;

- analyze the effects of silencing and overexpressing PPPDE1 *in vitro*, investigating whether this modulation affects neuronal biology and survival;
- relate the effects observed for PPPDE1 to its potential cellular functions.

Materials and Methods

Primary culture of mouse cortical neurons

Primary cortical neurons were derived from mouse C57BL/6 embryos and cultured in neurobasal medium with B27 supplement, in sterile conditions at 37°C and 5% CO_2, as described previously (Harms et al., 2007). Brain hemispheres of mouse embryos on embryonic day 15 (E15) were dissected for removal of the meninges and midbrain and isolation of the cerebral cortex. The tissue was washed in phosphate-buffered saline (PBS, Gibco, Life Technologies), incubated in 0.05% trypsin/EDTA (Biochrom, Berlin, Germany) for 15 minutes at 37°C, washed twice more in PBS and carefully resuspended in N-Med medium (MEM with 10% fetal bovine serum, 100 U/ml penicillin-streptomycin, 20 µM L-glutamine, 10 mM HEPES, 3.5 µg/ml insulin, and 44 mM glucose) using a glass pipette with reduced tip diameter to dissociate the cells. The preparation was centrifuged for 2 minutes at 1200 rpm and 4°C and the pellet resuspended in neuronal starter medium (neurobasal medium with B27 supplement, 100 U/ml penicillin-streptomycin, 4 µM L-glutamine and 25 µM glutamate). Concentration of cell suspension was adjusted to 3.25 million cells/ml. Cells were seeded in poly-L-lysine (PLL)-coated plates (Biochrom, Berlin, Germany) in the following amounts per well: 1.3 x 10^6 cells for 6-well plates (Falcon, Corning, USA), 3.25 x 10^5 cells for 24-well plates (Falcon, Corning, USA) and 2.3 x 10^5 cells for µ-Slide 8-well plates (Ibidi, Martinsried, Germany).

Cloning of PPPDE1 overexpression and RNA interference vectors

An overview of the cloned constructs is displayed below (Fig. 4). To induce neuronal expression of enhanced green fluorescent protein (EGFP)-labeled PPPDE1 protein, an N-terminal fusion of PPPDE1 to EGFP was constructed. AgeI and EcoRI sites were introduced at the C-terminus of EGFP in the pFSy(1.1)GW plasmid (Addgene #27232), a gift from Pavel Osten (Dittgen et al., 2004). This transfer vector drives exogenous genes via a neuronal-specific synapsin promoter. The stop codon of EGFP was eliminated and a Gly-Gly-Ser-Gly-Gly spacer introduced by polymerase chain reaction (PCR). pEGFP-N1 vector (Clontech, USA) was used as a template for a 769 base pair

(bp)-long PCR product using the following primers: 5'- GCA TAG GAT CCA CCA TGG TGA GCA AGG G-3' and 5'-GC TAT CAA TTG GAA TTC ACC GGT ACC ACC GGA CCC TCC CTT GTA CAG CTC GTC CAT GC-3' (the spacer is underlined). The PCR product was restricted with BamHI and MfeI and the pFSy(1.1)GW lentiviral transfer vector with BamHI and EcoRI (compatible to MfeI). The ligated vector was linearized using EcoRI and AgeI and a murine PPPDE1 gene synthesis of the coding sequence based on the NP_077244.1 amino acid sequence optimized for mammalian codon usage (Eurofins, Ebersberg, Germany) was inserted using AgeI and EcoRI restriction sites. The pFSy(1.1)GW plasmid was used as a control vector for expression of EGFP alone. Carbenicillin antibiotic was used to select the ampicillin-resistant clones.

To introduce PPPDE1 knockdown, a short hairpin RNA (shRNA) molecule was constructed to silence gene expression of PPPDE1 by degradation or translational repression of its target complementary messenger RNA (mRNA) coding for PPPDE1. MicroRNA 155-embedded shRNAs were expressed from an RNA polymerase II synapsin promoter based on a modified version of the pFSy(1.1)GW plasmid with EGFP harboring a stop codon followed by BlpI and XhoI restriction sites. The shRNAs were designed using BLOCK-iT RNAi Designer (Invitrogen, USA) with the accession number NM_024282 coding for murine PPPDE1 (DeSI2) and blasted against *Mus musculus* for control of off-target effects. Annealing and ligation of shRNAs targeting PPPDE1 at nucleotide positions 508 or 850 in the open reading frame (Eurofins, Ebersberg, Germany) were performed using sticky ends in a BbsI pre-digested vector (pcDNA6.2-GW/EmGFP with spectinomycin as a selection marker) following manufacturer's instructions (BLOCK-iT Pol II miR RNAi expression vector kit, Invitrogen). The ligated shRNAs were subcloned via BlpI and XhoI (204 bp-long fragments) into the lentiviral transfer vector for equal co-expression of the shRNA and EGFP (reporter protein). A LacZ non-targeting shRNA served as control. Ampicillin-resistant clones of the final constructs were selected using carbenicillin.

The pFSy(1.1)GW plasmid (Addgene #27232) with a sequence for EGFP was modified to express mRuby2 as a control for fusion protein expression of murine RAB1A, RAB2A or SAR1A by lentiviral gene delivery. pTALYM4SpMi-05 plasmid (Addgene #47880), a gift from Maria-Elena Torres-Padilla (Miyanari et al., 2013), served as template for a PCR amplification of mRuby2 using the following primers: 5'-GCA TAG GAT CCT AAC CAT GGT GTC TAA GGG CGA AG -3' and 5'-GCT AAC CGG TAC CAC CGG ACC

CTC CCT TGT ACA GCT CGT CCA TCC C -3' (Gly-Gly-Ser-Gly-Gly spacer is underlined), resulting in a 738 bp-long product. AgeI and EcoRI were used for unidirectional sticky-end insertion of the mRuby2 PCR product into the pFSy(1.1)GW plasmid backbone after removal of EGFP.

EGFP was replaced by mRuby2 in the lentiviral transfer vector for fusion protein expression of PPPDE1 using the same PCR product and BamHI and AgeI restriction digests prior to ligation. The resulting vector was further used to subclone the N-terminal fusion proteins of murine RAB1A, RAB2A or SAR1A to mRuby2. This was accomplished by inserting the coding sequence based on NM_008996 for mRab1a (615 bp), NM_021518.3 for mRab2a (645 bp) or NM_009120.3 for mSar1a (603 bp) optimized for mammalian codon usage and produced by gene synthesis (Eurofins, Ebersberg, Germany). These synthetic genes harboring the coding sequences were generated in pEX-128 plasmid, selected by ampicillin resistance using the carbenicillin analogue and isolated for ligation using AgeI and EcoRI restriction sites.

In all vectors (overexpression, knockdown and controls), a Woodchuck Hepatitis Virus (WHP) Post-transcriptional Regulatory Element (WPRE) sequence was included to enhance gene expression.

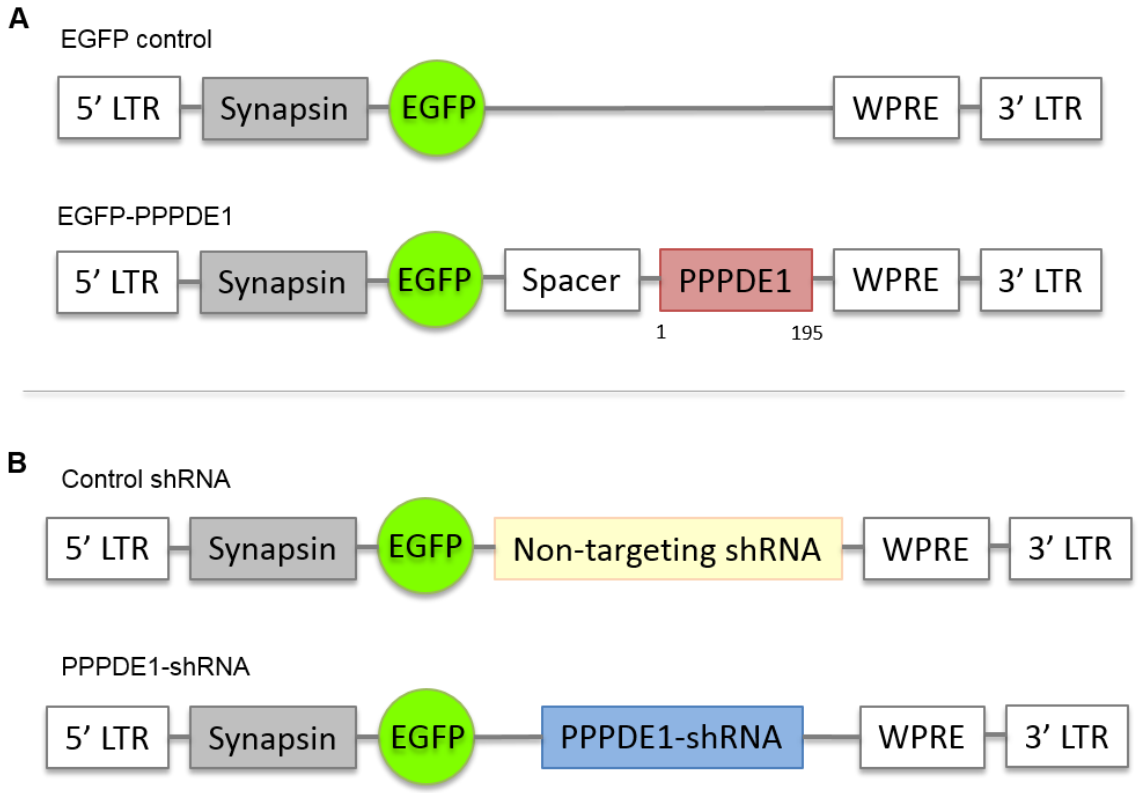

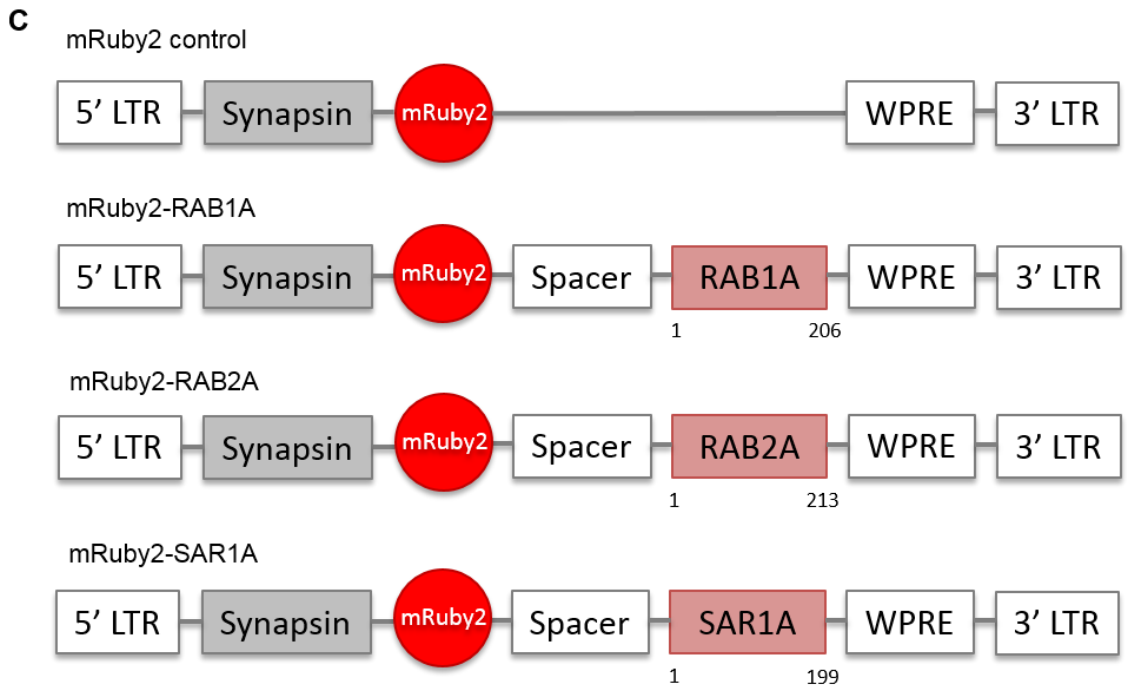

Fig. 4. Schematic overview of the overexpression and knockdown vectors used and their respective non-targeting controls. (A) EGFP control and EGFP-PPPDE1. **(B)** Control shRNA and PPPDE1-shRNA. **(C)** mRuby2 control, mRuby2-RAB1A, mRuby2-RAB2A and mRuby2-SAR1A. All vectors were driven by a neuronal-specific synapsin promoter and hosted a sequence coding for WPRE to increase gene expression.

Generation and titration of lentiviral particles

After sequence verification of the constructed vectors, third-generation lentiviral particles were generated by co-transfecting the plasmids with pMD2.G (Addgene #12259) and psPAX2 (Addgene #12260) packaging vectors into human embryonic kidney (HEK) 293TN cells (BioCat, Heidelberg, Germany) using XtremeGene HP DNA transfection reagent (Roche, Mannheim, Germany) in OptiMEM medium (Gibco, Life Technologies, Carlsbad, USA). Lentiviral supernatants were collected 48 and 72 hours after transfection, centrifuged to discard cell debris (4000 rpm, 10 minutes, 4°C) and filtered with a 0.45 µm pore size Millex filter (Millipore, Darmstadt, Germany). Supernatants were then concentrated by 72-hour precipitation with polyethylene glycol (PEG) 20000 (Carl Roth, Karlsruhe, Germany) at 4°C, followed by a 30-minute

centrifugation at 4000 rpm and 4°C, resuspension of the pellet in PBS and aliquoted storage at -80°C.

Cultured neurons were transduced on days in vitro (DIV) 2. Viral titers and transduction efficiency were determined by analyzing the fluorescence of the EGFP or mRuby2 reporters after 10-fold serial dilutions (undiluted, 1:10, 1:100 and 1:1000), as well as confirmed by immunoblot. Transmission and green fluorescence images of the dilution fold that reached between 1-30% EGFP- or mRuby2-positive cells were acquired on DIV 7. The number of EGFP- or mRuby2-positive cells, as well as the total number of live cells per image were measured manually in at least 3 images per condition using the Adobe Photoshop counting tool. Viral titers (transducing units, TU, per ml) were calculated as follows:

Titer (TU/ml) = [(average ratio x amount of cells) / volume of inoculum] x dilution fold

The average frequency ratio (EGFP- or mRuby2-positive cells divided by the total amount of cells) in the different images was calculated for each condition, then multiplied by the amount of cells per well used for transduction (3.25×10^5 for a 24-well). The value was divided by the volume of viral suspension that was added to the well (volume of inoculum) in milliliters (2 µl, so 0.002 ml), and the result multiplied by the dilution fold.

Lentiviral particles were delivered to cultured neurons in concentrations that reached at least 90% transduction efficiency, meaning a multiplicity of infection (MOI) of 6 TU/cell for the overexpression vectors and their controls, and of 90 TU/cell for the knockdown vector and its control.

Live cell imaging

Microscopic images were acquired on DIV 8. Neurons were maintained under culturing conditions at 37°C and 5% CO_2 during imaging. Images in figures 6-8, 10-12 and 16 were acquired using a confocal microscope (Nikon) with uniform spinning disk illumination (Andor Borealis) and Andor Revolution SD System (CSU-X) equipped with an EMCCD Camera (iXon3 DU-888 Ultra), a 60x Plan APO oil immersion objective (Nikon) and NIS-Elements Advanced Research software (Nikon, version 5.02). In

figures 6 and 10A, 0.5 µM SiR-DNA dye (Spirochrome, Switzerland; Lukinavicius et al., 2015) was added to the live neurons for visualization of the nucleus. In figure 11, 0.5 µM SiR-tubulin (Spirochrome, Switzerland), which is based on the microtubule-binding drug docetaxel, was added for visualization of microtubules. Images were taken with lasers exciting at 405 nm (>15 mW) to detect the nuclear marker 4',6-diamidino-2-phenylindole (DAPI), at 488 nm (>8 mW) to detect EGFP, at 561 nm (>15 mW) to detect SiR dyes or Alexa Fluor 546 and at 647 nm (>15 mW) to detect Alexa Fluor 647.

Immunoblot analysis

Neurons were harvested in RIPA buffer containing a cocktail of protease and phosphatase inhibitors (Thermo Fisher Scientific). Whole cell extracts were fractionated in 15% sodium dodecyl sulfate (SDS)-polyacrylamide gel electrophoresis and transferred to 0.45 µm pore size polyvinylidene fluoride (PVDF) membranes (Carl Roth, Karlsruhe, Germany). After 1 hour blocking with 5% milk, membranes were probed with rabbit anti-PPPDE1 (Proteintech 20517-1-AP, 1:1000), mouse anti-GAPDH (anti-glyceraldehyde 3-phosphate dehydrogenase, Millipore MAB374, 1:5000) or mouse anti-GFP (Santa Cruz sc-9996, 1:1000) primary antibodies overnight at 4°C. Incubation with either anti-mouse (VWR, NXA931) or anti-rabbit (Thermo Fisher Scientific, NA934) horseradish peroxidase-conjugated secondary antibodies (1:2500) for 1 hour at room temperature followed. Membranes were washed in Tris-buffered saline with Tween20 (TBS-T) buffer after each antibody incubation. A chemiluminescence system (GE Healthcare) was used to detect the immunoblot signal. Before being probed with the next primary antibody, membranes were incubated in 30% hydrogen peroxide solution for 30 minutes at room temperature, washed and blocked in 5% milk for 1 hour. Three independent replicates of the experiment were performed. The intensity signal of immunoblots was quantified using the Fiji software (Schindelin et al., 2012). PPPDE1 signal was normalized to the GAPDH signal (loading control) and to the total intensity of PPPDE1 signal in the same blot. Statistical significance between groups was calculated by unpaired t-test with Welch’s correction and plotted into graphs using GraphPad Prism software (version 6.0).

Immunocytochemistry

Cultured neurons were fixed on DIV 8 with methanol-free 4% formaldehyde (Thermo Fisher Scientific) for 5 minutes, permeabilized with 0.25% Triton X-100 for 10 minutes and blocked with 0.2% normal donkey serum for 30 minutes, all at room temperature. Cells were incubated with primary antibodies (see specifications and dilutions in the table below) overnight at 4°C. Most antibodies against markers of the endomembrane system were kindly provided by Prof. Dr. Michael Krauss. After 1 hour incubation at room temperature with donkey Alexa Fluor 546 or 647 secondary antibodies (Invitrogen, 0.8 µg/ml), cells were incubated with DAPI solution (Thermo Fisher Scientific, 1 µg/ml) for 10 minutes at room temperature to stain the nuclei.

Antibody target	**Manufacturer**	**Catalog number**	**Source species**	**Dilution**
Adaptin γ	BD Biosciences	610386	mouse	1:200
Clathrin heavy chain	Thermo Fisher Scientific	MA1-065	mouse	1:200
GGA1	Abnova	H00026088-B01	mouse	1:100
Golgin-97	Invitrogen	A-21270	mouse	1:50
EEA1	Cell Signaling	2411	rabbit	1:200
Transferrin receptor	Zymed	13-6800, clone H68.4	mouse	1:200
GM130	Abcam	610822	rabbit	1:200
ERGIC-53	Santa Cruz	sc-398893	mouse	1:100
COP-I	Gift from F.T. Wieland (Faulstich et al., 1996)	---	mouse	1:50
COP-II (Sec23)	Thermo Fisher Scientific	PA1-069A	rabbit	1:200
MAP2	Sigma-Aldrich	M9942	mouse	1:200
GFP	Chromotek 3H9	029762	rat	1:200

Table 1. Primary antibodies used and their specifications. Antibody targets, manufacturers, catalog numbers, source species and employed dilutions are displayed.

Colocalization analysis

The nuclear plus perinuclear areas of EGFP-positive cells were selected as regions of interest (ROIs) using the Icy software (de Chaumont et al., 2012). Pearson's correlation coefficients of the co-localization between the EGFP signal and the fluorescent signal from a given antibody or mRuby2 construct were quantified using Icy's Colocalization Studio tool and selecting the correlation (pixel-based) method in the tool settings (Lagache et al., 2015). At least 8 different cells per staining of three independent replicates of the experiment were analyzed.

Time lapse imaging after brefeldin A treatment

Cultured neurons were transduced with EGFP-PPPDE1 on DIV 2. On DIV 9, live cells were imaged under culturing conditions (37°C and 5% CO_2). Next, 2 µg/ml of either brefeldin A (BFA, Sigma-Aldrich) or the vehicle dimethyl sulfoxide (DMSO) were added to the cells. Immediately after, time lapse images of the same frame were acquired every 1 minute for a duration of 30 minutes. Neurons were fixed with 4% formaldehyde 1 hour after BFA treatment and immunostained for GM130, ERGIC-53 and MAP2, as specified in the 'Immunocytochemistry' section. Using the Fiji software (Schindelin et al., 2012), maximum intensity images of Z-stack planes were generated. Next, the EGFP-positive perinuclear areas of different cells were selected as regions of interest (ROIs) and the mean EGFP fluorescence intensity of ROIs over time was quantified. At least 14 different cells of four independent replicates of the experiment were analyzed. Values were corrected to the photobleaching rate that naturally occurred with time lapse imaging and compared between BFA and DMSO-treated groups for each minute of the time points using a two-way ANOVA with Sidak's multiple comparisons test. Graphs and statistical analysis were done using GraphPad Prism software (version 6.0).

Immunocytochemistry for Structured Illumination Microscopy (SIM) imaging

Immunostaining was performed as described above, with the following modifications: cells were seeded on PLL-coated glass precision cover slips with 18 mm diameter (Carl Roth, Karlsruhe, Germany) in 12-well plates (Falcon, Corning, USA) at 1.3 million cells

per well. Neurons were transduced with EGFP-PPPDE1 on DIV 2 and fixed on DIV 8 with methanol-free 4% formaldehyde (Thermo Fisher Scientific) for 5 minutes at room temperature. In order to amplify the EGFP fluorescent signal from PPPDE1 for high-resolution SIM, EGFP-PPPDE1-transduced neurons were immunostained using a rat anti-GFP primary antibody (Chromotek 3H9, 1:200), concomitantly with rabbit anti-GM130 (Abcam, 1:200) and mouse anti-ERGIC-53 (Santa Cruz, 1:100). Cells were then incubated with Alexa Fluor anti-rat 488, anti-rabbit 546 and anti-mouse 647 secondary antibodies (Invitrogen, 0.8 µg/ml) for 1 hour at room temperature, counter-stained with DAPI (Thermo Fisher Scientific, 1 µg/ml) and post-fixed with methanol-free 4% formaldehyde (Thermo Fisher Scientific) for 5 minutes at room temperature. Cover slips were mounted using Vectashield antifade mounting medium (Vector Laboratories, USA) before imaging.

SIM imaging, 3D rendering and nearest neighbor analysis

Three-dimensional (3D) 3-color SIM images of three independent experiments were acquired using 405 nm, 488 nm, 568 nm and 680 nm laser lines, standard filter sets and 125 nm Z-sectioning of the OMX V4 Blaze system (GE Healthcare) as previously described (Gimber et al., 2015). 100 nm fluorescent beads (Tetraspeck, T7284, Thermo Fisher Scientific) were used for registration of the detection channels, achieving less than 40 nm registration error for all four channels. 3D rendering, as well as image and movie exportations, were performed using Arivis Vision 4D and ImageJ softwares (Schneider et al., 2012). Objects were identified in Arivis with a histogram-based threshold procedure (Otsu's method, Trier & Jain, 1995). The nearest neighbor (NN) distribution was calculated from boundaries of rendered 3D objects using a custom-written Python script (Dr. Niclas Gimber, Charité). The negative control for co-localization was generated by performing a 1 µm toroidal shift of one channel against the other along the X-axis. The difference between NN traces from shifted and original images was tested against zero by multiple one sample t-tests and Bonferroni correction for multiple tests.

Fluorescence Recovery After Photobleaching (FRAP)

Cultured neurons were transduced with either EGFP-PPPDE1 or EGFP control on DIV 2 and used for FRAP experiments on DIV 8. Neurons were maintained in culturing conditions (37°C and 5% CO_2) during the experiments. Images were acquired using a spinning-disc confocal microscope (Nikon CSU-X) with a 60x Plan APO oil immersion objective (Nikon). Regions of interest (ROIs) to be bleached were adjusted to cover the whole area containing high intensity EGFP signal in the perinuclear region, but not the neuronal projections. Photobleaching was reached by applying a 488 nm laser (100% power) to the ROIs for 10 seconds. Immediately after photobleaching, images of the EGFP fluorescent signal were acquired every 300 milliseconds for 10 minutes. EGFP fluorescence recovery over time of circular selections with 0.7 µm diameter was measured using the NIS-Elements Advanced Research software (Nikon, version 5.02). The circular regions of interest inside the photobleached area were selected based on fluorescence intensity, to distinguish the EGFP signal of vesicular structures (high fluorescence intensity) from the diffused EGFP signal (low intensity), both present in the photobleached perinuclear region. Background was subtracted from measurements and values were corrected to the natural photobleaching rate over time of reference cells which were not targeted by the photobleaching laser. At least 10 cells were quantified per condition in each of the three independent experiments. Statistical significance between the two groups of measured ROIs was calculated for each time point by two-way ANOVA multiple comparisons. Graphs and statistical analysis were done using GraphPad Prism software (version 6.0).

Propidium iodide incorporation

Neurons were transduced with either EGFP-PPPDE1, EGFP control, PPPDE1-shRNA or control shRNA lentiviral constructs on DIV2. To assess cell viability, transduced neurons were stained on DIV 8 with 4 µM propidium iodide (PI), a DNA marker of dead cells, allowing to distinguish them from healthy, PI-negative cells. Widefield and fluorescence images in figure 13 were acquired using an inverted IX81 microscope (Olympus) equipped with an MT10 illumination system, CCD camera (Hamamatsu, Ammersee, Germany), a 20x LCACHN NA 0.4 objective (Olympus, Hamburg, Germany) and Xcellence Software (Olympus, Hamburg, Germany). The following filter

settings were used: for EGFP, excitation 470/20 nm, emission 520/15 nm; for PI, excitation 504/36 nm, emission 550/18 nm. Twelve images were acquired per condition in every of the four independent experiments. PI particles were counted using the Spot Detector tool of the Icy software (de Chaumont et al., 2012) with the following settings: detection of bright spots over dark background, size filtering and scale 4 object size (~13 pixels). Cell death was calculated as the number of PI-positive particles, normalized to the total amount of cells (EGFP-positive plus PI-positive cells). Statistical significance between groups was calculated using the Mann-Whitney test in GraphPad Prism software (version 6.0).

Immunoprecipitation for proteomics analysis

Neurons cultured in 6-well plates (Falcon, Corning, USA) at a rate of 1.3 x 10^6 cells per well were transduced with either EGFP-PPPDE1 or EGFP control on DIV 2. On DIV 9, cells were treated with either 2 µg/ml brefeldin A (BFA, Sigma-Aldrich) or DMSO as control for 1 hour at 37°C, then washed 3 times with 1x balanced salt solution (BSS) containing 5.5 mM glucose, 10 mM 4-(2-hydroxyethyl)-1-piperazineethanesulfonic acid (HEPES) buffer, 20 mM sodium hydrogen carbonate, 50 µM glycine and 2 mM calcium chloride. Next, cells in the glutamate group were treated with 50 µM glutamate solution for 1 hour at 37°C. Whole cell extracts were collected in RIPA buffer containing the following inhibitors: 10 mM 4-(2-aminoethyl) benzenesulfonyl fluoride hydrochloride (AEBSF), 1 mM sodium orthovanadate, 1 mM ethylenediaminetetraacetic acid (EDTA), 1 mM dithiothreitol (DTT), 1 mM sodium fluoride (NaF) and 10 mM N-ethylmaleimide (NEM). Whole cell extracts were sonicated 3 times of 5 seconds each with a 10% amplitude and cell debris was removed by centrifugation (14000 rpm, 10 minutes at 4°C). Samples were incubated with equilibrated GFP-Trap magnetic beads (ChromoTek, Martinsried, Germany) for 1 hour at 4°C for immunoprecipitation. GFP-Trap beads were washed twice with 50 mM Tris hydrochloride buffer (Tris-HCl) pH 8.0, first containing 250 mM sodium chloride and subsequently 150 mM, frozen in liquid nitrogen and stored at -80°C until analyzed. Three independent replicates of the experiment were performed.

Preparation of samples for mass spectrometry (MS)

After immunoprecipitation, further preparation and MS analysis of the samples, as well as statistical analysis, was conducted by Dr. Marieluise Kirchner (MDC). Trap beads were resuspended in 50 µl urea buffer (6 M urea, 2 M thiourea, 10 mM HEPES, pH 8.0), reduced for 30 minutes at room temperature in 12 mM dithiothreitol solution, followed by alkylation by 40 mM chloroacetamide for 20 minutes in the dark at room temperature. The samples were first digested using 1 µg endopeptidase LysC (Wako, Osaka, Japan) for 4 hours. The samples were diluted by adding 100 µl of 50 mM ammonium bicarbonate (pH 8.5), and finally digested with 1 µg trypsin (Promega) for 16 hours. The digestion was stopped by acidifying each sample to pH < 2.5 by adding 10% trifluoroacetic acid solution. The peptides were extracted and desalted using StageTip protocol (Rappsilber et al., 2003).

Liquid chromatography mass spectrometry (LC-MS) / MS analyses

Peptides were eluted using Buffer B (80% Acetonitrile and 0.1% formic acid) and organic solvent was evaporated using a speedvac (Eppendorf). Samples were diluted in Buffer A (5% acetonitrile and 0.1% formic acid). Peptides were separated on a reversed-phase column (20 cm fritless silica microcolumns with an inner diameter of 75 µm, packed with ReproSil-Pur C18-AQ 3 µm resin (Dr. Maisch GmbH) using a 90 minute gradient with a 250 nl/min flow rate of increasing Buffer B concentration (from 2% to 60%) on a High Performance Liquid Chromatography (HPLC) system (Thermo Fisher Scientific). Peptides were ionized using an electrospray ionization (ESI) source (Thermo Fisher Scientific) and analyzed on an Orbitrap Fusion (Q-OT-qIT, Thermo Fisher Scientific). The mass spectrometer was run in data-dependent mode selecting the top 10 most intense ions in the MS full scans, selecting ions from 350 to 2000 m/z, using 60K resolution with a 4×10^5 ion count target and 50 ms injection time. Tandem MS was performed by isolation at 0.7 m/z with the quadrupole, higher-energy collisional dissociation (HCD) fragmentation with normalized collision energy of 28 and resolution of 15K. The MS^2 ion count target was set to 5×10^4 with a maximum injection time of 250 ms. Only precursors with charge state 2-7 were sampled for MS^2. The dynamic exclusion duration was set to 30 seconds with a 10 ppm tolerance around the selected precursor and its isotopes.

MS data analyses

Data were analyzed using MaxQuant software package (version 1.5.6.5). The internal Andromeda search engine was used to search MS^2 spectra against a decoy mouse UniProt database (MOUSE.2016-08) containing forward and reverse sequences. The search included variable modifications of methionine oxidation and N-terminal acetylation, deamidation (N and Q), di-Glycine on lysine and fixed modification of carbamidomethyl cysteine. Minimal peptide length was set to seven amino acids and a maximum of 3 missed cleavages was allowed. The FDR (false discovery rate) was set to 1% for peptide and protein identifications. Unique and razor peptides were considered for quantification. Retention times were recalibrated based on the built-in nonlinear time-rescaling algorithm. MS^2 identifications were transferred between runs with the “match between runs” option, in which the maximal retention time window was set to 0.7 minutes. The resulting text files were filtered to exclude reverse database hits, potential contaminants, and proteins only identified by site. Statistical data analysis was performed using Perseus software (version 1.5.2.4). Technical and biological replicates for each condition were defined as groups and intensity values were filtered for “minimum value of 3” per group. After log2 transformation, missing values were imputed with random noise simulating the detection limit of the mass spectrometer. Imputed values are taken from a log normal distribution with 0.25× the standard deviation of the measured, logarithmized values, down-shifted by 1.8 standard deviations. Differences in protein abundance between EGFP-PPPDE1 and EGFP control samples (untreated and BFA-treated) were calculated using two-sample Student's t-test. Proteins passing the significance cut-off ("+": p-value ≤ 0.05 and log2 t-test difference > 2; "++": permutation-based FDR, or false discovery rate: 5%) were considered specific PPPDE1 binders. Gene ontology (GO) term classification of the proteins significantly enriched by PPPDE1 was assigned using the STRING database version 10.5 (Szklarczyk et al., 2017). Information on the proteins’ functions and intracellular localizations were retrieved from the UniProt database (Chen et al., 2017).

Results

PPPDE1 localizes to tubular-shaped compartments in the perinuclear region of neurons

In order to investigate the localization and cellular functions of PPPDE1, we constructed a short hairpin RNA (shRNA) to silence its expression and an N-terminal fusion of PPPDE1 to an enhanced green fluorescent protein (EGFP) to visualize it. All constructs were driven by the neuronal-specific synapsin promoter, carried EGFP for microscopic visualization and were delivered to the neurons by lentivirus-mediated transduction.

We cloned two variants of PPPDE1-shRNA: one targeting the 508 nucleotide position of the open reading frame (ORF) and the other targeting the 805 ORF position, as well as two non-targeting control vectors: scrambled and LacZ. The #508 shRNA variant promoted proper knockdown of PPPDE1 expression, while the #850 variant did not (Fig. 5). Therefore, we selected the #508 variant for use in experiments and in the EGFP-PPPDE1 fusion construct. No difference was observed between the two controls and the LacZ type was chosen for use.

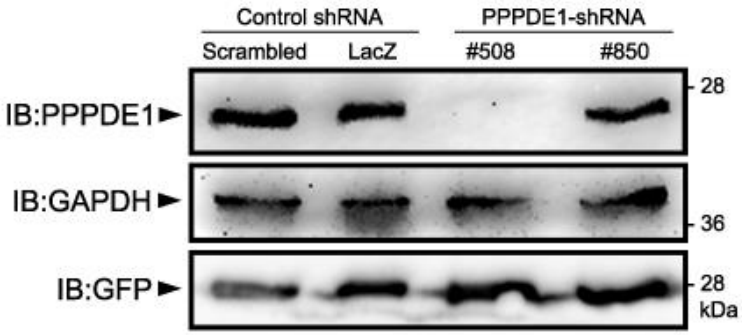

Fig. 5. Comparison between two variants of PPPDE1-shRNAs and of control shRNAs. Immunoblot (IB) analysis of PPPDE1, loading control GAPDH and expression control GFP in neurons expressing scrambled or LacZ control shRNAs, or PPPDE1-shRNAs targeting either the position 508 or 850 in the open reading frame (ORF) of PPPDE1.

Immunoblot analysis confirmed the knockdown and expression of PPPDE1 after transduction with the respective constructs (Fig. 6). RNA interference with the #508 variant resulted in a significantly decreased expression of the predicted ~21 kDa

PPPDE1 band compared to the non-targeting shRNA control (Fig. 6A, left). Neurons expressing the EGFP-PPPDE1 fusion exhibited significantly higher amounts of a ~55 kDa band, corresponding to PPPDE1 after fusion with EGFP, compared to its EGFP control (Fig. 6B, left).

We found that EGFP-PPPDE1 has a particular intracellular expression pattern in neurons, highly contrasting to its control. The fluorescent expression of the EGFP control vector is located homogeneously throughout both the cytoplasm and nucleus – the latter visualized using a DNA dye for live cells. EGFP-PPPDE1, on the other hand, is strongly excluded from the nucleus, mildly expressed throughout the cytoplasm and highly concentrated in tubular-shaped compartments in the perinuclear region of the neurons (Fig. 6B, right). PPPDE1 knockdown did not alter overall neuronal morphology, as no difference in EGFP expression pattern was observed between neurons transduced with PPPDE1-shRNA and its non-targeting control (Fig. 6A, right).

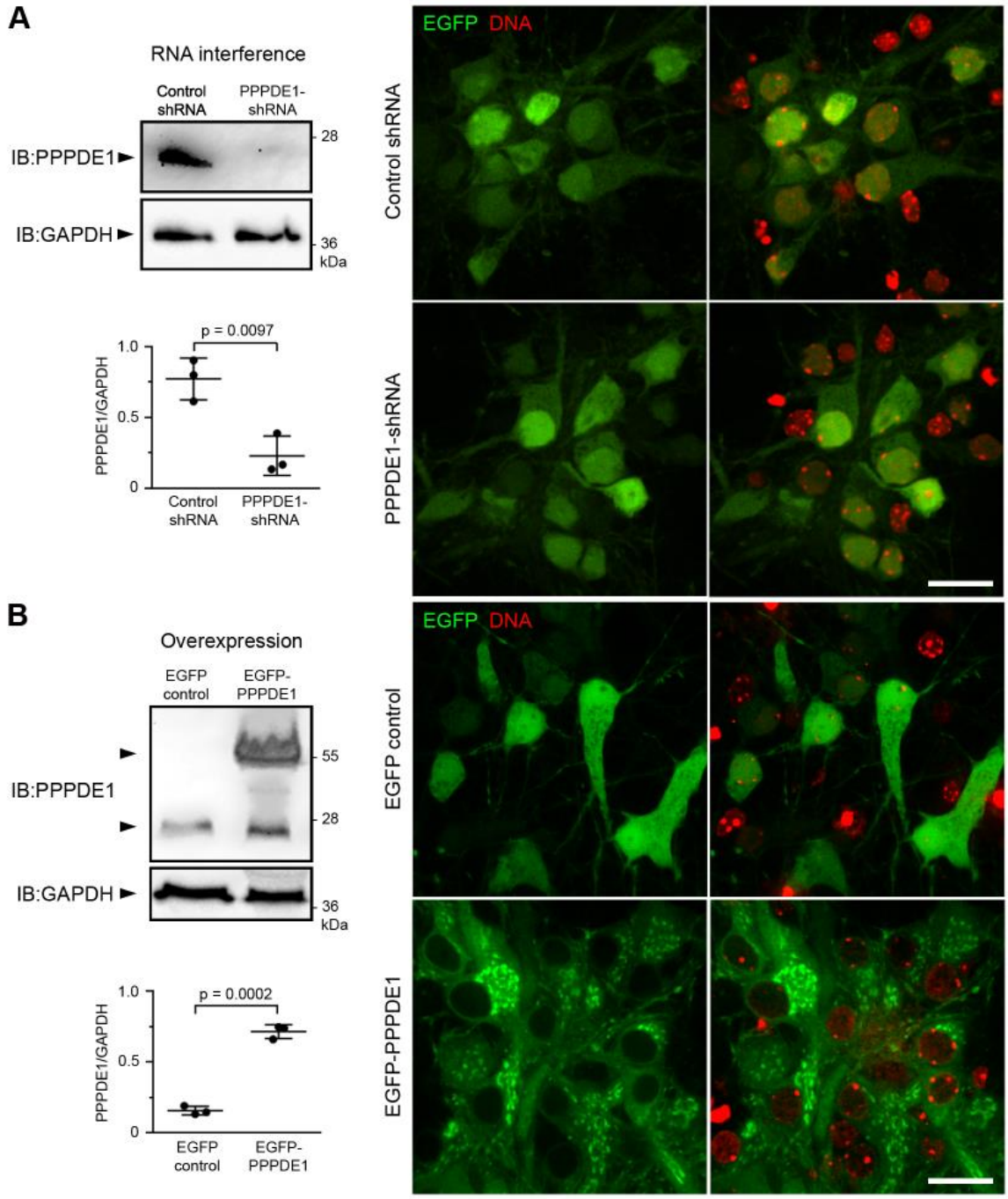

Fig. 6. Establishment of PPPDE1 knockdown and expression of EGFP-PPPDE1 after lentiviral-mediated transduction of mouse primary cortical neurons. (A) Neurons expressing non-targeting control shRNA or PPPDE1-shRNA. **(B)** Neurons expressing EGFP control or EGFP-PPPDE1. Left: immunoblot (IB) analyses of PPPDE1 and loading control GAPDH, followed by their quantification after three independent experiments (mean with standard deviation, unpaired t-test with Welch's correction). Right: representative images of the fluorescent expression of the reporter EGFP (green) and a DNA dye (red) in mouse cortical neurons. Scale bar: 20 µm.

PPPDE1 co-localizes with markers of the cis-Golgi and ER-Golgi intermediate compartment

Since PPPDE1 exhibited an expression pattern that is indicative of proteins associated with the endomembrane system, we screened for the cellular compartments or organelles that could correspond to the PPPDE1 localization observed. For this, we performed an immunostaining with antibodies for several different markers of endomembrane system components, compared their expression to that of PPPDE1 and quantified their correlation by measuring the Pearson's coefficient (Fig. 7). The closer this coefficient is to 1.0, the higher the positive correlation between the two channels. Coefficients above 0.6, or 60%, are considered to indicate high correlation.

PPPDE1 expression in cortical neurons displayed a specific co-localization with ERGIC-53, a marker of the endoplasmic reticulum (ER)-Golgi intermediate compartment (ERGIC) and GM130, a cis-Golgi matrix protein, with average correlation coefficients of 72% and 68%, respectively (Fig. 7B). GGA1 and Golgin-97, markers of the trans-Golgi network (TGN), and Adaptin γ, involved in protein sorting between the TGN and endosomes, showed similarly high correlation coefficients with PPPDE1 (59%, 66% and 73%, respectively). However, these markers exhibited a diffuse expression pattern throughout the cells and therefore did not co-localize specifically with the PPPDE1-positive perinuclear structures, as can be observed in the composite images.

Other antibodies tested which revealed low correlation coefficients were: clathrin heavy chain, the main component of vesicle coats between the TGN and the plasma membrane (45%); EEA1, a marker of early endosomes (43%); and transferrin receptor, used as an endosomal marker (25%). Markers of the vesicle coats COP-I (Golgi to ER transport) and COP-II (ER to Golgi transport) showed the lowest correlation coefficients with PPPDE1 amongst the antibodies analyzed: 22% and 21%, respectively.

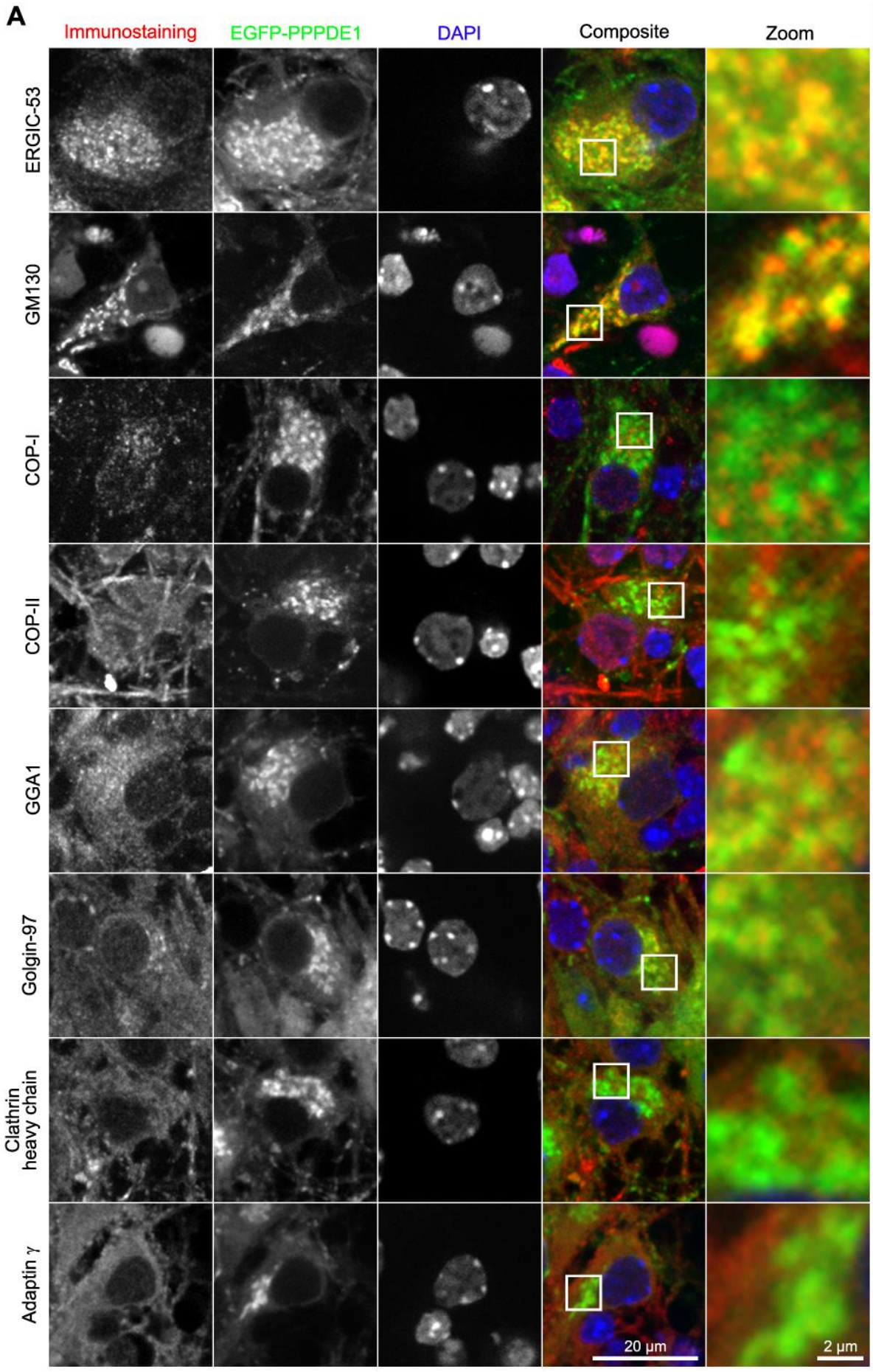
A
Immunostaining
EGFP-PPPDE1
DAPI
Composite
Zoom
ERGIC-53
GM130
COP-I
COP-II
GGA1
Golgin-97
Clathrin heavy chain
Adaptin γ
20 μm
2 μm

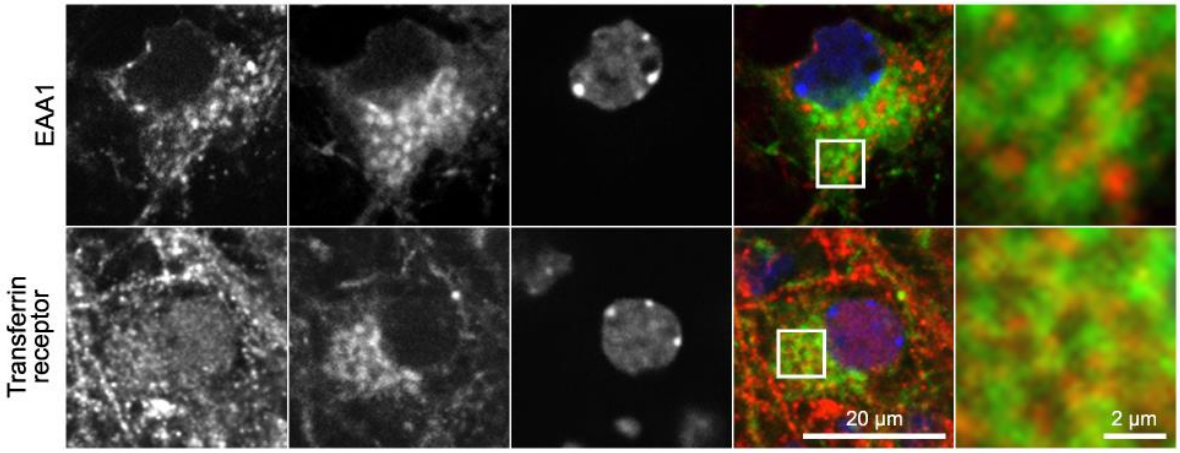
EAA1
Transferrin receptor
20 µm
2 µm

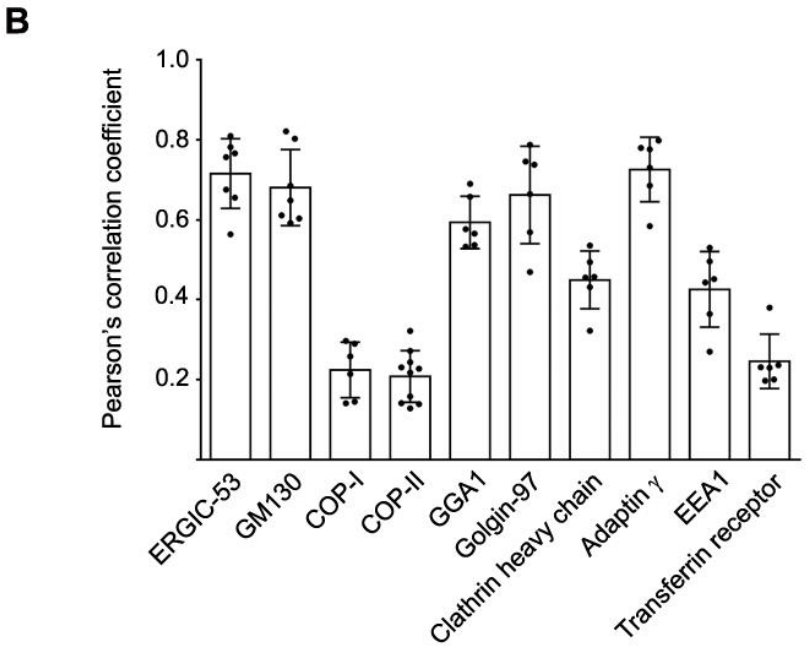
B
Pearson's correlation coefficient
1.0
0.8
0.6
0.4
0.2
ERGIC-53
GM130
COP-I
COP-II
GGA1
Golgin-97
Clathrin heavy chain
Adaptin γ
EEA1
Transferrin receptor

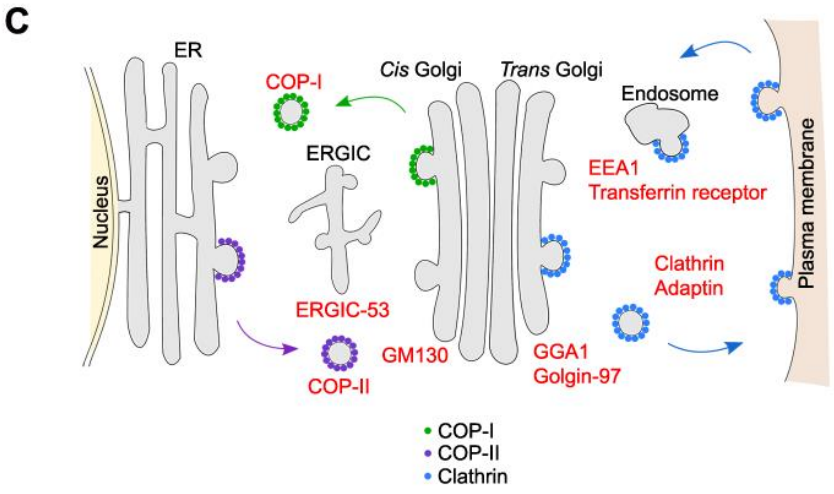
C
ER
COP-I
Cis Golgi
Trans Golgi
Endosome
ERGIC
EEA1
Transferrin receptor
Nucleus
Plasma membrane
Clathrin
Adaptin
ERGIC-53
GM130
GGA1
Golgin-97
COP-II
COP-I
COP-II
Clathrin

Fig. 7. Immunocytochemical screening of markers of the endomembrane system for co-localization with PPPDE1. (A) Expression patterns of the different endomembrane system markers tested (first column) compared to the expression of EGFP-PPPDE1 (second column). DAPI was used as a nuclear marker (third column). Composite images (fourth column, scale bar: 20 µm) display the merging between the expression of the immunostaining (red), of EGFP-PPPDE1 (green) and DAPI (blue). Zoom images display the amplified selected regions from the composite images (fifth column, scale bar: 2 µm). **(B)** Pearson's correlation coefficients of the co-localization between the different markers and EGFP-PPPDE1, measured in at least 8 cells per staining in each of three independent replicates (mean with standard deviation). **(C)** Schematic representation of the intracellular targets of the antibodies analyzed (red) and their localization in the endomembrane system. Based on Bonifacino & Glick, 2004.

PPPDE1 is in close proximity with the cis-Golgi and ERGIC, but is closer to the cis-Golgi

The immunocytochemical screening revealed that, amongst all markers of the endomembrane system analyzed, GM130 (cis-Golgi) and ERGIC-53 (ERGIC) co-localized most highly and specifically with PPPDE1. Therefore, we next investigated the nanoscale spatial distribution and relative localization of PPPDE1, cis-Golgi and ERGIC in relation to each other. For this, we performed structured illumination microscopy (SIM), which allows image reconstruction at a resolution that is two times higher than the conventional diffraction limited resolution: approximately 100 nm in XY and 250 nm in Z (Abbe, 1873; Gustafsson, 2000).

With the intention to improve the fluorescent signal from neurons expressing EGFP-PPPDE1 for SIM detection, we first tested whether we could enhance the signal by immunostaining for GFP. A strong amplification of the EGFP fluorescence was confirmed (Fig. 8A) and shown to represent the native localization of EGFP-PPPDE1 (Fig. 8B).

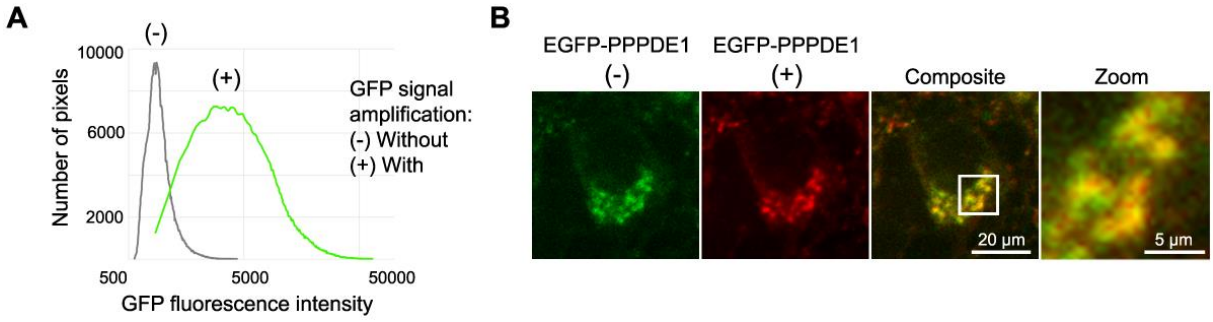

Fig. 8. Confirmation of EGFP fluorescence signal amplification and specificity for PPPDE1 after GFP immunostaining. (A) Histograms comparing EGFP-PPPDE1 signal distribution without and with amplification by GFP immunostaining. **(B)** Co-localization between EGFP-PPPDE1 signal without antibody amplification (green) and after GFP immunostaining (red).

After triple immunostaining for GM130, ERGIC-53 and GFP in cortical neurons expressing EGFP-PPPDE1, we performed SIM imaging and 3D rendering of PPPDE1, cis-Golgi and ERGIC structures (Fig. 9A). Nearest neighbor (NN) analysis of the rendered 3D objects provided measurement of the distance and frequency of occurrence of GM130 or ERGIC-53 objects in relation to PPPDE1 objects. NN results showed that the major fraction of PPPDE1-positive objects is closely associated with the cis-Golgi, as the highest frequency of GM130 objects was detected at a distance of 50 nm (0.05 µm) to PPPDE1 and decreased exponentially with increasing distances (Fig 9B, GM130). In contrast, PPPDE1 and ERGIC are more loosely connected, as distances between PPPDE1- and ERGIC-53-positive objects were most frequently found at a range of 150 to 200 nm (Fig 9B, ERGIC-53).

To control for non-specific co-clustering of objects that might happen by chance, we performed a toroidal randomization and shifted one channel towards the other by 1 µm. For both pairs analyzed (PPPDE1-GM130 and PPPDE1-ERGIC-53), randomization decreased the incidence of smaller NN distances and increased the frequency of longer distances (Fig. 9C), proving that the results from the NN analysis correspond to the specific co-clustering of PPPDE1 with cis-Golgi and ERGIC.

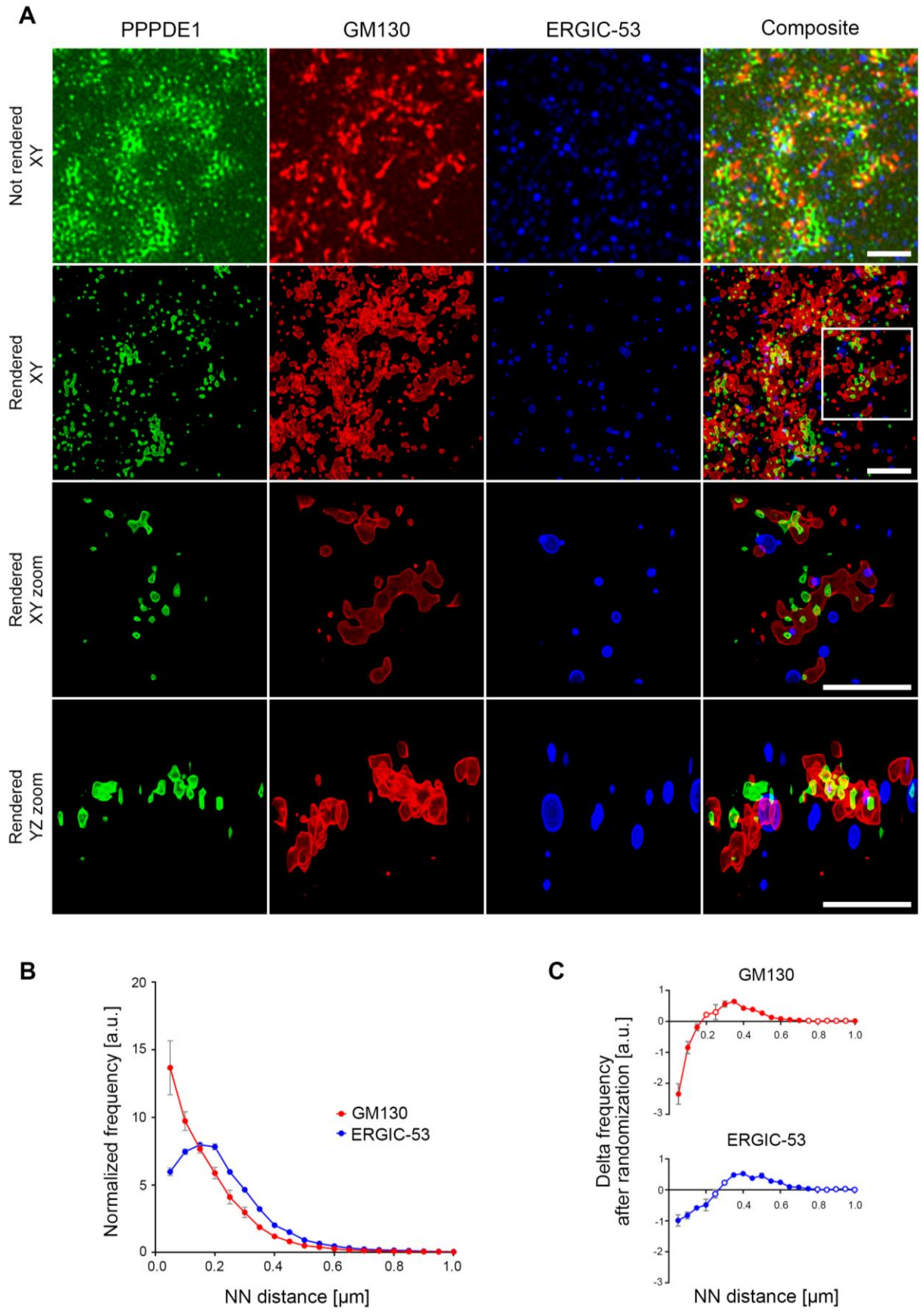
A
PPPDE1
GM130
ERGIC-53
Composite
Not rendered XY
Rendered XY
Rendered XY zoom
Rendered YZ zoom
B
Normalized frequency [a.u.]
GM130
ERGIC-53
NN distance [µm]
C
GM130
ERGIC-53
Delta frequency after randomization [a.u.]
NN distance [µm]

Fig. 9. Spatial distribution of cis-Golgi and ERGIC in relation to PPPDE1. (A) Representative images of 3D rendering after SIM imaging of mouse cortical neurons expressing EGFP-PPPDE1 after GFP enhancement (green) and immunostained for GM130 (red) and ERGIC-53 (blue). The composite images display the merging of the three markers. First row: not rendered XY-stack overview images. Second row: rendered XY-stack overview images. The white box indicates the zoomed-in area displayed in the next two rows. Third row: rendered XY-stack of zoomed-in region. Fourth row: rendered YZ-stack of zoomed-in region. Scale bars: 1 µm. **(B)** Nearest neighbor (NN) analysis of surfaces of GM130- (red) and ERGIC-53-positive (blue) rendered 3D objects in relation to PPPDE1 (mean with standard deviation). **(C)** NN frequency changes by 1 µm toroidal shift (delta frequency: shifted minus unshifted) of GM130- (red) and ERGIC-53-positive (blue) rendered 3D objects in relation to PPPDE1 after shift randomization to control for non-specific co-clustering (mean with standard deviation, filled circles: p-value ≤ 0.05, unfilled circles: p-value > 0.05, multiple one sample t-tests and Bonferroni correction for multiple tests).

Brefeldin A causes rapid dispersion of PPPDE1-positive tubular structures

In order to functionally characterize the association of PPPDE1 with the Golgi apparatus, we treated live cortical neurons expressing EGFP-PPPDE1 with brefeldin A (BFA) and analyzed the EGFP expression signal over time. The fungal metabolite BFA inhibits anterograde protein transport, induces redistribution of cis-Golgi proteins back to the ER and causes rapid and complete disassembly of the Golgi apparatus (Lippincott-Schwartz et al., 1989; Helms & Rothman, 1992; Klausner et al., 1992).

A few minutes after BFA treatment, the perinuclear, highly intense EGFP-PPPDE1-positive structures started to dissipate and disperse throughout the cytoplasm. The effect became gradually more evident over time (Fig. 10A). Quantification of the EGFP signal in the perinuclear region (Fig. 10B) confirmed a significant decrease in fluorescence intensity over time after BFA treatment compared to the vehicle control-treated neurons (p-value = 0.033 for minute 5, p-value = 0.0075 for minute 6 and p-value < 0.0001 for minutes 7 to 30, two-way ANOVA with Sidak's multiple comparisons test).

Immunostaining for GM130 and ERGIC-53 60 minutes after treatment showed that, in the DMSO vehicle-treated control group, expression patterns of both markers remained concentrated in perinuclear structures. In contrast, neurons in the BFA-treated group exhibited a scattered and more homogeneously distributed pattern of GM130 expression, similar to the effect observed with PPPDE1 after addition of BFA (Fig. 10C). ERGIC-53 showed a less pronounced diffusion and an overall slightly more intense expression after BFA treatment.

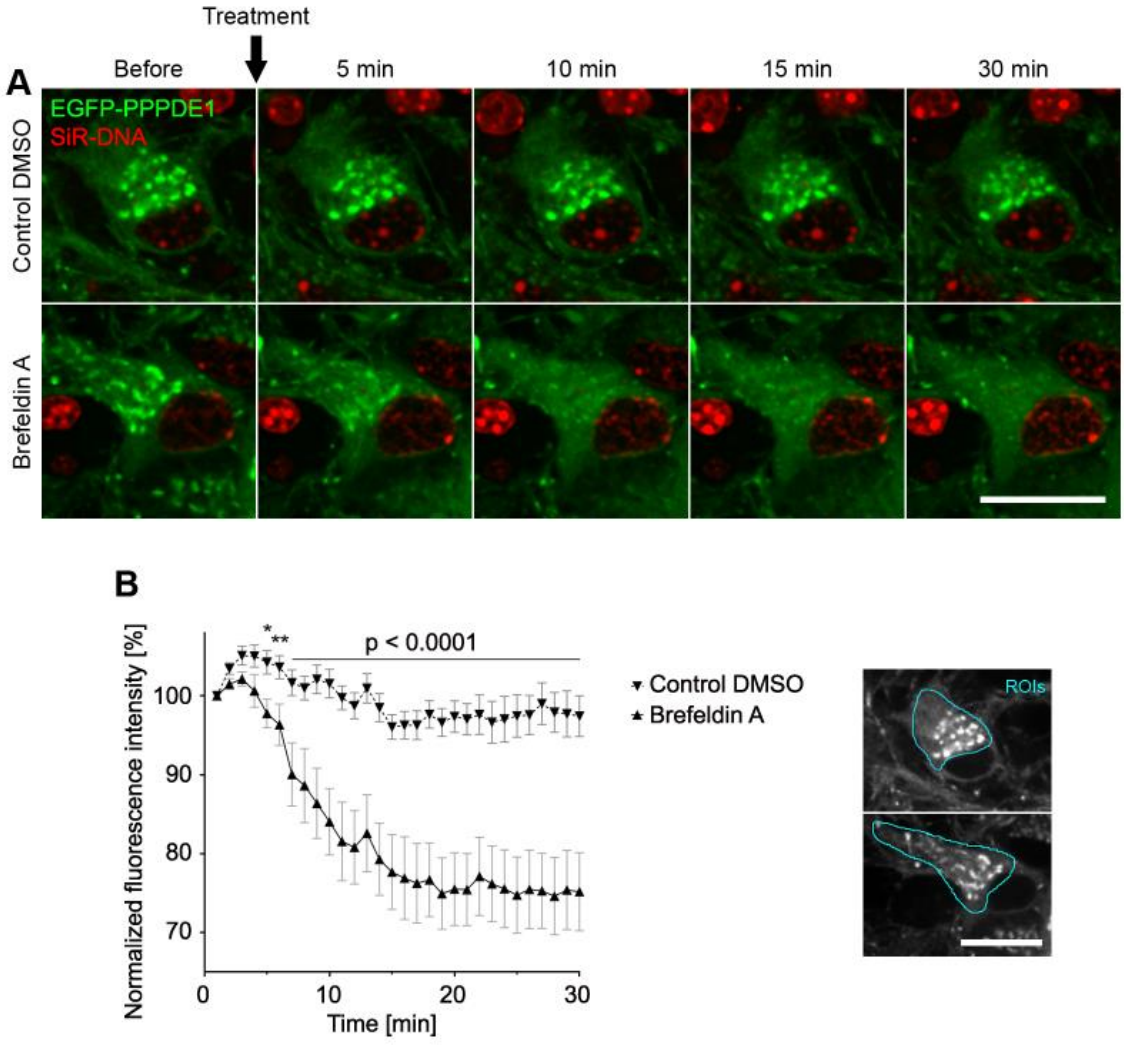

Fig. 10. (continues on the next page)

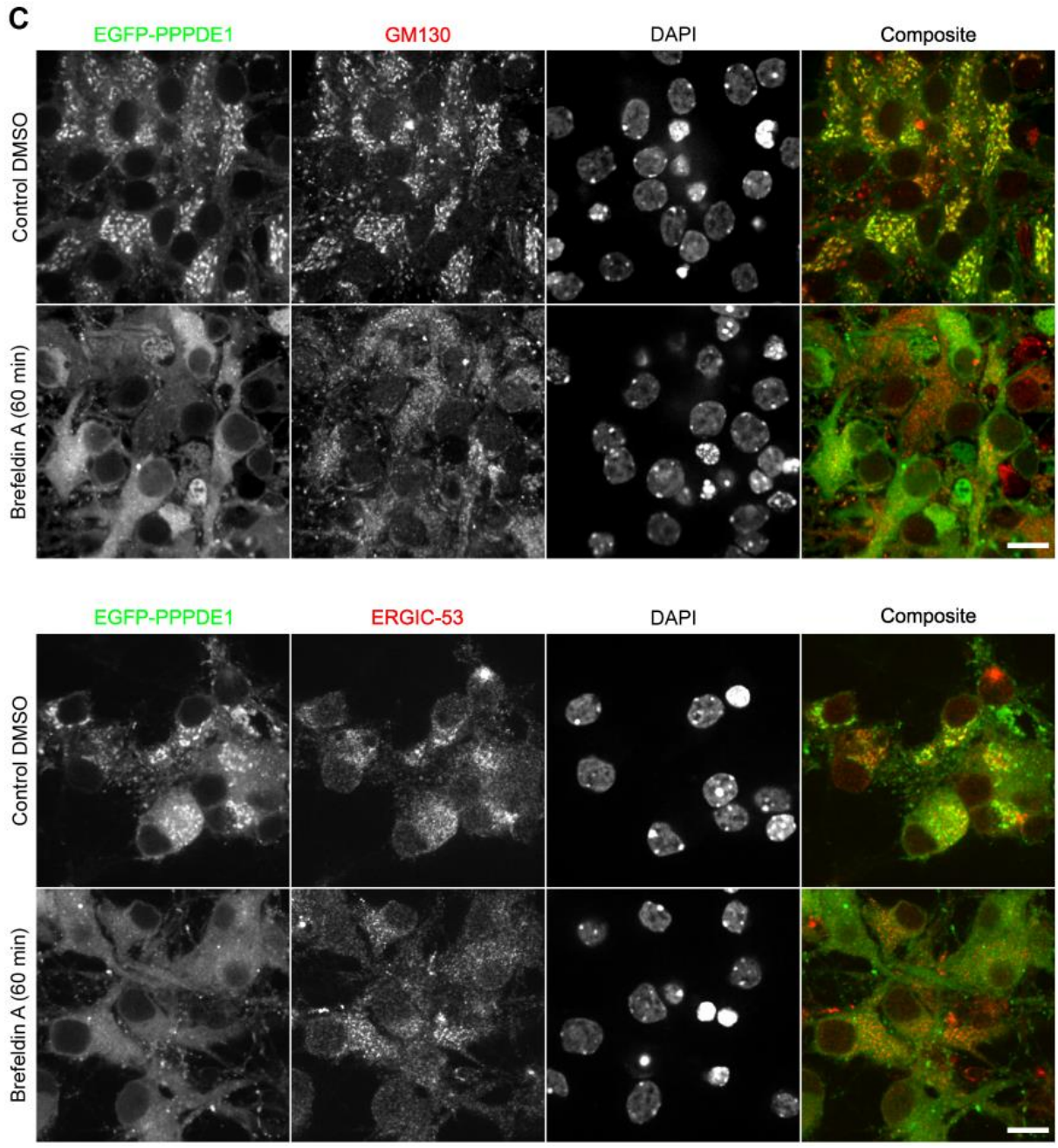

Fig. 10. Effect of brefeldin A (BFA) treatment on PPPDE1 in live cortical neurons. **(A)** Time lapse imaging of live mouse cortical neurons transduced with EGFP-PPPDE1 (green) before treatment or 5, 10, 15 or 30 minutes after treatment with either vehicle control dimethyl sulfoxide (DMSO) or BFA. A DNA tracker for live cells was used for visualization of the nucleus (red). **(B)** Quantification of normalized percentage of EGFP fluorescence intensity (mean with 95% confidence interval) over time (in minutes) in the perinuclear region after BFA or DMSO treatment (two-way ANOVA with Sidak's multiple comparisons test, *: p-value ≤ 0.05, **: p-value ≤ 0.01). **(C)** Immunostaining for GM130 and ERGIC-53 in EGFP-PPPDE1-expressing neurons 60 minutes after BFA or DMSO

treatment. DAPI was used as a nuclear marker. The composite images represent the merging between EGFP-PPPDE1 (green) and GM130 or ERGIC-53 (red). Scale bars: 20 μm.

PPPDE1 vesicles move bi-directionally through neuronal projections

Besides localizing to tubular-shaped structures in the perinuclear region corresponding to the ERGIC and cis-Golgi, PPPDE1 is also expressed homogeneously distributed in the cytoplasm and intensely in small vesicles present in neuronal projections. Interestingly, these vesicles constantly move over time through the projections, some of which in both directions, as observed in live time lapse imaging (Fig. 11). A SiR-tubulin tracker for live cells was used for visualization of microtubules in the neuronal projections (Fig. 11B).

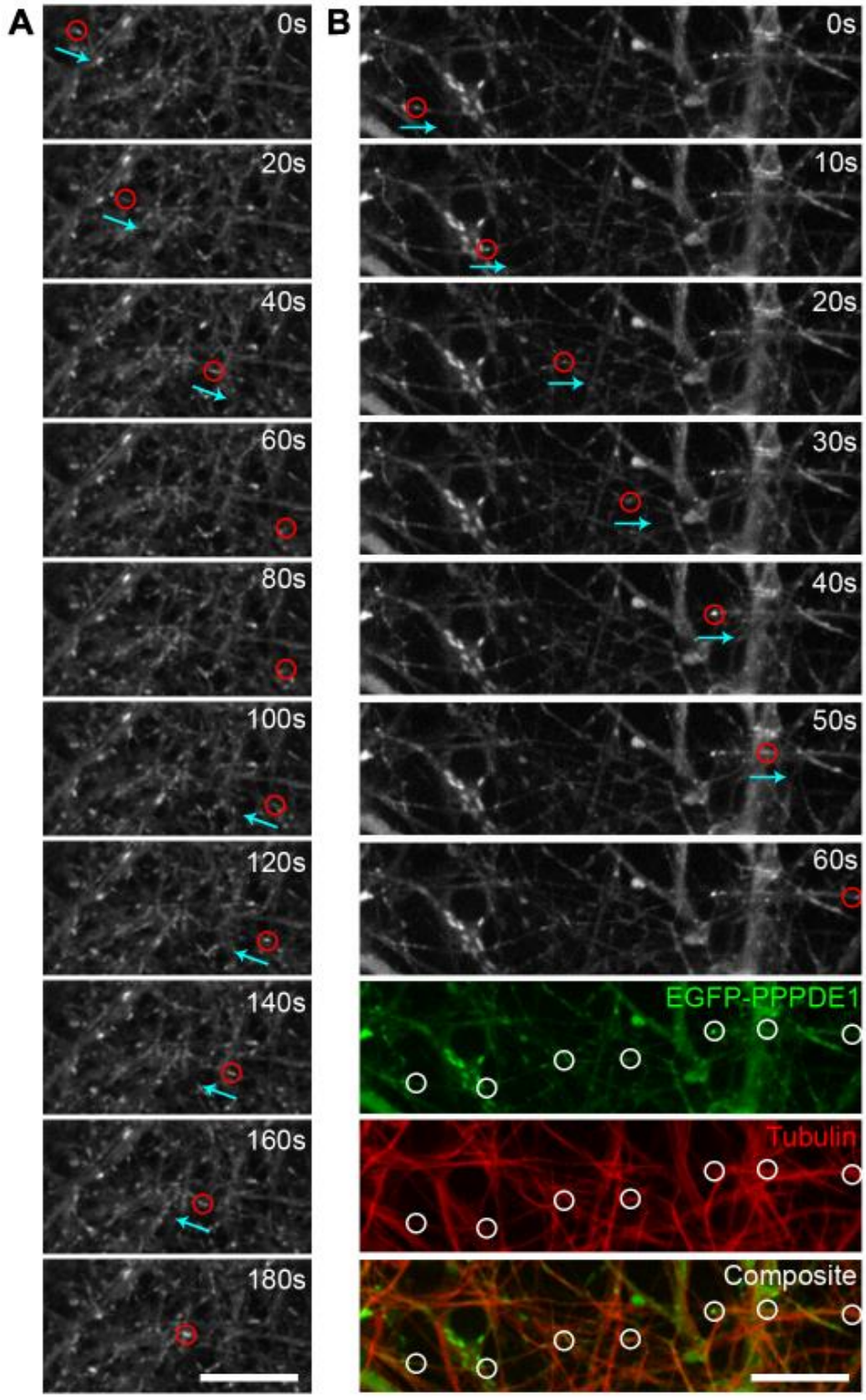

Fig. 11. Representative time lapse images of EGFP-PPPDE1 vesicles moving mono- or bi-directionally through neuronal projections over time. Two representative sets of positional tracking of EGFP-PPPDE1-positive vesicles (red circles) and their directionality (blue arrows) over time. **(A)** Example of bi-directional movement. Vesicle tracking every 20 seconds over the course of 180 seconds. **(B)**

Example of mono-directional movement. Tracking every 10 seconds over the course of 60 seconds. The white circles represent all positions tracked for the vesicle over time in the same image. The composite image displays the merging between EGFP-PPPDE1-positive projections (green) and a live cell marker for tubulin (red). Scale bar: 20 μm.

There is a faster- and a slower-moving pool of PPPDE1 molecules

Although PPPDE1 structures located in the projections of cortical neurons exhibited movement in live cell imaging, the ones concentrated in the perinuclear region did not seem to change position over time. Therefore, we hypothesized that there are two pools of PPPDE1 molecules with distinct properties regarding membrane association and mobility.

In order to measure the trafficking dynamics of single PPPDE1 molecules, we analyzed their fluorescence recovery after photobleaching (FRAP). The FRAP method allows to quantify mobility of cell components, either by diffusion or active movement (Reits & Neefjes, 2001). A region of the cell is photobleached using a high intensity laser. Next, unbleached mobile fluorescent structures coming from non-bleached areas of the cell gradually appear in the photobleached area over time (recovery). Thus, the recovery rate over time is used as a measurement of particle mobility. Less mobile components might be bound to an immobile structure or restrained inside a cellular compartment. Faster diffusing components are more likely to be unbound, freely moving molecules.

After whole-organelle photobleaching of the perinuclear EGFP signal (Fig. 12A), we measured the fluorescence recovery of two different groups of regions of interest (ROIs): in yellow, the less intense, homogeneously distributed PPPDE1-positive areas with undefined shape; and in magenta, the tubular-shaped, bright intensity structures (Fig. 12C). A significant difference between the recovery dynamics of the two groups was observed starting in early time points (p-value < 0.01 for second 40, p-value < 0.001 for second 47.3 and p-value < 0.0001 from second 54.9 forward, two-way ANOVA, Fig. 12B). The first group exhibited a faster recovery rate (half-life: 76.83 s) and larger mobile fraction (0.50 or 50%), while the second group showed slower kinetics (half-life: 121.89 s) and smaller mobile fraction (0.28 or 28%) (Fig. 12D).

These results indicate the existence of two different pools of EGFP-PPPDE1 molecules in terms of cellular mobility and dynamics. Slower recovery of pool 2 in comparison to pool 1 suggests that mobility of pool 2 PPPDE1 molecules is restricted by either a physical association with or a compartmentalization within a stable cell component.

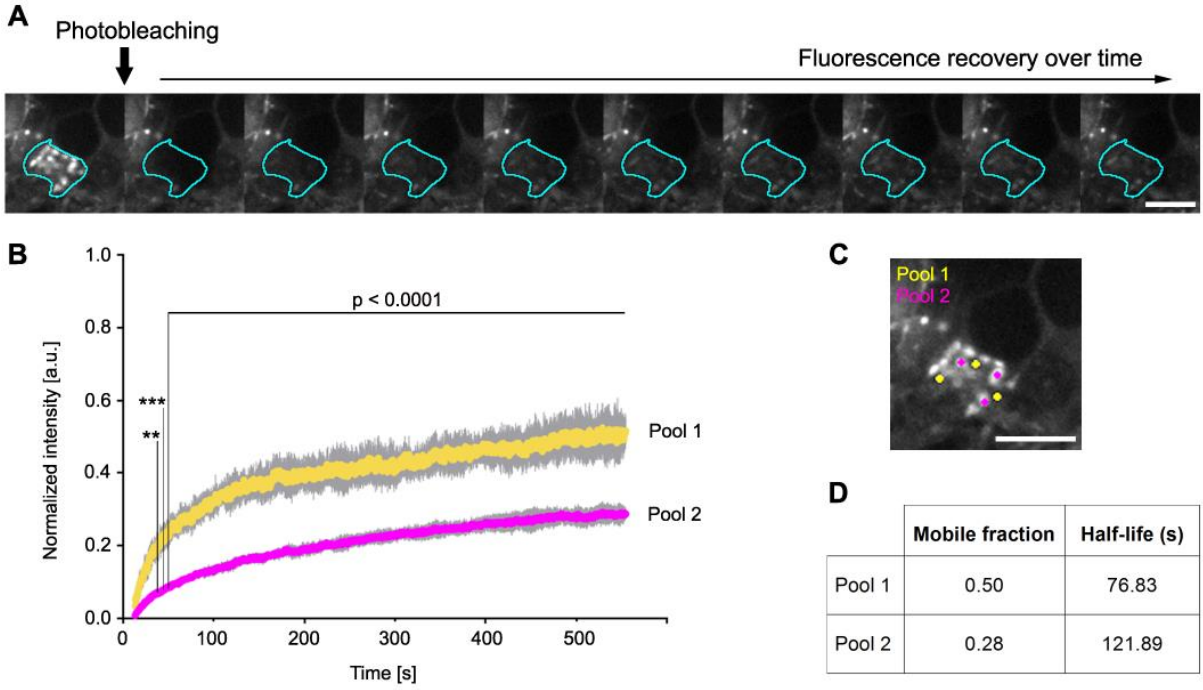

	Mobile fraction	Half-life (s)
Pool 1	0.50	76.83
Pool 2	0.28	121.89

Fig. 12. Quantification of the fluorescence recovery after photobleaching (FRAP) in live cortical neurons expressing EGFP-PPPDE1. (A) Representative images of the EGFP-positive perinuclear regions selected for photobleaching (blue ROIs) in live neurons expressing EGFP-PPPDE1. **(B)** Fluorescence recovery dynamics of the two groups of measured ROIs (mean with standard deviation, two-way ANOVA, **: p-value ≤ 0.01, ***: p-value ≤ 0.001). **(C)** Circular regions inside the photobleached area that were measured for FRAP (yellow and magenta ROIs). **(D)** Mobile fraction and half-life of recovery values, calculated based on the FRAP curves, for pool 1 (mobile fraction: 0.50; half-life: 76.83 s) and pool 2 (mobile fraction: 0.28; half-life: 121.89 s) of PPPDE1-positive vesicles. Scale bars: 10 µm.

Exogenous PPPDE1 has a positive effect on survival of cultured cortical neurons

The literature evidence that PPPDE1 seems to be involved in de-ubiquitination and apoptosis in non-neuronal cells raises the interesting possibility that this protein might have an effect on the survival of neurons. To test this hypothesis, we analyzed cell viability of cultured mouse cortical neurons 6 days after transduction with either RNA interference shRNA-PPPDE1, EGFP-PPPDE1 fusion, or their respective controls. Incorporation of propidium iodide (PI), a fluorescent nuclear marker that is only permeable to cells whose membrane is not intact, was used to distinguish healthy from apoptotic or necrotic cells and measured in the different experimental groups after imaging.

We found that neuronal viability was improved in cultures expressing EGFP-PPPDE1 (Fig. 13). These cortical neuronal cultures displayed a significantly smaller amount of PI-positive cells compared to those expressing EGFP control (Fig. 13B). The difference between cultures expressing PPPDE1-shRNA and control shRNA was not statistically significant, although a trend could be observed showing a higher number of dead neurons in cultures where PPPDE1 was silenced (Fig. 13A).

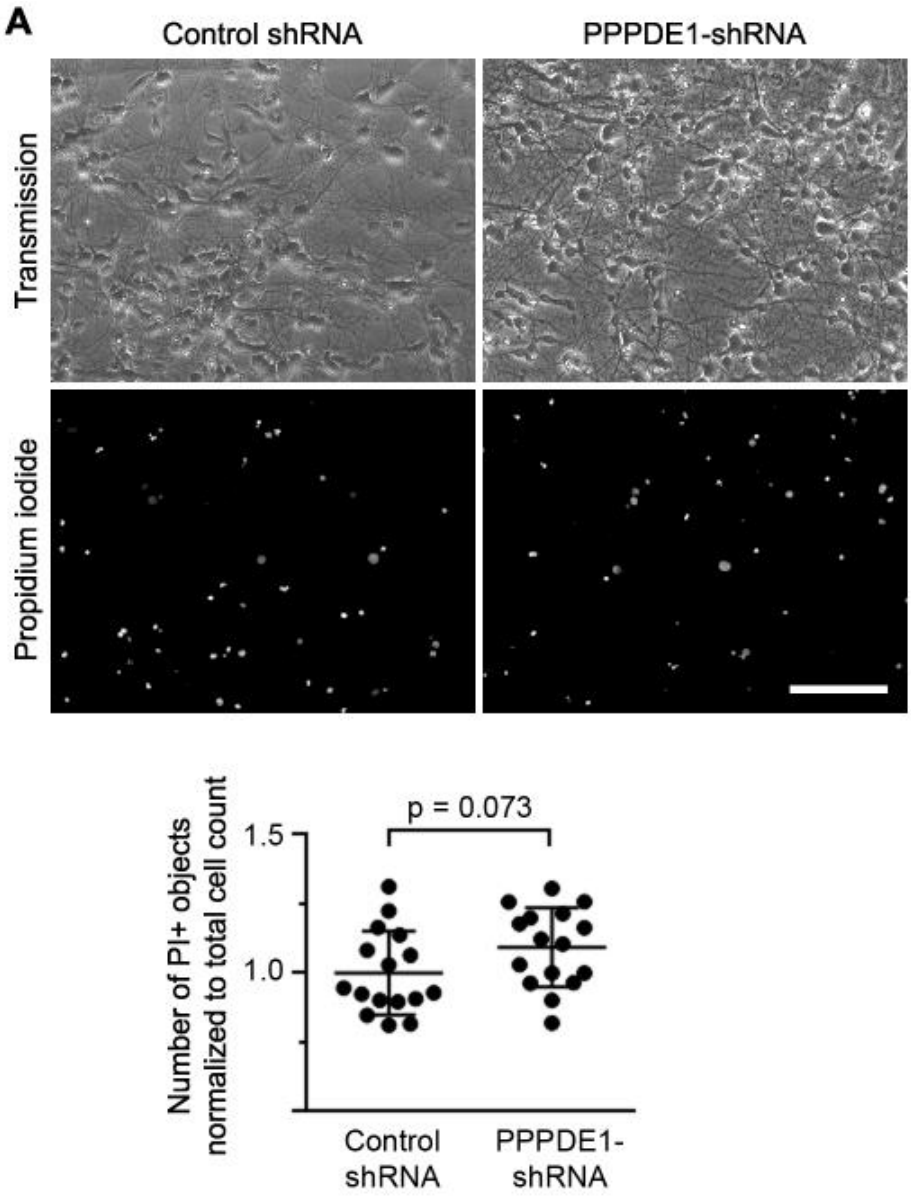

Fig. 13. (continues on the next page)

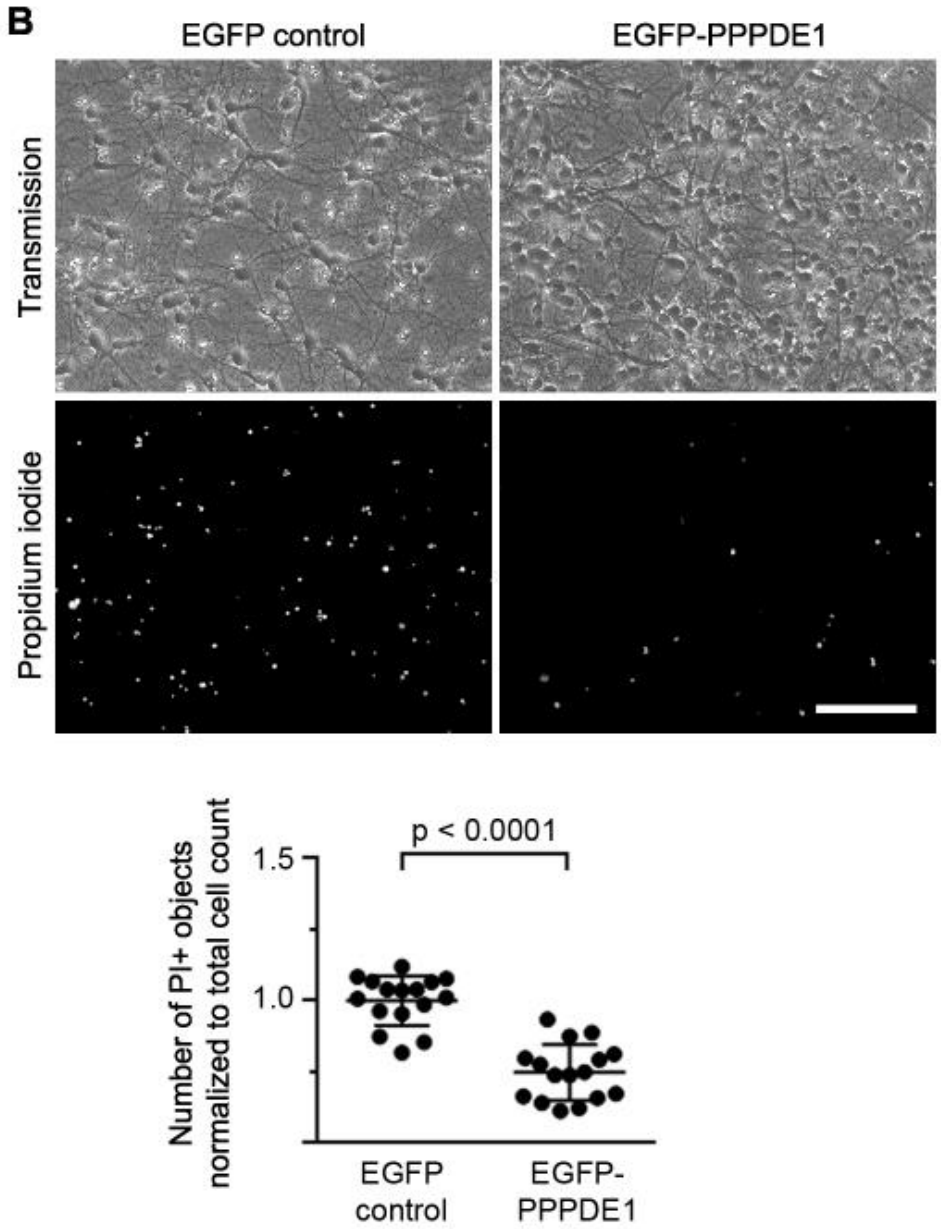

Fig. 13. Assessment of cell viability in cultured mouse cortical neurons after transduction with EGFP-PPPDE1. Neuronal cultures were transduced on DIV 2 with **(A)** non-targeting control shRNA or PPPDE1-shRNA or **(B)** EGFP control or EGFP-PPPDE1. Propidium iodide (PI) incorporation was analyzed on DIV 8 to assess and measure cell viability. Top: representative transmission images and fluorescent expression of PI. Scale bar: 100 µm. Bottom: quantification of PI-positive objects normalized to the total amount of cells in each image (mean with standard deviation, Mann-Whitney test).

PPPDE1 co-precipitates with ubiquitin, but not SUMO, and proteins involved in ER-Golgi vesicle trafficking

Identification of the binding partners of a particular protein can provide valuable clues and insights into its functions and involvement in particular cellular compartments or pathways. In order to investigate which proteins might interact with PPPDE1, we performed an interactome analysis by shotgun proteomics.

Cortical neurons expressing EGFP-PPPDE1 or EGFP control were either left untreated or received 1-hour treatment with brefeldin A (BFA), to promote intracellular dispersion of the Golgi and PPPDE1. After EGFP immunoprecipitation of the whole cell extracts, a mass spectrometry analysis of the proteome was conducted to identify candidate binding partners of PPPDE1 (Fig. 14). For consideration of statistical significance, two different parameters were used: "+" (-log10 p-value > 1.3 and log2 ratio > 2) and "++" (5% permutation-based false discovery rate)**,** both conservative but the latter more stringent.

In both treatment conditions, PPPDE1 was the most intensely enriched protein in neurons expressing EGFP-PPPDE1 compared to the control, confirming that the immunoprecipitation procedure was successful (Fig. 14A-B).

Ubiquitin was enriched by PPPDE1 in both conditions analyzed, and with high significance in the native condition (Fig. 14 A-B). On the other hand, SUMO was not detected at all by the proteomics analysis in any treatment group.

Most proteins that co-precipitated with PPPDE1 are involved in intracellular transport or protein trafficking: 58.3% of all significant proteins in the native interactome and 42.9% in the interactome after BFA treatment (Fig. 14C, Fig. 15).

A list of all proteins identified with their gene names and IDs is displayed in the Annex table.

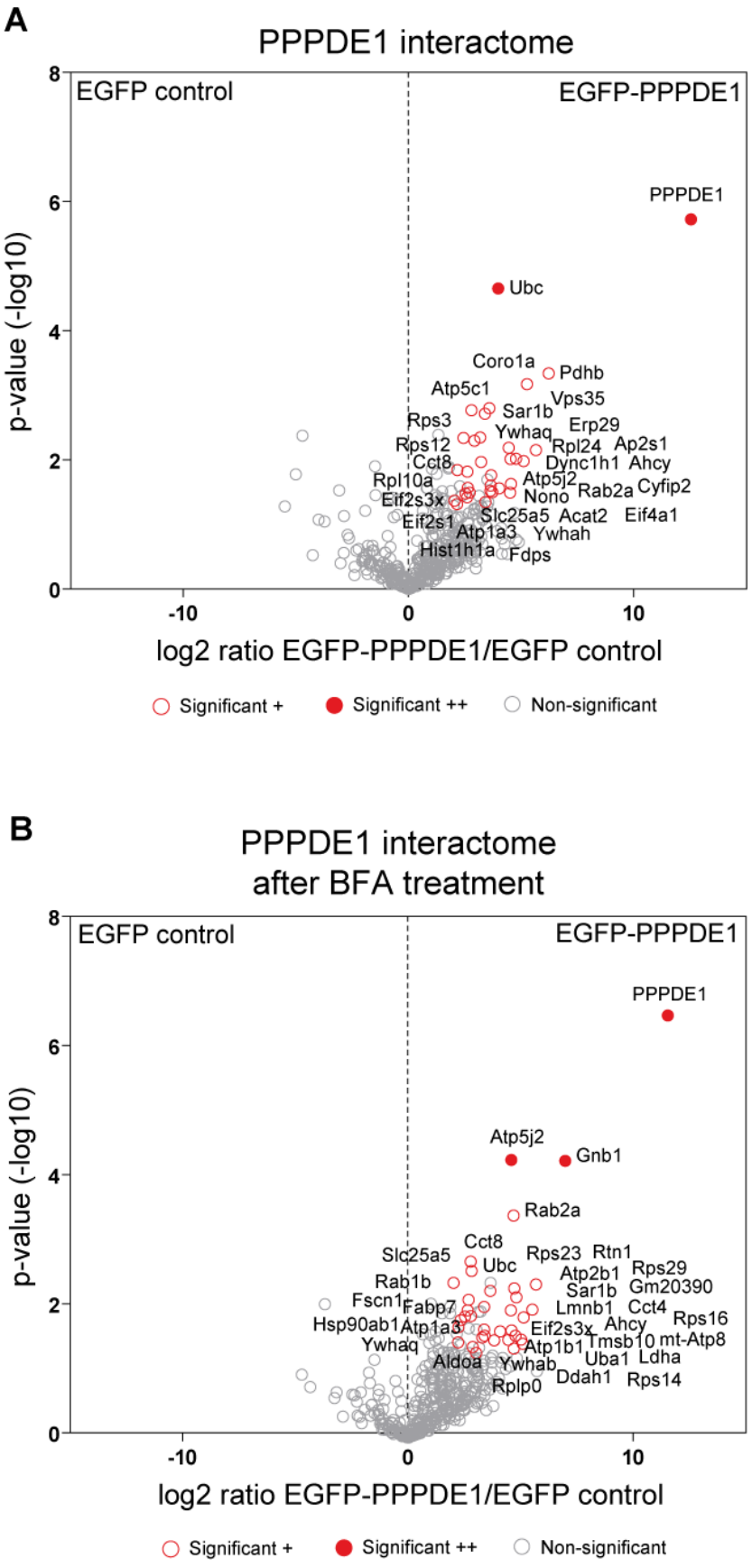

Fig. 14. (continues on the next pages)

C

PPPDE1 interactome	
Identified gene products in: Blue: native interactome Orange: interactome after BFA treatment Black: both	
Gene names	**Protein function and/or localization**
Sar1a, Sar1b	ER-Golgi transport; initiation of COP-II coat assembly
Rab1a, Rab1b	ER-Golgi transport; small GTPase
Rab2a, Rab2b	ER-Golgi transport; small GTPase
Ywhaq, Ywhah, Ywhab	Adapter protein; regulates signaling pathways
Ubc, Uba52, Rps27a, Ubb	Ubiquitin
Kxd1	Lysosomal protein; coupling to microtubules
Slc25a5	Mitochondrial ADP/ATP translocase 2
Ahcy	Adenosylhomocysteinase; L-homocysteine biosynthesis, part of amino acid biosynthesis
Eif2s1, Eif2s3x, Eif2s3y, Eif4a1	Eukaryotic translation initiation factor
Cct8, Cctq, Cct4	Cytoskeletal chaperone; folding of proteins upon ATP hydrolysis
Atp5j2, Atp5c1	ATP synthase subunits; mitochondrial membrane
Atp1a3, Atp1b1	Plasma membrane sodium/potassium-transporting ATPase subunits
Atp2b1	Plasma membrane calcium-transporting ATPase
Ap2s1	Adaptor protein complex 2 (AP-2) subunit; intracellular protein transport
Coro1a	Coronin-1A; cytoskeletal protein
Erp29	ER resident protein
Dync1h1	Dynein; cytoskeletal retrograde motor protein

Vps35	Endosomal protein; protein sorting into lysosomes
Nono	DNA- and RNA-binding protein; nuclear
Fdps	Farnesyl pyrophosphate synthase; lipid biosynthesis
Pdhb	Pyruvate dehydrogenase subunit; mitochondrial
Acat2, Acat3	Acetyl-CoA acetyltransferase
Cyfip2, Cyfip1	FMR1 (fragile X mental retardation 1)-interacting protein
Hist1h1a	Histone H1.1; DNA condensation; nuclear
Rps3, Rpl24, Rps12, Rpl10a	Ribosomal proteins
Rplp0, Rps14, Rps23, Rps16, Rps29	Ribosomal proteins
Gnb1, Gnb2	G protein subunits; GTPases
mt-Atp8, ATP8, Mtatp8	ATP synthase protein
Fabp7	Fatty acid-binding protein
Fscn1	Fascin; organization of cytoskeletal actin filaments
Tmsb10	Thymosin beta-10; organization of cytoskeleton; inhibits actin polymerization
Nme2	Nucleoside diphosphate kinase; nuclear
Aldoa	Fructose-bisphosphate aldolase; glycolysis and gluconeogenesis
Uba1	Ubiquitin-like modifier-activating enzyme 1 (E1)
Lmnb1	Lamin-B1; component of the nuclear lamina
Rtn1	Reticulon-1; ER protein
Ldha	L-lactate dehydrogenase; interconversion of lactate and pyruvate
Ddah1	N(G),N(G)-dimethylarginine dimethylaminohydrolase 1; inhibition of nitric oxide synthase
Hsp90ab1	Heat shock protein HSP 90-beta; chaperone

Fig. 14. Interactome analysis of binding partners of PPPDE1 by mass spectrometry. PPPDE1 interactome **(A)** without treatment and **(B)** after BFA treatment. X-axis: log2 ratio, or mean difference, between the two groups. Y-axis: p-value (-log10) of the comparison between the genotype groups (two-sample Student's t-test). Circles in the scattered dot plots represent the proteins identified (gene names are displayed). Red circles represent the proteins whose abundance was statistically significant in the EGFP-PPPDE1 group compared to EGFP control. Unfilled red circles or "+": -log10 p-value > 1.3 (corresponding to p-value ≤ 0.05) and log2 ratio > 2. Filled red circles or "++": 5% permutation-based false discovery rate. Grey circles represent non-significant identified proteins (gene names not displayed). **(C)** Table listing the gene names of all identified statistically significant proteins enriched by PPPDE1 (besides PPPDE1 itself), their function and/or intracellular localization, based on the UniProt database (Chen et al., 2017). In blue: gene products identified only in the native interactome; in orange: identified only in the interactome after BFA treatment; in black: identified in both groups. A complete list of all proteins detected, their gene names and IDs can be found in the Annex.

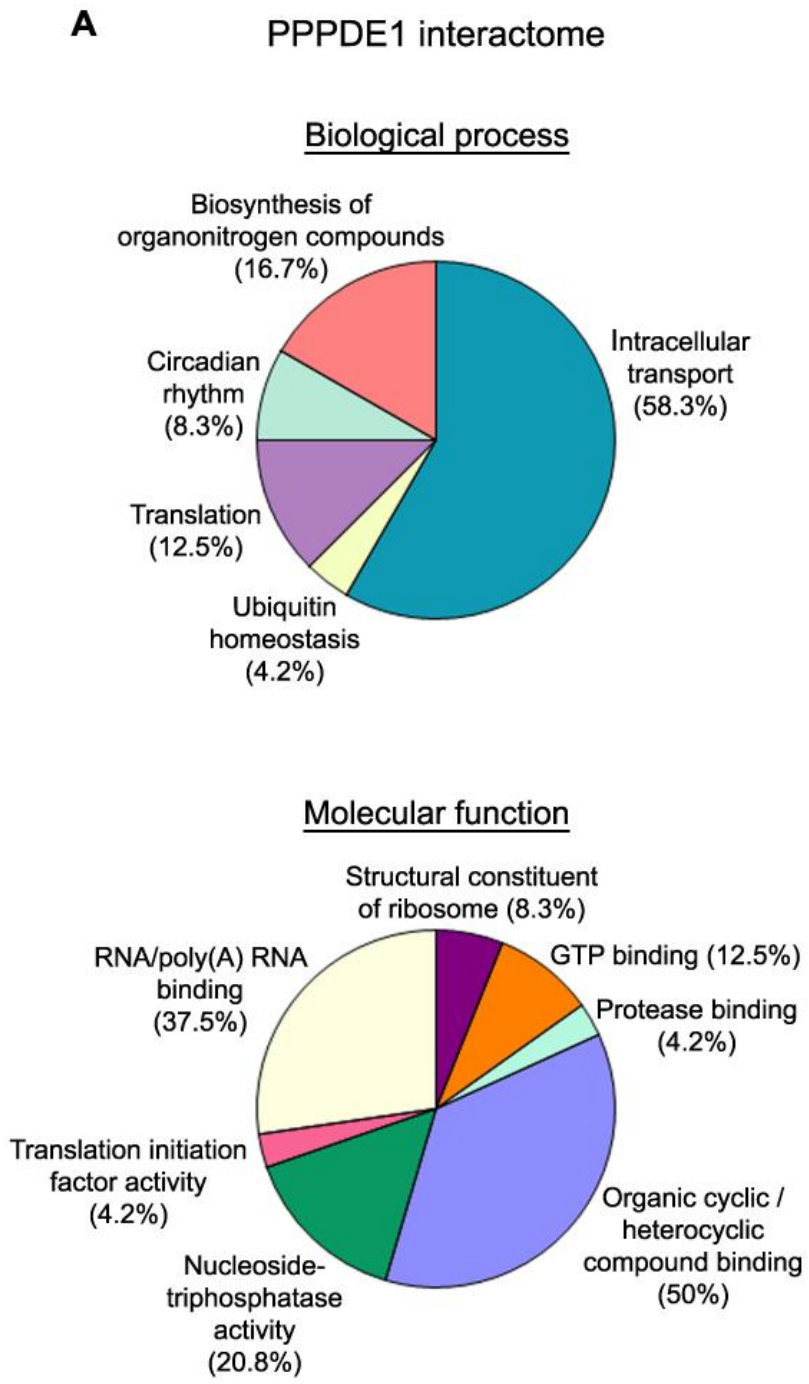

Fig. 15. (continues on the next page)

B

PPPDE1 interactome after BFA treatment

Biological process

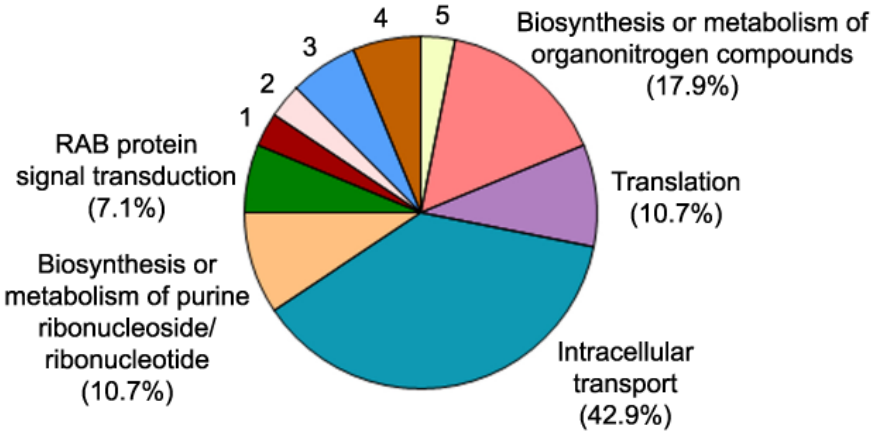

1- Sodium ion exportation / Potassium ion homeostasis (3.6%)
2- Peptidyl-histidine phosphorylation (3.6%)
3- Cellular homeostasis (7.1%)
4- Nucleoside diphosphate phosphorylation (7.1%)
5- Ubiquitin homeostasis (3.6%)

Molecular function

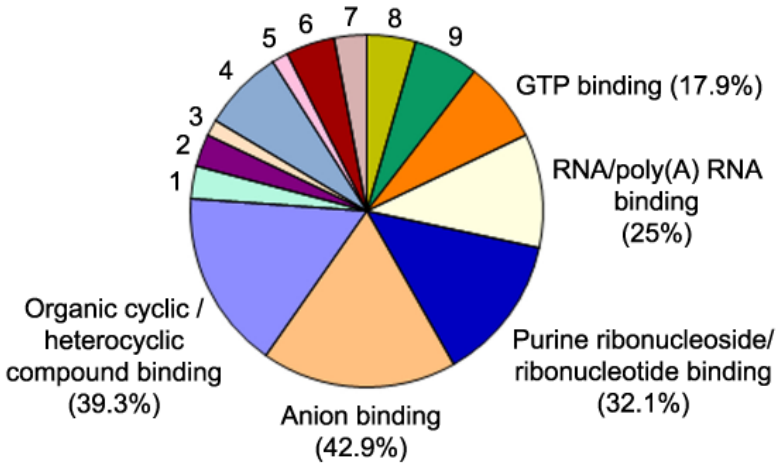

1- Protease binding (7.1%)
2- Structural constituent of ribosome (7.1%)
3- ATPase activity (3.6%)
4- Hydrolase activity (17.9%)
5- Protein histidine kinase activity (3.6%)
6- Structural molecule activity (10.7%)
7- MHC class II protein complex binding (7.1%)
8- GTPase activity (10.7%)
9- Nucleoside-triphosphatase activity (14.3%)

Fig. 15. Gene ontology (GO) term classification of proteins in the PPPDE1 interactome. GO assignment was performed to functionally classify the proteins significantly enriched by PPPDE1, summarized in two main categories of biological process and molecular function. Percentage values represent the percentage number of all proteins identified that fall into a certain category. Since some proteins may be included in more than one category, or none, sum of the percentages may not equal 100. **(A)** Categorization of the PPPDE1 native interactome, without treatment and **(B)** after BFA treatment.

PPPDE1 co-localizes with RAB1 and RAB2, but not with SAR1

We selected three proteins identified in the proteomics screening for further analysis of their potential association with PPPDE1: the small GTPases RAB1, RAB2 and SAR1, given that they exert activity between the ER and Golgi compartments, the same specific intracellular region where we described PPPDE1 to be located.

Protein members of the RAS-related RAB family are known to regulate all steps of vesicular trafficking in the cell – RAB1 and RAB2 being particularly involved in the transport between ER and Golgi (Simons & Zerial, 1993; Stenmark, 2009). SAR1, in turn, is the activating component of the COP-II coat that mediates transport from the ER to the cis-Golgi (Nakańo & Muramatsu, 1989; Kuge et al., 1994; Barlowe et al., 1994).

After cloning fusion proteins of mRuby2 to RAB1, RAB2 and SAR1 and co-expressing each of them with EGFP-PPPDE1 in live cortical neurons, we observed that RAB1 and RAB2 exhibited expression patterns with high similarity to those of PPPDE1 (Fig. 16A). Quantification of the correlation between the EGFP and mRuby2 fluorescent signals (Fig. 16B) confirmed that PPPDE1 co-localized highly with RAB1 (Pearson's coefficient: 89%) and RAB2 (87%), but poorly with the control vector (9%). Surprisingly, SAR1 was not found to be concentrated in tubular-vesicular structures in the perinuclear area. Instead, it showed a diffuse expression throughout the nucleus and cytoplasm (Fig. 16A) and a low co-localization with PPPDE1 (44%) (Fig. 16B).

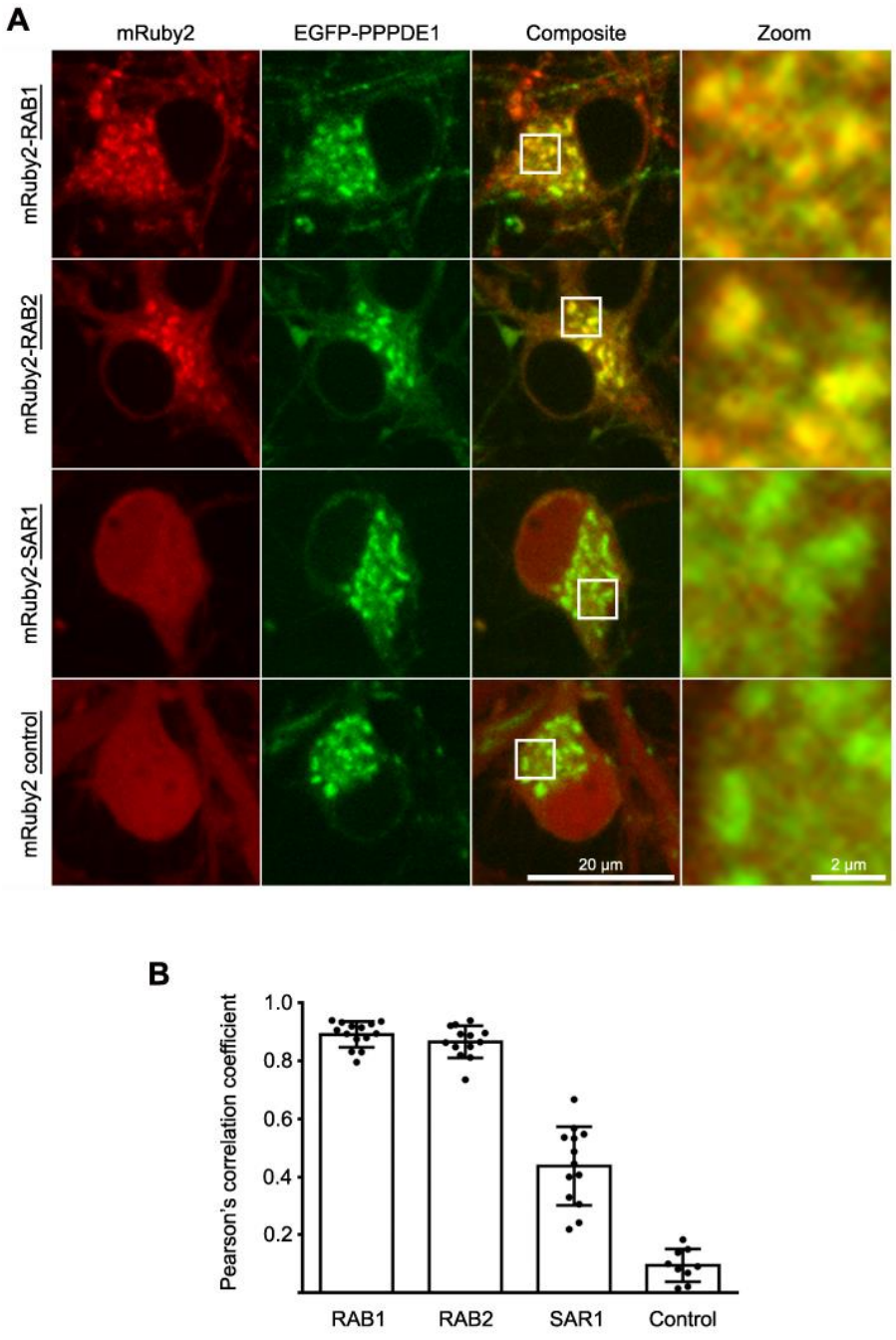

Fig. 16. Co-expression of EGFP-PPPDE1 and mRuby2-RAB1, -RAB2, -SAR1 or mRuby2 control in live cortical neurons. (A) Representative images of the live expression of the mRuby2 fusion constructs (first column, red) compared to the expression of EGFP-PPPDE1 (second column, green). Composite images (third column, scale bar: 20 µm) display the merging between the first two columns. Zoom images display the amplified selected regions from the composite images (third column, scale bar: 2 µm). **(B)** Pearson's correlation coefficients of the co-localization between EGFP-PPPDE1 and mRuby2-RAB1, -RAB2, -SAR1 and control (mean with standard deviation).

Annex

Gene names	Protein names	Protein IDs
Acat2, Acat3	Acetyl-CoA acetyltransferase	Q8CAY6; G3XA25; Q80X81; Q8R4V3; F2Z459
Ahcy	Adenosylhomocysteinase	Q5M9P0; Q3U5U5; Q3U4D1; Q3TF14; P50247; A2ALT5; Q8BPI7
Aldoa	Fructose-bisphosphate aldolase	Q5FWB7; P05064; Q6NY00; A6ZI44; D3YWI1; A0A0U1RPN8; Q9CPQ9; A6ZI46; A0A0U1RPT5
Ap2s1	AP-2 complex subunit sigma	A0A0U1RPS0; Q3UJ76;P62743
Atp1a3, Atp1b1	Sodium/potassium-transporting ATPase subunit alpha-3	A0A0G2JGX4; Q8VCE0; Q6PIC6; Q8R0E8
Atp2b1	Plasma membrane calcium-transporting ATPase 1	G5E829; Q8K314
Atp5j2, Atp5c1	ATP synthase subunit	F8WHP8; P56135; Q8C2Q8; A2AKU9; Q9D9D7; Q3UD06; Q91VR2; A2AKV1; A2AKV2; A2AKV3; Q9ERA8
Cct8, Cctq, Cct4	T-complex protein 1 subunit	H3BL49; Q9WVS5; Q8BVY8; Q3UL22; Q6A0F1; P42932; Q3UKQ2; Q9CS06; Q9CRW7; H3BJB6; Q564F4; Q3UJZ8; Q3TII0; P80315; G5E839; G3UYW5
Coro1a	Coronin-1A	Q3U9K3; Q3U232; Q3U1N0; Q3T9L1; O89053; A0A0U1RPY8; G3UYK8
Cyfip2, Cyfip1	Cytoplasmic FMR1-interacting protein	Q810V4; F6QD74; Q5SQX6; Q8K118; A0A0R4J119; Q7TMB8-2; Q7TMB8
Ddah1	N(G),N(G)-dimethylarginine dimethylaminohydrolase 1	Q9CWS0; D3YU15; Q3UF01
Dync1h1	Cytoplasmic dynein 1 heavy chain 1	Q9JHU4; Q80U36
Eif2s1, Eif2s3x, Eif2s3y, Eif4a1	Eukaryotic translation initiation factor	Q9CV24; Q6ZWX6; A2AAW9; Q3UDF8; Q3UIJ2; Q3TML6; Q9Z0N1; Q3U5H6; Q9CRE9; Q9D791; Q9Z0N2; Q4FZL1; Q5F2A7; Q3UXC2; Q3TGK7; Q3TFG3; P60843; Q3U8I0; Q3TLL6
Erp29	Endoplasmic reticulum resident protein 29	P57759
Fabp7	Fatty acid-binding protein	Q5NDA4; P51880; E9Q0H6
Fdps	Farnesyl pyrophosphate synthase	Q5M8R9; Q4FJN9; Q3US29; Q920E5; A0A0G2JDJ5; A0A0G2JEB3; Q3TMB3; A0A0G2JEA5
Fscn1	Fascin	Q61553; A0A0G2JDU7
Gnb1, Gnb2	Guanine nucleotide-binding protein G(I)/G(S)/G(T) subunit beta-1	Q3U1B1; Q3TQ70; P62874; H3BLF7; H3BKR2; D3YZX3; E9QKR0; Q61621
Hist1h1a	Histone H1.1	P43275
Hsp90ab1	Heat shock protein HSP 90-beta	Q71LX8; P11499
Kxd1	KxDL motif-containing protein 1	Q80XH1
Ldha	L-lactate dehydrogenase	Q3UDU4; Q564E2; Q3TI99; G5E8N5; P06151; Q99K20; Q3THB4; Q3TCI7;

		D3Z736; D3YZQ9; Q3UIC3
Lmnb1	Lamin-B1	P14733; Q8C553
mt-Atp8, ATP8, Mtatp8	ATP synthase protein 8	Q7JCZ0; A3R404; A0A141CM32; A0A075DCI0; P03930
Nme2	Nucleoside diphosphate kinase	E9PZF0; B0LAA8
Nono	Non-POU domain-containing octamer-binding protein	Q4FK11; Q3TTV7; Q3TFC2; Q3UM20; Q3TF40; Q99K48; Q3TMM5; Q99K48-2
Pdhb	Pyruvate dehydrogenase E1 component subunit beta	Q9D051
Rab1a, Rab1b	Ras-related in brain protein Rab-1	Q0PD66; Q9D1G1; Q3V3C2; Q5SW88; Q3UB66; Q0PD67; Q6ZPF0; P62821; Q5SW87
Rab2a, Rab2b	Ras-related in brain protein Rab-2	Q0PD65; P53994; Q8BXY4; Q6PDZ3; Q3TEG7; Q5U628; Q0PD64; P59279
Rplp0, Rps14, Rps23, Rps16, Rps29	Ribosomal protein	D3YVM5; Q5M8R8; Q5FWB6; E9Q070; P14869; O89073; S4R1N1, D3YVF4; D3Z7I1; O70569; P62264; Q3UJS5; Q9CWI9; Q497E1; Q9CZI5; P62267; Q9CSN9; A4FUS1; Q641N3; Q5CZY9; P14131; P62274
Rps3, Rpl24, Rps12, Rpl10a	Ribosomal protein	Q9CZP6; Q5YLW3; Q3UCL7; P62908; Q9D0A2; Q3UK56; A0A140LI77; D3YV43; Q8BP67; Q3UW40; Q6ZWZ6; P63323; Q5XJF6; Q3U561; P53026
Rtn1	Reticulon-1	Q4FJL2; Q8K0T0; Q05CD8; Q7M6W1; A3QM89; Q4FZ95
Sar1a, Sar1b	GTP-binding protein Sar1	Q3U281; Q0VGU0; Q9CQC9; Q99JZ4; Q3TXJ4; P36536
Slc25a5	ADP/ATP translocase 2	Q545A2; P51881
Tmsb10	Thymosin beta-10	A6H6H4; Q6ZWY8
Uba1	Ubiquitin-like modifier-activating enzyme 1	B9EHN0; Q02053
Ubc, Uba52, Rps27a, Ubb	Ubiquitin	A5JUZ1; A0A0A6YW67; E9Q9J0; Q66JP1; Q8C2K3; Q642L7; E9Q5F6; Q922B0; Q5SX22; Q3TH47; Q78XY9; Q6NZC5; Q8R0Z9; Q922Z8; Q8VC46; P62984; P62983; P0CG49; P0CG50; E9Q4P0; E9QNP0; B0LAC2; J3QK04
Vps35	Vacuolar protein sorting-associated protein 35	Q3UQJ1; Q3TRJ1; Q3TKU6; Q3TJ43; Q9EQH3
Ywhaq, Ywhah, Ywhab	14-3-3 protein	A3KML3; P68254-2; P68254; F6YY69; F6VW30; P68510; A2A5N2; Q9CQV8; Q9CQV8-2; A2A5N1

Table 2. Specifications of the proteins identified in the PPPDE1 interactome. List of gene and protein names, as well as protein IDs, of all products found in both conditions (with and without BFA treatment), in alphabetical order.

Discussion

In the present work, we extensively characterized different aspects of PPPDE1, a ubiquitous yet poorly understood protein, in mouse cortical neurons.

We constructed a lentivirus-mediated vector coding for a fusion protein that induces neuronal-specific co-expression of PPPDE1 and EGFP. A disadvantage of employing an expression construct is that introduction of exogenous gene expression leads to artificially increased PPPDE1 levels in the cells. Further, attachment to an EGFP molecule might also cause alteration of a protein's localization, structure or function, as it may interfere with potential interaction interfaces (Agbulut et al., 2006; Wiedenmann et al., 2009). EGFP can also form weak dimers, which could dimerize PPPDE1 and affect the fusion protein properties (Kimple et al., 2013).

Even though EGFP is a relatively large protein with 238 amino acids or 26.9 kDa, its size does not usually impair the access of the fusion protein to the different cellular compartments. Unlike other frequently used protein tags, such as the FLAG epitope and the human influenza hemagglutinin (HA), EGFP has intrinsic fluorescence that allows native detection without the use of antibodies or other co-factors (Kimple et al., 2013).

To ensure that the effects we described were attributed to the PPPDE1 protein, and not to its EGFP tag, we consistently used a vector expressing EGFP alone as a control throughout this study. We also employed a 5 amino acid long spacer between the EGFP and the PPPDE1 sequences.

Despite its drawbacks, transduction of a protein of interest together with a fluorescent protein is a valuable and frequently employed tool to allow its visualization and to aid in elucidating its localization and function. By using the EGFP-PPPDE1 construct, we were able to study PPPDE1 in live cells and to follow treatment effects over time, thus adding another dimension when compared to other types of localization microscopy. Furthermore, using a fluorescent fusion protein allowed our investigation to be performed under physiological conditions that are more comparable to the natural cellular environment than after chemical fixation or protein extraction methods.

Live cell expression of the EGFP-PPPDE1 fusion protein (Fig. 6) showed that PPPDE1 localizes to tubular-shaped structures in the perinuclear region and is excluded from the

nucleus in neurons. This observation is in accordance with studies that have also found a perinuclear distribution of PPPDE1 in other cell types: HEK cells (Yan et al., 2010; Deng et al., 2010; Shin et al., 2012), pig kidney epithelial cells (Mo et al., 2008) and HeLa cells (He et al., 2013).

The antibody we used to detect PPPDE1 in immunoblots (Proteintech 20517-1-AP) showed a diffuse localization of PPPDE1 throughout the nucleus and cytoplasm in cortical neurons after immunocytochemistry (Fig. 17). This immunostaining signal was incompatible with the perinuclear pattern we observed in live cells and that was also reported by the other studies cited above. For this reason, for the localization analysis, we used neurons expressing EGFP-tagged PPPDE1, instead of employing the PPPDE1 antibody.

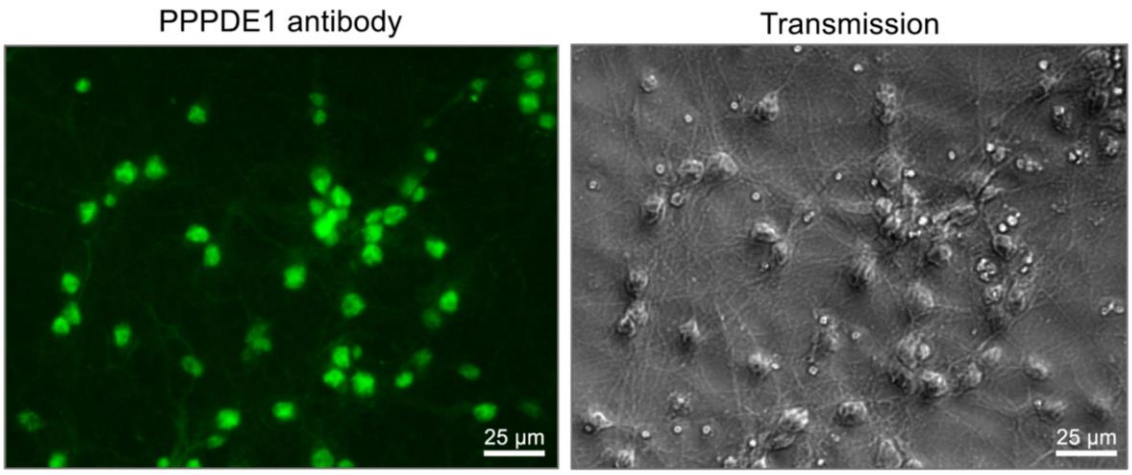

Fig. 17. Expression pattern of PPPDE1 immunostaining in mouse cortical neurons. Representative images of immunocytochemistry using the Proteintech 20517-1-AP anti-PPPDE1 antibody (green) and transmission microscopy.

The immunocytochemical screening for a potential co-localization with PPPDE1 using different markers of the endomembrane system (Fig. 7) demonstrated that this protein correlated most highly and specifically with markers of the cis-Golgi and of the ERGIC and poorly or non-specifically with trans- or post-Golgi markers. Some of the late-stage markers showed diffuse expression throughout the cytoplasm, which translated into relatively high Pearson's correlation coefficients with PPPDE1, although their localization was not specific for the PPPDE1 expression pattern.

The immunostaining analysis indicates that the PPPDE1-positive perinuclear structures localize in the region that comprises the ER and the cis-Golgi network. In addition, it shows that the localization of PPPDE1 is not compatible with cellular compartments involved in endocytosis or in late stages of the secretion pathway, between the trans-Golgi network and the cell membrane.

We expected the primary antibody against Sec23, a subunit of the COP-II coat (Thermo Fisher Scientific, PA1-069A) to exhibit a punctual and perinuclear localization, similar to that of COP-I, as reported in other studies that have used the same antibody (Brandon et al., 2006; Bhattacharyya & Glick, 2007). Instead, we observed a diffuse immunostaining pattern throughout both the nucleus and cytoplasm in mouse cortical neurons, after fixation with 4% formaldehyde or methanol. In order to test whether this effect occurred only in neurons, we performed the same immunostaining in human embryonic kidney (HEK) cells and in C2C12 mouse myoblast cells – but a similar localization was observed (data not shown).

In addition, the expression pattern of the mRuby2-SAR1 fusion protein (Fig. 16) showed that SAR1, a component of the COP-II coat, also localized diffusely throughout nuclear and cytoplasmic compartments in live neurons, similarly to the COP-II marker. This indicates that, although unexpected, the intracellular signal of the antibody against Sec23 seemed to relate accurately to the localization of SAR1 and, by association, of the COP-II coat.

The co-localization analysis showed that COP-I and COP-II markers exhibited the lowest correlation coefficients with PPPDE1 amongst the tested antibodies. Thus, it is plausible that PPPDE1 is not physically or permanently associated with the coat protein complexes of vesicles trafficking between Golgi and ER. It might, however, still influence other molecules involved in vesicle budding or fusion.

Brefeldin A (BFA) is a fungal toxin that has been extensively used in studies investigating components of the endomembrane system, as it inhibits ER to Golgi transport and secretory trafficking (Lippincott-Schwartz et al., 1989; Klausner et al., 1992). COP-I coat assembly is initiated by the activation of the small GTPase ADP ribosylation factor (ARF). BFA prevents conversion of GDP- to GTP-bound form of ARF, therefore blocking its activation and COP-I formation. This results on a redistribution of cis-Golgi resident proteins to the ER via tubular structures and accumulation of

recycling proteins in the ERGIC (Lippincott-Schwartz et al., 1990; Orci et al. 1991; Donaldson et al., 1992; Helms & Rothman, 1992; Peyroche et al., 1999, Hauri et al, 2000). Thus, BFA blocks the anterograde trafficking through secretory organelles and, consequently, inhibits secretion (Misumi et al., 1986; Kunze et al., 1995).

The Golgi apparatus rapidly disassembles after BFA treatment – an effect that is reversible, as morphology is reestablished after removal (Fishman & Curran, 1992; Sciaky et al., 1997). BFA causes dispersion of Golgi marker GM130 (Mardones et al., 2006) and accumulation of ERGIC-53 in the ERGIC (Hauri et al., 2000), consistent to the effects we observed after fixation and immunostaining one hour after BFA addition.

After treatment with BFA in live neurons (Fig. 10), PPPDE1-positive perinuclear structures were rapidly dispersed throughout the cytoplasm. Therefore, the effect of BFA on PPPDE1 expression was similar to that of its effect on GM130, but not to that on ERGIC-53. This demonstrates that PPPDE1 not only localizes in very close proximity to the cis-Golgi, but that its stability and localization depend on a functional and structured Golgi apparatus. It also suggests that PPPDE1 might play a role in the secretory pathway.

Neurons have extensive surface areas, about 10,000 times bigger than typical animal cells, and extremities located very far from the soma. They also have special requirements for protein biosynthesis and insertion into the membrane at synaptic sites (Horton & Ehlers, 2004). Therefore, this cell type must rely on a specialized organization of secretory organelles.

Early studies identified the presence of polyribosomes in dendrites (Steward & Lewy, 1982) and the capability of neurons to locally synthetize proteins within dendrites (Rao & Steward, 1991; Torre & Steward, 1992). It has also been shown that satellite components of the secretory pathway, including functional ER exit sites and Golgi structures, can extend to both proximal and distal parts of neuronal dendrites (Broadwell & Cataldo, 1983; Krijnse-Locker et al., 1995; Pierce et al., 2001). Intermediate compartment markers of ER-Golgi transport, such as the RAS-related small GTPases RAB1 and RAB2, p58 and the KDEL (Lys-Asp-Glu-Leu) receptor, have also been found by immunostaining in dendrites (Krijnse-Locker et al., 1995; Torre & Steward, 1996; Gardiol et al., 1999).

In addition to the somatic Golgi apparatus with classical perinuclear distribution, neurons have smaller, discontinuous Golgi structures distributed through the dendrites, named Golgi outposts (GOPs), which function similarly to the somatic Golgi (Horton & Ehlers, 2003). 70-80% of cultured hippocampal neurons display dendritic Golgi (Horton et al., 2005; Quassollo et al., 2015). GOPs can occur as single- or multi-compartments, with elements of cis-, medial- and trans-Golgi cisternae that are disconnected from each other, unlike somatic Golgi (Horton & Ehlers, 2003; Zhou et al., 2014). Golgi structures have not yet been reported, however, to be naturally present in axons.

This peripheral distribution might confer neurons a more controlled secretory ability in the dendrites for an efficient turnover of plasma membrane proteins, especially necessary near synaptic clefts (Gardiol et al., 1999). GOPs have also been shown to help shape dendritic morphology by assisting with microtubule organization, as does the somatic Golgi (Ori-McKenney et al., 2012).

Using live cell imaging of cortical neurons expressing EGFP-PPPDE1, we observed that this protein not only localizes to the perinuclear area, but also to vesicular-tubular structures distributed throughout neuronal projections. Interestingly, these vesicles move either mono- or bi-directionally through the projections (Fig. 11), a characteristic that we had not observed with the pronounced, tubular-shaped perinuclear PPPDE1 structures, and that had not been previously reported in the literature.

The fluorescence recovery after photobleaching (FRAP) analysis (Fig. 12) confirmed the existence of two populations of PPPDE1 molecules with different kinetics during recovery. The mobile fraction of PPPDE1-positive structures corresponds to freely moving, unbound PPPDE1 molecules. The more stationary population corresponds to the perinuclear structures we identified to be in close proximity with the cis-Golgi and the ERGIC, and closer to the Golgi. Possibly, part of this population present in neuronal projections is related to dendritic GOPs. The less mobile pool could not be replenished by the more mobile molecules. The slower recovery observed compared to the cytoplasmic population indicates that PPPDE1 molecules in the perinuclear pool are probably attached to a stationary cellular compartment, most likely the cis-Golgi complex.

We cannot exclude the possibility that PPPDE1 is a component protein of the Golgi apparatus, as has been claimed by a few researchers based purely on its expression

similarity with Golgi markers (Mo et al., 2008; He et al., 2013). However, our SIM and confocal microscopy images and nearest neighbor analysis suggest that PPPDE1 is located very close to the cis-Golgi, perhaps somehow associated to its membrane, as suggested by the FRAP analysis, but not in the organelle lumen. These observations argue against the assumption that PPPDE1 is a Golgi resident protein, but rather indicate that it is membrane-bound.

Whether and how PPPDE1 associates to the cis-Golgi membrane remains elusive, but could be explained by its interaction with binding partners, such as RAB1 and RAB2, or other membrane-anchored proteins. Alternatively, PPPDE1 could be inserted directly into a membrane by its C-terminal amino acids, as a primary structure analysis revealed a probability, despite low, for membrane insertion of the C-terminal part of its transmembrane helices between amino acid 165 and 184 (data not shown).

In addition to describing its intracellular localization, identification of the molecules that might interact with or bind to a protein of interest offer important information about its potential cellular functions. Thus, we analyzed the PPPDE1 interactome after immunoprecipitation via the EGFP fusion both in a native, untreated condition, and upon inhibition of forward secretory trafficking with BFA treatment (Fig. 14). After PPPDE1 immunoprecipitation and mass spectrometry analysis, PPPDE1 was the most abundant protein identified in both conditions, confirming that the purification steps were successful and validating the analysis.

Since an interactome analysis has screening purposes, it is expected to detect several tens, or even hundreds of statistically significant candidate proteins. Even though we employed a conservative statistical analysis, it is likely that not all peptides identified in the interactome bind directly to PPPDE1, as complexes with this protein are also possible, and some binders might not have been detected. In this work, we selected the most relevant candidates to have an association with PPPDE1 for discussion and further confirmation, based on the features of PPPDE1 described here and in the literature, such as its localization and activity reported in non-neuronal cell types.

Ubiquitin co-precipitated with PPPDE1 in both treatment conditions and was the most significantly enriched protein in the native interactome, only after PPPDE1 itself. This suggests two possibilities: first, that PPPDE1 might interact with ubiquitin, which supports previous indications of its potential de-ubiquitinating activity (Iyer et al., 2004;

Xie et al., 2017). Second, that PPPDE1 does not bind to ubiquitin directly, but rather associates with ubiquitinated proteins.

The ubiquitin-like modifier SUMO, on the other hand, was not identified in the interactome analysis in any of the conditions, not even outside the statistical significance parameters. This finding excludes SUMO as a binding partner of PPPDE1, indicating that PPPDE1 most likely does not play a role in de-SUMOylation. For this reason, it should not be referred to as deSUMOylating isopeptidase 2 (DeSI2), which has been used as a synonym for PPPDE1 in the literature (Shin et al., 2012), as well as in gene and protein databases.

Our interactome analysis also identified several proteins involved in intracellular trafficking as potential binding partners of PPPDE1, many of which are located particularly between the ER and Golgi, which is consistent with the intracellular localization of PPPDE1 that we and other groups have described.

One of these proteins is SAR1, a small GTPase responsible for initiating coat assembly of COP-II vesicles budding from the ER (Nakańo & Muramatsu, 1989; Kuge et al., 1994; Barlowe et al., 1994). Another small GTPase, the RAB2 protein, was significantly enriched by PPPDE1 in the untreated condition, and both RAB1 and RAB2 after treatment with BFA.

RABs (RAS-related proteins) constitute a large family of small GTPases, part of the RAS superfamily, that coordinate intracellular vesicle trafficking in all its stages (Touchot et al., 1987; Simons & Zerial, 1993; Novick & Zerial, 1997; Zerial & McBride, 2001). Amongst the several members of the RAB family (over 70 in humans - Colicelli, 2004), RAB1 and RAB2 are located between the ER and Golgi and regulate vesicular traffic between these organelles (Stenmark, 2009; Bhuin & Roy, 2014).

Small GTPases, such as SAR1, RAB1 and RAB2, can bind and hydrolyze guanosine triphosphate (GTP). They are in their active, membrane-attached form when bound to GTP, and inactive and free in the cytoplasm when bound to guanosine diphosphate (GDP) (Yang, 2002). Regulatory proteins control their switching mechanism: guanine nucleotide exchange factors (GEFs) cause GDP to dissociate from the GTPases, enabling GTP binding and resulting in their activation, while GTPase activating proteins

(GAPs) stimulate their GTPase activity, allowing conversion of GTP to GDP and resulting in their inactivation (Cherfils & Zeghouf, 2013).

Activated SAR1 binds to the ER membrane on exit sites (ERES) and recruits assembly of Sec23/Sec24 protein complexes, and subsequently of Sec13/Sec31, promoting formation of the COP-II coat (Matsuoka et al., 1998; Antonny et al., 2001). Activated RAB1 and RAB2 anchor via prenyl groups to the cytoplasmic face of membranes of vesicles trafficking between the ER and Golgi and facilitate vesicle tethering, i.e. enable proximity of the vesicle with the target membrane prior to docking and fusion (Moyer et al., 2001; Stenmark, 2009; Barrowman et al., 2010). Functional defects in RAB1 or SAR1 proteins cause disassembly and dispersion of the Golgi complex (Wilson et al., 1994; Zaal et al., 1999; Ward et al., 2001).

Using super-resolution microscopy with structured illumination and subsequent nearest neighbor analysis (Fig. 9), we investigated the spatial distribution of cis-Golgi and ERGIC markers in relation to PPPDE1. We saw that, even though PPPDE1 is in close proximity with both the cis-Golgi marker GM130 and the ERGIC marker ERGIC-53, it is located closer to GM130.

The Golgi matrix protein GM130 acts as an effector molecule for both RAB1 and RAB2 (Saraste, 2016). GM130 forms a complex with other proteins, which then interacts with activated RAB1, facilitating COP-II vesicle tethering and fusion to the Golgi (Moyer et al., 2001; Bhuin & Roy, 2014). PPPDE1 might, therefore, be a component protein of the effector complex for RAB1 and RAB2.

Analysis of the PPPDE1 interactome after BFA treatment identified proteins related to a larger number of categories of molecular processes than the untreated condition, as can be seen in the gene ontology classification (Fig. 15). Since BFA caused dispersion of PPPDE1 throughout the cell, it most likely also caused temporary alteration of its binding partners, increasing the range of biological pathways in which they are involved. Some proteins, including ubiquitin, SAR1 and RAB2, were found in both treatment conditions (Fig. 14C, labeled in black). These represent strong candidates for interacting with PPPDE1, as they still co-precipitate with PPPDE1 even after BFA-induced diffusion of the Golgi and PPPDE1 structures.

Our interactome screening also identified the farnesyl pyrophosphate synthase as a potential binding partner of PPPDE1. This enzyme is a prenyl transferase, meaning it catalyzes the transfer of hydrophobic prenyl groups (in this case, farnesyl) to acceptor molecules, such as RABs, allowing their insertion into target membranes (Hutagalung & Novick, 2011). This raises the possibility that PPPDE1 could be involved in the facilitation of RAB1 and RAB2 farnesylation that is necessary for their active localization in vesicular membranes.

Several proteins related to the cytoskeleton were identified in the PPPDE1 interactome, such as coronin 1-A, subunits of the cytoskeletal chaperone T-complex protein (CCT), as well as fascin and thymosin beta-10, involved in cytoskeleton organization. Another protein enriched by PPPDE1 in the untreated condition was dynein, a cytoskeleton motor protein that carries vesicular cargos by moving along microtubules. In neurons, dynein usually transports cargo in a retrograde direction (towards the soma), while kinesin moves in an anterograde direction (towards the axonal end). In neuronal dendrites, however, dynein can move bi-directionally (Kapitein et al., 2010).

The identification of dynein as a potential binding partner of PPPDE1 is in accordance with the localization of PPPDE1. Transport from the ERGIC to the cis-Golgi requires dynein movement along microtubules (Appenzeller-Herzog & Hauri, 2006). RAB4 and RAB6, which coordinate endosomal and Golgi-to-ER transport, respectively, were found to interact with dynein light chain (Bielli et al., 2001; Wanschers et al., 2008). In addition, RAB2 recruits dynein, but not kinesin, for coupling with microtubules (Tisdale et al., 2009). Therefore, interaction of PPPDE1 with dynein could be indirect, through its association with RAB1 and RAB2. We also observed through vesicle tracking that the cytoplasmic population of PPPDE1 structures moves along tubulin-positive neuronal projections, which could mean that PPPDE1 movement is microtubule-dependent.

After BFA treatment, dynein was not detected in the PPPDE1 interactome. The G-protein subunits GNB1 and 2, which were not identified in the untreated condition, were enriched by PPPDE1 with high significance upon addition of BFA. This is consistent with the indication of a strong association between PPPDE1 and small GTPases, as they are monomeric, small types of G-proteins (Purves et al., 2001).

Because of their particular localization and activity in the regulation of vesicular traffic between the ER and Golgi, where PPPDE1 is located, we considered the proteins

RAB1, RAB2 and SAR1 identified in the PPPDE1 interactome to be likely candidates to effectively interact with PPPDE1. To further examine this possibility, we generated fusion vectors of mRuby2 to each of these three proteins and co-expressed them with EGFP-PPPDE1 in cultured neurons.

There are two isoforms of RAB1, RAB2 and SAR1: A and B. Since they share high sequence identity, – of 92% for RAB1A/B, 84% for RAB2A/B and 91% for SAR1A/B in mice – we generated fusion proteins with only the A isoforms. For simplicity, we referred to the proteins expressed by these constructs as RAB1, RAB2 and SAR1.

Live cell imaging and correlation quantification (Fig. 16) demonstrated that RAB1 and RAB2 co-localized highly and specifically with PPPDE1 (approximately 90%), more strongly than any of the antibodies tested in the immunocytochemical screening. This finding corroborates the interaction between PPPDE1 and RAB1 and RAB2 in neurons observed in the interactome analysis and demonstrates a strong association of PPPDE1 with these two RAS-related small GTPases regulating ER-Golgi transport.

SAR1, on the other hand, exhibited a diffuse expression in both nucleus and cytoplasm and showed less correlation with PPPDE1. This does not fully exclude, however, a possible functional interaction between these two proteins, as SAR1 was detected in the PPPDE1 interactome both with and without BFA treatment.

A schematic summary of the localization of PPPDE1, RAB1/RAB2 and SAR1 based on the compilation of the observations of this work is displayed below (Fig. 18).

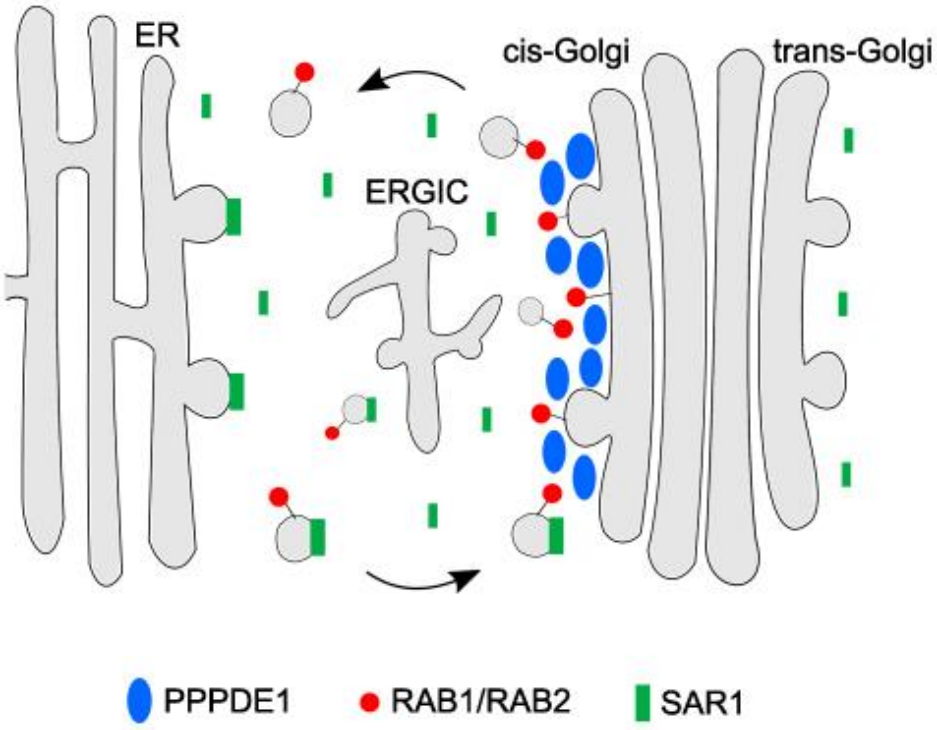

Fig. 18. Schematic representation of the intracellular localization of perinuclear PPPDE1, RAB1/RAB2 and SAR1 in neurons. Perinuclear EGFP-PPPDE1 localized to tubular, stationary structures in close proximity with the cis-Golgi marker GM130 and the ERGIC marker ERGIC-53, but closer to GM130. Whether PPPDE1 is attached to the cis-Golgi membrane directly or indirectly remains unclear. Activated RAB1 and RAB2 are membrane-anchored via a prenyl group. Fusion of RAB1 and RAB2 to mRuby2 exhibited approximately 90% co-localization with PPPDE1 in live imaging of mouse cortical neurons. mRuby2-SAR1 displayed a diffuse and homogeneous signal throughout the cytoplasm and nucleus and a low correlation with PPPDE1-positive structures.

Although PPPDE1 seems to interact with RAB1 and RAB2, it is most likely not a GTPase itself. The size and the fold of the PPPDE1 isoform, PPPDE2, is similar to that of small GTPases. However, it lacks one of the most important regions for nucleotide binding, the phosphate-binding loop (P-loop) (Saraste et al., 1990), meaning that this feature is presumably also missing in the structure of PPPDE1.

Previous studies have pointed out a role of PPPDE1 in apoptosis (Yan et al., 2009; Deng et al., 2010; Li 2013 et al.; Yuan et al., 2015), as well as in de-ubiquitinating (Iyer

et al., 2004; Xie et al., 2017) and de-SUMOylating processes (Shin et al., 2012), known to have an implication on cell fate and survival (Kirkin & Dikic, 2007; Gilberto & Peter, 2017). Therefore, we hypothesized that PPPDE1 might exert an effect on neuronal viability.

We observed that cortical neuronal cultures overexpressing PPPDE1 displayed significantly lower rates of dead cells in comparison to those transduced with the control vector (Fig. 13). In contrast, cultures where PPPDE1 had been silenced exhibited higher, although not significant, amounts of apoptotic or necrotic neurons. These results suggest that increased levels of PPPDE1 provide a beneficial outcome towards neuronal survival, even in the absence of exogenous triggers of cellular stress. PPPDE1 may, therefore, serve as a target for improving viability in neurons.

Our findings contradict preceding data supporting a pro-apoptotic role of PPPDE1 (Yan et al., 2009; Deng et al., 2010; Li 2013 et al.; Yuan et al., 2015). However, these studies employed other, proliferating cell types. The only previous study of PPPDE1 in neurons has shown that its knockdown did not influence apoptosis during mouse brain development (Cai et al., 2010). This suggests that functions of PPPDE1 in post-mitotic neurons might be distinct from those in proliferating cell types, and unrelated to programmed cell death.

Our result that PPPDE1 expression improved neuronal viability could be explained by its potential activity as a de-ubiquitinating enzyme (DUB) in neurons. Intracellular environments host a dynamic equilibrium between free ubiquitin, which is available for attachment, and conjugated ubiquitin, which is attached to target proteins. A reduction in the availability of free ubiquitin has been associated with compromised neuronal function and survival (Park et al., 2012). Ubiquitin homeostasis is closely related to cellular vulnerability and DUBs play a major role in its maintenance (Park & Ryu, 2014). Thus, PPPDE1 expression might exert a beneficial effect on the viability of neurons through the regulation of appropriate intracellular levels of free ubiquitin.

The evidence that exogenous PPPDE1 impacts neuronal survival might also be related to its association with the RAB1 and RAB2 small GTPases. Malfunctioning of several RAB proteins, including RAB1, and impaired membrane trafficking have been linked to neurodegeneration, either as its cause or as its effect (Kiral et al., 2018). Upregulation of RAB1 restored ER-Golgi transport and prevented apoptosis induction in an *in vitro*

model of amyotrophic lateral sclerosis (ALS) (Soo et al., 2015). Therefore, overexpression of PPPDE1 might cause decrease in neuronal death rates by improving RAB1-mediated vesicle trafficking.

Our results provide indications of a potential association of PPPDE1 with proteins involved in ER-Golgi vesicle trafficking and in ubiquitin modification. These two cellular processes are, in fact, related. Ubiquitination of membrane proteins is known to regulate a broad range of pathways in the endomembrane system (Helliwell et al., 2001; Risinger & Kaiser, 2008). It acts, for example, as a signal for internalization, endosomal sorting and turnover of plasma membrane transporters, including G protein-coupled receptors (Hicke and Riezman, 1996; Galan et al., 1996; Kölling & Losko, 1997; Marchese & Trejo, 2013). In addition, monoubiquitination of COP-II component Sec31 controls vesicle coat size, allowing loading of larger cargo molecules leaving the ER (Jin et al., 2012). De-ubiquitination of the COP-II protein Sec23 and of β'-COP, a structural subunit of the COP-I complex, also regulate coat turnover and failure of this mechanism impairs vesicular traffic (Cohen et al., 2003 a/b; Jarmoszewicz, 2012). Therefore, modification by ubiquitin conjugation and deconjugation seems to be a regulatory mechanism in both anterograde and retrograde transport between the ER and Golgi.

Increasing evidence has demonstrated that activity of RAB proteins can also be controlled by ubiquitination, so far shown for RAB6, RAB8, RAB11 (Lachance et al., 2014) and RAB5 (Shin et al., 2017). GEFs, GAPs and effector molecules that regulate the activity of small GTPases can also be ubiquitinated (Pham & Rotim, 2001; Ang et al., 2008). Even though some small GTPases have not been shown so far to be targets of ubiquitination themselves, they often bind to or complex with ubiquitinated proteins, as is the case of SAR1 (de la Vega et al., 2011).

Whether or not PPPDE1 acts directly as a de-ubiquitinating enzyme as suggested by a previous study (Xie et al., 2017) still remains unclear. A broad range of proteins is necessary for proper vesicular transport between ER and Golgi, many of which either have their function controlled by ubiquitination or interact with proteins that do. We cannot exclude the possibility that PPPDE1 is either an adapter molecule or a component of an effector protein complex that assists the modulation of ubiquitin conjugation or deconjugation in an indirect manner.

Bringing together the current literature knowledge and our findings that PPPDE1 is in close proximity with the cis-Golgi and is likely associated with ubiquitin and the small GTPases RAB1 and RAB2, we hypothesize that the cellular functions of PPPDE1 lie at the intersection of these molecules. PPPDE1 might help regulate vesicle trafficking between the ER and Golgi compartments, possibly by interacting with RAB1 and RAB2 and by modulating the ubiquitination status of target proteins.

As an outlook of this project, we aim to further investigate the potential activity of PPPDE1 on de-ubiquitination in neurons and to identify the proteins it may modify. After transduction with either the knockdown PPPDE1-shRNA construct or its non-targeting control, neuronal cultures expressing an EGFP-ubiquitin fusion protein or its control (already generated) will be immunoprecipitated for EGFP. A proteomics analysis using mass spectrometry will then be performed, allowing us to better evaluate the role of PPPDE1 in ubiquitination processes and analyze its function based on its endogenous expression.

In the present work, we examined the intracellular localization and the interactome of PPPDE1 in mouse cortical neurons, and identified two populations of PPPDE1 molecules with different mobility kinetics. We also analyzed the functional consequences of PPPDE1 RNA interference and expression of an EGFP-PPPDE1 fusion protein. We demonstrated for the first time that PPPDE1 is physically and structurally associated with the *cis* face of the Golgi complex in neurons and linked its localization to its potential binding partners and cellular functions. We identified ubiquitin, RAB1 and RAB2 as likely candidates for interacting with PPPDE1 and observed a high correlation of PPPDE1 with RAB1 and RAB2 in live neurons, providing clues towards the mechanisms and pathways in which it plays a role. In addition, we found that delivery of exogenous PPPDE1 increased survival rates of cultured neuronal cells, raising the exciting possibility that modulation of PPPDE1 levels may represent a mechanism to improve viability of neurons.

Our results contribute to the understanding of structural and functional aspects of PPPDE1 in neurons and provide novel insight into its impact on regulatory mechanisms of intracellular trafficking and neuronal survival.

References

Abbe E. Beiträge zur Theorie des Mikroskops und der mikroskopischen Wahrnehmung. Archiv für Mikroskopische Anatomie. 1873; 9:413-418.

Agbulut O, Coirault C, Niederländer N, Huet A, Vicart P, Hagège A, Puceat M, Menasché P. GFP expression in muscle cells impairs actin-myosin interactions: implications for cell therapy. Nat Methods. 2006 May;3(5):331.

Alberts B, Johnson A, Lewis J, Raff M, Roberts K, Walter P. Transport from the ER through the Golgi Apparatus. In: Molecular Biology of the Cell. 4th edition. New York: Garland Science; 2002.

Ang XL, Seeburg DP, Sheng M, Harper JW. Regulation of postsynaptic RapGAP SPAR by Polo-like kinase 2 and the SCFbeta-TRCP ubiquitin ligase in hippocampal neurons. J Biol Chem. 2008 Oct 24;283(43):29424-32.

Antonny B, Madden D, Hamamoto S, Orci L, Schekman R. Dynamics of the COPII coat with GTP and stable analogues. Nat Cell Biol. 2001 Jun;3(6):531-7.

Appenzeller-Herzog C, Hauri HP. The ER-Golgi intermediate compartment (ERGIC): in search of its identity and function. J Cell Sci. 2006 Jun 1;119(Pt 11):2173-83.

Aridor M, Bannykh SI, Rowe T, Balch WE. Sequential coupling between COPII and COPI vesicle coats in endoplasmic reticulum to Golgi transport. J Cell Biol. 1995 Nov;131(4):875-93.

Bannykh SI, Rowe T, Balch WE. The organization of endoplasmic reticulum export complexes. J Cell Biol. 1996 Oct;135(1):19-35.

Barlowe C, Orci L, Yeung T, Hosobuchi M, Hamamoto S, Salama N, Rexach MF, Ravazzola M, Amherdt M, Schekman R. COPII: a membrane coat formed by Sec proteins that drive vesicle budding from the endoplasmic reticulum. Cell. 1994 Jun 17;77(6):895-907.

Barrowman J, Bhandari D, Reinisch K, Ferro-Novick S. TRAPP complexes in membrane traffic: convergence through a common Rab. Nat Rev Mol Cell Biol. 2010 Nov;11(11):759-63.

Bentivoglio M. The discovery of the Golgi apparatus. J Hist Neurosci. 1999 Aug;8(2):202-8.

Bhattacharyya D, Glick BS. Two mammalian Sec16 homologues have nonredundant functions in endoplasmic reticulum (ER) export and transitional ER organization. Mol Biol Cell. 2007 Mar;18(3):839-49.

Bhuin T, Roy JK. Rab proteins: the key regulators of intracellular vesicle transport. Exp Cell Res. 2014 Oct 15;328(1):1-19.

Bielli A, Thörnqvist PO, Hendrick AG, Finn R, Fitzgerald K, McCaffrey MW. The small GTPase Rab4A interacts with the central region of cytoplasmic dynein light intermediate chain-1. Biochem Biophys Res Commun. 2001 Mar;281(5):1141-53.

Blum R, Stephens DJ, Schulz I. Lumenal targeted GFP, used as a marker of soluble cargo, visualises rapid ERGIC to Golgi traffic by a tubulo-vesicular network. J Cell Sci. 2000 Sep;113 (Pt 18):3151-9.

Bonifacino JS, Glick BS. The mechanisms of vesicle budding and fusion. Cell. 2004 Jan 23;116(2):153-66.

Brandon E, Szul T, Alvarez C, Grabski R, Benjamin R, Kawai R, Sztul E. On and off membrane dynamics of the endoplasmic reticulum-golgi tethering factor p115 in vivo. Mol Biol Cell. 2006 Jul;17(7):2996-3008.

Broadwell RD, Cataldo AM. The neuronal endoplasmic reticulum: its cytochemistry and contribution to the endomembrane system. I. Cell bodies and dendrites. J Histochem Cytochem. 1983 Sep;31(9):1077-88.

Cai P, Xia X, Li F, Cui Y, Yang Q, Chen M. PNAS4 knockout does not induce obviously neurocytes apoptosis and abnormal development in mice brain. Mol Biol Rep. 2012 Jan;39(1):621-8.

Cappadocia L, Lima CD. Ubiquitin-like Protein Conjugation: Structures, Chemistry, and Mechanism. Chem Rev. 2018 Feb 14;118(3):889-918.

Chen C, Huang H, Wu CH. Protein Bioinformatics Databases and Resources. Methods Mol Biol. 2017;1558:3-39.

Chen ZJ, Sun LJ. Nonproteolytic functions of ubiquitin in cell signaling. Mol Cell. 2009 Feb 13;33(3):275-86.

Cherfils J, Zeghouf M. Regulation of small GTPases by GEFs, GAPs, and GDIs. Physiol Rev. 2013 Jan;93(1):269-309.

Cohen M, Stutz F, Belgareh N, Haguenauer-Tsapis R, Dargemont C. Ubp3 requires a cofactor, Bre5, to specifically de-ubiquitinate the COPII protein, Sec23. Nat Cell Biol. 2003 Jul;5(7):661-7.

Cohen M, Stutz F, Dargemont C. Deubiquitination, a new player in Golgi to endoplasmic reticulum retrograde transport. J Biol Chem. 2003 Dec 26;278(52):51989-92.

Colicelli J. Human RAS superfamily proteins and related GTPases. Sci STKE. 2004 Sep 7;(250):RE13.

Cooper GM. The Mechanism of Vesicular Transport. In: The Cell: A Molecular Approach. 2nd edition. Sunderland (MA): Sinauer Associates; 2000.

Datwyler AL, Lättig-Tünnemann G, Yang W, Paschen W, Lee SL, Dirnagl U, Endres M, Harms C. SUMO2/3 conjugation is an endogenous neuroprotective mechanism. J Cereb Blood Flow Metab. 2011 Nov;31(11):2152-9.

de Chaumont F, Dallongeville S, Chenouard N, Hervé N, Pop S, Provoost T, Meas-Yedid V, Pankajakshan P, Lecomte T, Le Montagner Y, Lagache T, Dufour A, Olivo-Marin JC. Icy: an open bioimage informatics platform for extended reproducible research. Nat Methods. 2012 Jun 28;9(7):690-6.

de la Vega M, Burrows JF, Johnston JA. Ubiquitination: Added complexity in Ras and Rho family GTPase function. Small GTPases. 2011 Jul;2(4):192-201.

Deng H, Jiang Q, Liang S, Yan F, Hou S, Qian Z, Li J, Wen Y, Yang J, Wei Y. Prokaryotic expression, purification and characterization of a novel pro-apoptosis protein hPNAS-4. Biotechnol Appl Biochem. 2010 Feb 11;55(2):63-72.

Denuc A, Marfany G. SUMO and ubiquitin paths converge. Biochem Soc Trans. 2010 Feb;38(Pt 1):34-9.

Dittgen T, Nimmerjahn A, Komai S, Licznerski P, Waters J, Margrie TW, Helmchen F, Denk W, Brecht M, Osten P. Lentivirus-based genetic manipulations of cortical neurons and their optical and electrophysiological monitoring in vivo. Proc Natl Acad Sci U S A. 2004 Dec 28;101(52):18206-11.

Donaldson JG, Finazzi D, Klausner RD. Brefeldin A inhibits Golgi membrane-catalysed exchange of guanine nucleotide onto ARF protein. Nature. 1992 Nov 26;360(6402):350-2.

English AR, Voeltz GK. Endoplasmic Reticulum Structure and Interconnections with Other Organelles. Cold Spring Harb Perspect Biol. 2013 Apr; 5(4): a013227.

Faulstich D, Auerbach S, Orci L, Ravazzola M, Wegchingel S, Lottspeich F, Stenbeck G, Harter C, Wieland FT, Tschochner H. Architecture of coatomer: molecular characterization of delta-COP and protein interactions within the complex. J Cell Biol. 1996 Oct;135(1):53-61.

Fishman PH, Curran PK. Brefeldin A inhibits protein synthesis in cultured cells. FEBS Lett. 1992 Dec 21;314(3):371-4.

Flick K, Kaiser P. Protein degradation and the stress response. Semin Cell Dev Biol. 2012 Jul;23(5):515-22.

Galan JM, Moreau V, Andre B, Volland C, Haguenauer-Tsapis R. Ubiquitination mediated by the Npi1p/Rsp5p ubiquitin-protein ligase is required for endocytosis of the yeast uracil permease. J Biol Chem. 1996 May 3;271(18):10946-52.

Gardiol A, Racca C, Triller A. Dendritic and postsynaptic protein synthetic machinery. J Neurosci. 1999 Jan 1;19(1):168-79.

Gilberto S, Peter M. Dynamic ubiquitin signaling in cell cycle regulation. J Cell Biol. 2017 Aug 7;216(8):2259-2271.

Giles J. Chemistry Nobel for trio who revealed molecular death-tag. Nature. 2004 Oct 14;431(7010):729.

Gimber N, Tadeus G, Maritzen T, Schmoranzer J, Haucke V. Diffusional spread and confinement of newly exocytosed synaptic vesicle proteins. Nat Commun. 2015 Sep 24;6:8392.

Glickman MH, Ciechanover A. The ubiquitin-proteasome proteolytic pathway: destruction for the sake of construction. Physiol Rev. 2002 Apr;82(2):373-428.

Goldstein G, Scheid M, Hammerling U, Schlesinger DH, Niall HD, Boyse EA. Isolation of a polypeptide that has lymphocyte-differentiating properties and is probably represented universally in living cells. Proc Natl Acad Sci U S A. 1975 Jan;72(1):11-5.

Gong L, Millas S, Maul GG, Yeh ET. Differential regulation of sentrinized proteins by a novel sentrin-specific protease. J Biol Chem. 2000 Feb 4;275(5):3355-9.

Guo C, Henley JM. Wrestling with stress: roles of protein SUMOylation and deSUMOylation in cell stress response. IUBMB Life. 2014 Feb;66(2):71-7.

Gustafsson MG. Surpassing the lateral resolution limit by a factor of two using structured illumination microscopy. J Microsc. 2000 May;198(Pt 2):82-7.

Harms C, Albrecht K, Harms U, Seidel K, Hauck L, Baldinger T, Hübner D, Kronenberg G, An J, Ruscher K, Meisel A, Dirnagl U, von Harsdorf R, Endres M, Hörtnagl H. Phosphatidylinositol 3-Akt-kinase-dependent phosphorylation of p21(Waf1/Cip1) as a novel mechanism of neuroprotection by glucocorticoids. J Neurosci. 2007 Apr 25;27(17):4562-71.

Harris N. Organization of the Endomembrane System. Ann. Rev. Plant Physiol. 1986 37:73-92.

Hauri HP, Kappeler F, Andersson H, Appenzeller C. ERGIC-53 and traffic in the secretory pathway. J Cell Sci. 2000 Feb;113 (Pt 4):587-96.

Hauri HP, Schweizer A. The endoplasmic reticulum-Golgi intermediate compartment. Curr Opin Cell Biol. 1992 Aug;4(4):600-8.

He Y, Wang J, Gou L, Shen C, Chen L, Yi C, Wei X, Yang J. Comprehensive analysis of expression profile reveals the ubiquitous distribution of PPPDE peptidase domain 1, a Golgi apparatus component, and its implications in clinical cancer. Biochimie. 2013 Jul;95(7):1466-75.

Helenius A, Mellman I, Wall D, Hubbard A. Endosomes. Trends Biochem Sci. 1983; 8:245–250.

Helliwell SB, Losko S, Kaiser CA. Components of a ubiquitin ligase complex specify polyubiquitination and intracellular trafficking of the general amino acid permease. J Cell Biol. 2001 May 14;153(4):649-62.

Helms JB, Rothman JE. Inhibition by brefeldin A of a Golgi membrane enzyme that catalyses exchange of guanine nucleotide bound to ARF. Nature. 1992 Nov 26;360(6402):352-4.

Herrup K, Yang Y. Cell cycle regulation in the postmitotic neuron: oxymoron or new biology? Nat Rev Neurosci. 2007 May;8(5):368-78.

Hershko A, Ciechanover A, Heller H, Haas AL, Rose IA. Proposed role of ATP in protein breakdown: conjugation of protein with multiple chains of the polypeptide of ATP-dependent proteolysis. Proc Natl Acad Sci U S A. 1980 Apr;77(4):1783-6.

Hicke L, Riezman H. Ubiquitination of a yeast plasma membrane receptor signals its ligand-stimulated endocytosis. Cell. 1996 Jan 26;84(2):277-87.

Hirschberg K, Miller CM, Ellenberg J, Presley JF, Siggia ED, Phair RD, Lippincott-Schwartz J. Kinetic analysis of secretory protein traffic and characterization of golgi to plasma membrane transport intermediates in living cells. J Cell Biol. 1998 Dec 14;143(6):1485-503.

Horton AC, Ehlers MD. Dual modes of endoplasmic reticulum-to-Golgi transport in dendrites revealed by live-cell imaging. J Neurosci. 2003 Jul 16;23(15):6188-99.

Horton AC, Ehlers MD. Secretory trafficking in neuronal dendrites. Nat Cell Biol. 2004 Jul;6(7):585-91.

Horton AC, Rácz B, Monson EE, Lin AL, Weinberg RJ, Ehlers MD. Polarized secretory trafficking directs cargo for asymmetric dendrite growth and morphogenesis. Neuron. 2005 Dec 8;48(5):757-71.

Hutagalung AH, Novick PJ. Role of Rab GTPases in Membrane Traffic and Cell Physiology. Physiological Reviews. 2011; 91(1):119-149.

Iyer LM, Koonin EV, Aravind L. Novel predicted peptidases with a potential role in the ubiquitin signaling pathway. Cell Cycle. 2004 Nov;3(11):1440-50.

Jarmoszewicz K, Łukasiak K, Riezman H, Kaminska J. Rsp5 ubiquitin ligase is required for protein trafficking in Saccharomyces cerevisiae COPI mutants. PLoS One. 2012;7(6):e39582.

Jin L, Pahuja KB, Wickliffe KE, Gorur A, Baumgärtel C, Schekman R, Rape M. Ubiquitin-dependent regulation of COPII coat size and function. Nature. 2012 Feb 22;482(7386):495-500.

Johnson ES, Schwienhorst I, Dohmen RJ, Blobel G. The ubiquitin-like protein Smt3p is activated for conjugation to other proteins by an Aos1p/Uba2p heterodimer. EMBO J. 1997 Sep 15;16(18):5509-19.

Kapitein LC, Schlager MA, Kuijpers M, Wulf PS, van Spronsen M, MacKintosh FC, Hoogenraad CC. Mixed microtubules steer dynein-driven cargo transport into dendrites. Curr Biol. 2010 Feb 23;20(4):290-9.

Karve TM, Cheema AK. Small changes huge impact: the role of protein posttranslational modifications in cellular homeostasis and disease. Amino Acids. 2011;207691.

Khoury GA, Baliban RC, Floudas CA. Proteome-wide post-translational modification statistics: frequency analysis and curation of the swiss-prot database. Sci Rep. 2011 Sep 13;1.

Kimple ME, Brill AL, Pasker RL. Overview of affinity tags for protein purification. Curr Protoc Protein Sci. 2013 Sep 24;73:Unit 9.9.

Kiral FR, Kohrs FE, Jin EJ, Hiesinger PR. Rab GTPases and Membrane Trafficking in Neurodegeneration. Curr Biol. 2018 Apr 23;28(8):R471-R486.

Kirkin V, Dikic I. Role of ubiquitin- and Ubl-binding proteins in cell signaling. Curr Opin Cell Biol. 2007 Apr;19(2):199-205.

Klausner RD, Donaldson JG, Lippincott-Schwartz J. Brefeldin A: insights into the control of membrane traffic and organelle structure. J Cell Biol. 1992 Mar;116(5):1071-80.

Knorre DG, Kudryashova NV, Godovikova TS. Chemical and functional aspects of posttranslational modification of proteins. Acta Naturae. 2009 Oct;1(3):29-51.

Kölling R, Losko S. The linker region of the ABC-transporter Ste6 mediates ubiquitination and fast turnover of the protein. EMBO J. 1997 May 1;16(9):2251-61.

Komander D. The emerging complexity of protein ubiquitination. Biochem Soc Trans. 2009 Oct;37(Pt 5):937-53.

Krijnse-Locker J, Parton RG, Fuller SD, Griffiths G, Dotti CG. The organization of the endoplasmic reticulum and the intermediate compartment in cultured rat hippocampal neurons. Mol Biol Cell. 1995 Oct;6(10):1315-32.

Kuge O, Dascher C, Orci L, Rowe T, Amherdt M, Plutner H, Ravazzola M, Tanigawa G, Rothman JE, Balch WE. Sar1 promotes vesicle budding from the endoplasmic reticulum but not Golgi compartments. J Cell Biol. 1994 Apr;125(1):51-65.

Kunze I, Horstmann C, Manteuffel R, Kunze G, Müntz K. Brefeldin A differentially affects protein secretion from suspension cultured tobacco cells (Nico-tiana tabacum L.). In: Terzi M., Cella R., Falavigna A. (eds) Current Issues in Plant Molecular and Cellular Biology. Current Plant Science and Biotechnology in Agriculture, 1995, vol 22. Springer, Dordrecht.

Lachance V, Degrandmaison J, Marois S, Robitaille M, Génier S, Nadeau S, Angers S, Parent JL. Ubiquitylation and activation of a Rab GTPase is promoted by a β_2AR-HACE1 complex. J Cell Sci. 2014 Jan 1;127(Pt 1):111-23.

Lagache T, Sauvonnet N, Danglot L, Olivo-Marin JC. Statistical analysis of molecule colocalization in bioimaging. Cytometry A. 2015 Jun;87(6):568-79.

Lee MC, Miller EA, Goldberg J, Orci L, Schekman R. Bi-directional protein transport between the ER and Golgi. Annu Rev Cell Dev Biol. 2004;20:87-123.

Lee YJ, Castri P, Bembry J, Maric D, Auh S, Hallenbeck JM. SUMOylation participates in induction of ischemic tolerance. J Neurochem. 2009 Apr;109(1):257-67.

Li L, Chen DB, Lin C, Cao K, Wan Y, Zhao XY, Nie CL, Yuan Z, Wei YQ. hPNAS-4 inhibits proliferation through S phase arrest and apoptosis: underlying action mechanism in ovarian cancer cells. Apoptosis. 2013 Apr;18(4):467-79.

Lippincott-Schwartz J, Donaldson JG, Schweizer A, Berger EG, Hauri HP, Yuan LC, Klausner RD. Microtubule-dependent retrograde transport of proteins into the ER in the presence of brefeldin A suggests an ER recycling pathway. Cell. 1990 Mar 9;60(5):821-36.

Lippincott-Schwartz J, Yuan LC, Bonifacino JS, Klausner RD. Rapid redistribution of Golgi proteins into the ER in cells treated with brefeldin A: evidence for membrane cycling from Golgi to ER. Cell. 1989 Mar 10;56(5):801-13.

Lodish H, Berk A, Zipursky SL, Matsudaira P, Baltimore D, Darnell J. Kinesin, Dynein, and Intracellular Transport. In: Molecular Cell Biology. 4th edition, section 19.3. New York: W. H. Freeman; 2000.

Luini A, Ragnini-Wilson A, Polishchuck RS, De Matteis MA. Large pleiomorphic traffic intermediates in the secretory pathway. Curr Opin Cell Biol. 2005 Aug;17(4):353-61.

Lukinavičius G, Blaukopf C, Pershagen E, Schena A, Reymond L, Derivery E, Gonzalez-Gaitan M, D'Este E, Hell SW, Gerlich DW, Johnsson K. SiR-Hoechst is a far-red DNA stain for live-cell nanoscopy. Nat Commun. 2015 Oct 1;6:8497.

Marchese A, Trejo J. Ubiquitin-dependent regulation of G protein-coupled receptor trafficking and signaling. Cell Signal. 2013 Mar;25(3):707-16.

Mardones GA, Snyder CM, Howell KE. Cis-Golgi matrix proteins move directly to endoplasmic reticulum exit sites by association with tubules. Mol Biol Cell. 2006 Jan;17(1):525-38. Epub 2005 Oct 26.

Marsh BJ, Volkmann N, McIntosh JR, Howell KE. Direct continuities between cisternae at different levels of the Golgi complex in glucose-stimulated mouse islet beta cells. Proc Natl Acad Sci U S A. 2004 Apr 13;101(15):5565-70.

Martínez-Menárguez JA, Geuze HJ, Slot JW, Klumperman J. Vesicular tubular clusters between the ER and Golgi mediate concentration of soluble secretory proteins by exclusion from COPI-coated vesicles. Cell. 1999 Jul 9;98(1):81-90.

Massol RH, Larsen JE, Kirchhausen T. Possible role of deep tubular invaginations of the plasma membrane in MHC-I trafficking. Exp Cell Res. 2005 May 15;306(1):142-9.

Matsuoka K, Orci L, Amherdt M, Bednarek SY, Hamamoto S, Schekman R, Yeung T. COPII-coated vesicle formation reconstituted with purified coat proteins and chemically defined liposomes. Cell. 1998 Apr 17;93(2):263-75.

Meller R, Thompson SJ, Lusardi TA, Ordonez AN, Ashley MD, Jessick V, Wang W, Torrey DJ, Henshall DC, Gafken PR, Saugstad JA, Xiong ZG, Simon RP. Ubiquitin proteasome-mediated synaptic reorganization: a novel mechanism underlying rapid ischemic tolerance. J Neurosci. 2008 Jan 2;28(1):50-9.

Mellman I. Endocytosis and molecular sorting. Annu Rev Cell Dev Biol. 1996; 12:575-625.

Mellman I. Organelles observed: lysosomes. Science. 1989 May 19;244(4906):853-4.

Misumi Y, Misumi Y, Miki K, Takatsuki A, Tamura G, Ikehara Y. Novel blockade by brefeldin A of intracellular transport of secretory proteins in cultured rat hepatocytes. J Biol Chem. 1986 Aug 25;261(24):11398-403.

Miyanari Y, Ziegler-Birling C, Torres-Padilla ME. Live visualization of chromatin dynamics with fluorescent TALEs. Nat Struct Mol Biol. 2013 Nov;20(11):1321-4.

Mo D, Zhu Z, te Pas MF, Li X, Yang S, Wang H, Wang H, Li K. Characterization, expression profiles, intracellular distribution and association analysis of porcine PNAS-4 gene with production traits. BMC Genet. 2008 Jun 30;9:40.

Morré DJ, Mollenhauer HH. The endomembrane concept: a functional integration of endoplasmic reticulum and Golgi apparatus. In: Dynamic Aspects of Plant infrastructure (ed. A. W. Robards), 1974, pp. 84–137.

Moyer BD, Allan BB, Balch WE. Rab1 interaction with a GM130 effector complex regulates COPII vesicle cis-Golgi tethering. Traffic. 2001 Apr;2(4):268-76.

Mukhopadhyay D, Riezman H. Proteasome-independent functions of ubiquitin in endocytosis and signaling. Science. 2007 Jan 12;315(5809):201-5.

Müller S, Hoege C, Pyrowolakis G, Jentsch S. SUMO, ubiquitin's mysterious cousin. Nat Rev Mol Cell Biol. 2001 Mar;2(3):202-10.

Nakańo A, Muramatsu M. A novel GTP-binding protein, Sar1p, is involved in transport from the endoplasmic reticulum to the Golgi apparatus. J Cell Biol. 1989 Dec;109(6 Pt 1):2677-91.

Nayak A, Müller S. SUMO-specific proteases/isopeptidases: SENPs and beyond. Genome Biol. 2014 Jul 31;15(7):422.

Novick P, Zerial M. The diversity of Rab proteins in vesicle transport. Curr Opin Cell Biol. 1997 Aug;9(4):496-504.

Orci L, Tagaya M, Amherdt M, Perrelet A, Donaldson JG, Lippincott-Schwartz J, Klausner RD, Rothman JE. Brefeldin A, a drug that blocks secretion, prevents the assembly of non-clathrin-coated buds on Golgi cisternae. Cell. 1991 Mar 22;64(6):1183-95.

Ori-McKenney KM, Jan LY, Jan YN. Golgi outposts shape dendrite morphology by functioning as sites of acentrosomal microtubule nucleation in neurons. Neuron. 2012 Dec 6;76(5):921-30.

Palade G. Intracellular aspects of the process of protein synthesis. Science. 1975 Aug 1;189(4200):347-58.

Park CW, Ryu HW, Ryu KY. Locus coeruleus neurons are resistant to dysfunction and degeneration by maintaining free ubiquitin levels although total ubiquitin levels decrease upon disruption of polyubiquitin gene Ubb. Biochem Biophys Res Commun. 2012 Feb 17;418(3):541-6.

Park CW, Ryu KY. Cellular ubiquitin pool dynamics and homeostasis. BMB Rep. 2014 Sep;47(9):475-82.

Peyroche A, Antonny B, Robineau S, Acker J, Cherfils J, Jackson CL. Brefeldin A acts to stabilize an abortive ARF-GDP-Sec7 domain protein complex: involvement of specific residues of the Sec7 domain. Mol Cell. 1999 Mar;3(3):275-85.

Pham N, Rotin D. Nedd4 regulates ubiquitination and stability of the guanine-nucleotide exchange factor CNrasGEF. J Biol Chem. 2001 Dec 14;276(50):46995-7003.

Pickart CM. Ubiquitin and the Stress Response. In: Latchman D.S. (eds) Stress Proteins. Handbook of Experimental Pharmacology, vol 136. Springer, Berlin, Heidelberg, 1999.

Pierce JP, Mayer T, McCarthy JB. Evidence for a satellite secretory pathway in neuronal dendritic spines. Curr Biol. 2001 Mar 6;11(5):351-5.

Polishchuk RS, Capestrano M, Polishchuk EV. Shaping tubular carriers for intracellular membrane transport. FEBS Lett. 2009 Dec 3;583(23):3847-56.

Polishchuk RS, Polishchuk EV, Marra P, Alberti S, Buccione R, Luini A, Mironov AA. Correlative light-electron microscopy reveals the tubular-saccular ultrastructure of carriers operating between Golgi apparatus and plasma membrane. J Cell Biol. 2000 Jan 10;148(1):45-58.

Purves D, Augustine GJ, Fitzpatrick D, Katz LC, LaMantia A, McNamara JO, Williams SM. G-Proteins and Their Molecular Targets. In: Neuroscience. 2nd edition. Sunderland (MA): Sinauer Associates; 2001.

Quassollo G, Wojnacki J, Salas DA, Gastaldi L, Marzolo MP, Conde C, Bisbal M, Couve A, Cáceres A. A RhoA Signaling Pathway Regulates Dendritic Golgi Outpost Formation. Curr Biol. 2015 Apr 20;25(8):971-82.

Rao A, Steward O. Evidence that protein constituents of postsynaptic membrane specializations are locally synthesized: analysis of proteins synthesized within synaptosomes. J Neurosci. 1991 Sep;11(9):2881-95.

Rappsilber J, Ishihama Y, Mann M. Stop and go extraction tips for matrix-assisted laser desorption/ionization, nanoelectrospray, and LC/MS sample pretreatment in proteomics. Anal Chem. 2003 Feb 1;75(3):663-70.

Reits EA, Neefjes JJ. From fixed to FRAP: measuring protein mobility and activity in living cells. Nat Cell Biol. 2001 Jun;3(6):E145-7.

Reyes-Turcu FE, Ventii KH, Wilkinson KD. Regulation and cellular roles of ubiquitin-specific deubiquitinating enzymes. Annu Rev Biochem. 2009;78:363-97.

Risinger AL, Kaiser CA. Different ubiquitin signals act at the Golgi and plasma membrane to direct GAP1 trafficking. Mol Biol Cell. 2008 Jul;19(7):2962-72.

Saraste J. Spatial and Functional Aspects of ER-Golgi Rabs and Tethers. Front Cell Dev Biol. 2016 Apr 18;4:28.

Saraste M, Sibbald PR, Wittinghofer A. The P-loop -- a common motif in ATP- and GTP-binding proteins. Trends Biochem Sci. 1990 Nov;15(11):430-4.

Schindelin J, Arganda-Carreras I, Frise E, Kaynig V, Longair M, Pietzsch T, Preibisch S, Rueden C, Saalfeld S, Schmid B, Tinevez JY, White DJ, Hartenstein V, Eliceiri K, Tomancak P, Cardona A. Fiji: an open-source platform for biological-image analysis. Nat Methods. 2012 Jun 28;9(7):676-82.

Schneider CA, Rasband WS, Eliceiri KW. NIH Image to ImageJ: 25 years of image analysis. Nat Methods. 2012 Jul;9(7):671-5.

Schwartz DC, Hochstrasser M. A superfamily of protein tags: ubiquitin, SUMO and related modifiers. Trends Biochem Sci. 2003 Jun;28(6):321-8.

Schweizer A, Fransen JA, Bächi T, Ginsel L, Hauri HP. Identification, by a monoclonal antibody, of a 53-kD protein associated with a tubulo-vesicular compartment at the cis-side of the Golgi apparatus. J Cell Biol. 1988 Nov;107(5):1643-53.

Sciaky N, Presley J, Smith C, Zaal KJ, Cole N, Moreira JE, Terasaki M, Siggia E, Lippincott-Schwartz J. Golgi tubule traffic and the effects of brefeldin A visualized in living cells. J Cell Biol. 1997 Dec 1;139(5):1137-55.

Shin D, Na W, Lee JH, Kim G, Baek J, Park SH, Choi CY, Lee S. Site-specific monoubiquitination downregulates Rab5 by disrupting effector binding and guanine nucleotide conversion. Elife. 2017 Oct 2;6. pii: e29154.

Shin EJ, Shin HM, Nam E, Kim WS, Kim JH, Oh BH, Yun Y. DeSUMOylating isopeptidase: a second class of SUMO protease. EMBO Rep. 2012 Apr;13(4):339-46.

Simons K, Zerial M. Rab proteins and the road maps for intracellular transport. Neuron. 1993 Nov;11(5):789-99.

Simpson JC, Nilsson T, Pepperkok R. Biogenesis of tubular ER-to-Golgi transport intermediates. Mol Biol Cell. 2006 Feb;17(2):723-37.

Soo KY, Halloran M, Sundaramoorthy V, Parakh S, Toth RP, Southam KA, McLean CA, Lock P, King A, Farg MA, Atkin JD. Rab1-dependent ER-Golgi transport dysfunction is a common pathogenic mechanism in SOD1, TDP-43 and FUS-associated ALS. Acta Neuropathol. 2015 Nov;130(5):679-97.

Stenmark H. Rab GTPases as coordinators of vesicle traffic. Nat Rev Mol Cell Biol. 2009 Aug;10(8):513-25.

Steward O, Levy WB. Preferential localization of polyribosomes under the base of dendritic spines in granule cells of the dentate gyrus. J Neurosci. 1982 Mar;2(3):284-91.

Swatek KN, Komander D. Ubiquitin modifications. Cell Res. 2016 Apr;26(4):399-422.

Szklarczyk D, Morris JH, Cook H, Kuhn M, Wyder S, Simonovic M, Santos A, Doncheva NT, Roth A, Bork P, Jensen LJ, von Mering C. The STRING database in 2017: quality-controlled protein-protein association networks, made broadly accessible. Nucleic Acids Res. 2017 Jan 4;45(D1):D362-D368.

Tisdale EJ, Azizi F, Artalejo CR. Rab2 utilizes glyceraldehyde-3-phosphate dehydrogenase and protein kinase C{iota} to associate with microtubules and to recruit dynein. J Biol Chem. 2009 Feb 27;284(9):5876-84.

Toomre D, Keller P, White J, Olivo JC, Simons K. Dual-color visualization of trans-Golgi network to plasma membrane traffic along microtubules in living cells. J Cell Sci. 1999 Jan;112 (Pt 1):21-33.

Torre ER, Steward O. Demonstration of local protein synthesis within dendrites using a new cell culture system that permits the isolation of living axons and dendrites from their cell bodies. J Neurosci. 1992 Mar;12(3):762-72.

Torre ER, Steward O. Protein synthesis within dendrites: glycosylation of newly synthesized proteins in dendrites of hippocampal neurons in culture. J Neurosci. 1996 Oct 1;16(19):5967-78.

Touchot N, Chardin P, Tavitian A. Four additional members of the ras gene superfamily isolated by an oligonucleotide strategy: molecular cloning of YPT-related cDNAs from a rat brain library. Proc Natl Acad Sci U S A. 1987 Dec;84(23):8210-4.

Trier OD, Jain AK. Goal-directed evaluation of binarization methods. IEEE Transactions on Pattern Analysis and Machine Intelligence. 1995 Dec; 17(12):1191-1201.

Trucco A, Polishchuk RS, Martella O, Di Pentima A, Fusella A, Di Giandomenico D, San Pietro E, Beznoussenko GV, Polishchuk EV, Baldassarre M, Buccione R, Geerts WJ, Koster AJ, Burger KN, Mironov AA, Luini A. Secretory traffic triggers the formation of tubular continuities across Golgi sub-compartments. Nat Cell Biol. 2004 Nov;6(11):1071-81.

Wanschers B, van de Vorstenbosch R, Wijers M, Wieringa B, King SM, Fransen J. Rab6 family proteins interact with the dynein light chain protein DYNLRB1. Cell Motil Cytoskeleton. 2008 Mar;65(3):183-96.

Ward TH, Polishchuk RS, Caplan S, Hirschberg K, Lippincott-Schwartz J. Maintenance of Golgi structure and function depends on the integrity of ER export. J Cell Biol. 2001 Nov 12;155(4):557-70.

Waterhouse AM, Procter JB, Martin DM, Clamp M, Barton GJ. Jalview Version 2 – a multiple sequence alignment editor and analysis workbench. Bioinformatics. 2009 May 1;25(9):1189-91.

Wiedenmann J, Oswald F, Nienhaus GU. Fluorescent proteins for live cell imaging: opportunities, limitations, and challenges. IUBMB Life. 2009 Nov;61(11):1029-42.

Wilson BS, Nuoffer C, Meinkoth JL, McCaffery M, Feramisco JR, Balch WE, Farquhar MG. A Rab1 mutant affecting guanine nucleotide exchange promotes disassembly of the Golgi apparatus. J Cell Biol. 1994 May;125(3):557-71.

Xie X, Wang X, Jiang D, Wang J, Fei R, Cong X, Wei L, Wang Y, Chen H. PPPDE1 is a novel deubiquitinase belonging to a cysteine isopeptidase family. Biochem Biophys Res Commun. 2017 Jun 24;488(2):291-296.

Yan F, Gou L, Yang J, Chen L, Tong A, Tang M, Yuan Z, Yao S, Zhang P, Wei Y. A novel pro-apoptosis gene PNAS4 that induces apoptosis in A549 human lung adenocarcinoma cells and inhibits tumor growth in mice. Biochimie. 2009 Apr;91(4):502-7.

Yan F, Ruan XZ, Yang HS, Yao SH, Zhao XY, Gou LT, Ma FX, Yuan Z, Deng HX, Wei YQ. Identification, characterization, and effects of Xenopus laevis PNAS-4 gene on embryonic development. J Biomed Biotechnol. 2010;134764.

Yang Z. Small GTPases: Versatile Signaling Switches in Plants. The Plant Cell. 2002;14:s375-s388.

Yao S, Xie L, Qian M, Yang H, Zhou L, Zhou Q, Yan F, Gou L, Wei Y, Zhao X, Mo X. Pnas4 is a novel regulator for convergence and extension during vertebrate gastrulation. FEBS Lett. 2008 Jun 25;582(15):2325-32.

Yuan Z, Guo W, Yang J, Li L, Wang M, Lei Y, Wan Y, Zhao X, Luo N, Cheng P, Liu X, Nie C, Peng Y, Tong A, Wei Y. PNAS-4, an Early DNA Damage Response Gene, Induces S Phase Arrest and Apoptosis by Activating Checkpoint Kinases in Lung Cancer Cells. J Biol Chem. 2015 Jun 12;290(24):14927-44.

Zaal KJ, Smith CL, Polishchuk RS, Altan N, Cole NB, Ellenberg J, Hirschberg K, Presley JF, Roberts TH, Siggia E, Phair RD, Lippincott-Schwartz J. Golgi membranes are absorbed into and reemerge from the ER during mitosis. Cell. 1999 Dec 10;99(6):589-601.

Zerial M, McBride H. Rab proteins as membrane organizers. Nat Rev Mol Cell Biol. 2001 Feb;2(2):107-17.

Zhao S, Ulrich HD. Distinct consequences of posttranslational modification by linear versus K63-linked polyubiquitin chains. Proc Natl Acad Sci U S A. 2010 Apr 27;107(17):7704-9.

Zhou W, Chang J, Wang X, Savelieff MG, Zhao Y, Ke S, Ye B. GM130 is required for compartmental organization of dendritic golgi outposts. Curr Biol. 2014 Jun 2;24(11):1227-33.

Affidavit

I, Mariana de Souza Leão Cerdeira, certify under penalty of perjury by my own signature that I have submitted the thesis on the topic "*Characterization of the PPPDE1 protein in neurons: intracellular localization, binding partners and functional implications*". I wrote this thesis independently and without assistance from third parties, I used no other aids than the listed sources and resources.

All points based literally or in spirit on publications or presentations of other authors are, as such, in proper citations (see "uniform requirements for manuscripts (URM)" of the ICMJE www.icmje.org) indicated. The sections on methodology (in particular practical work, laboratory requirements, statistical processing) and results (in particular images, graphics and tables) correspond to the URM (s.o) and are answered by me. My contributions in the selected publications for this dissertation correspond to those that are specified in the following joint declaration with the responsible person and supervisor. All publications resulting from this thesis and which I am author of correspond to the URM (see above) and I am solely responsible.

The importance of this affidavit and the criminal consequences of a false affidavit (section 156,161 of the Criminal Code) are known to me and I understand the rights and responsibilities stated therein.

_____ _____

Date Signature

Curriculum Vitae

My curriculum vitae does not appear in the electronic version of my dissertation for reasons of data protection.

My curriculum vitae does not appear in the electronic version of my dissertation for reasons of data protection.

My curriculum vitae does not appear in the electronic version of my dissertation for reasons of data protection.

Acknowledgements

I would like to express my sincere gratitude and appreciation:

to my supervisors, Prof. Dr. Christoph Harms and Dr. Gilla Lättig, who have been tremendously kind and accessible to me, for the continuous support and guidance throughout my PhD;

to Prof. Dr. Ulrich Dirnagl, for the opportunity of taking part in the Department of Experimental Neurology;

to all lab members of AG Harms, in special to Magdalena Jochner, Melanie Kuffner and Stephanie Lorenz, a big thank you for the daily support and enriching discussions;

to our collaborators, Prof. Dr. Michael Krauss (FMP), Dr. Marieluise Kirchner (MDC), Dr. Niclas Gimber and Dr. Jan Schmoranzer (Charité), for the valuable suggestions and contributions to our project;

to my MedNeuro colleagues and friends, in special to Ahmed Khalil, Aarti Swaminathan, Dr. Apoorva Madipakkam, Valérie Boujon and Meron Maricos, for sharing this road with me;

to David Furkert, for the daily encouragement and inspiring passion for science;

to my family, in special my parents, Ana Leão and Antonio Cerdeira, for the endless wisdom and unconditional support;

and to you, dear reader, for your attention.